UNIVERSITÀ
DI PARMA

DOTTORATO DI RICERCA IN
INGEGNERIA INDUSTRIALE

CICLO XXX

Adaptive manufacturing and quality control of freeform parts: engineering, implementation and validation of a laser triangulation based system

Coordinatore:
Chiar.mo Prof. G.F.M.A. Royer Carfagni

Tutore:
Chiar.mo Prof. Marco Silvestri

Co-Tutore:
Chiar.mo Prof. Paolo Pedrazzoli

Dottorando: Matteo Confalonieri

Anni 2014/2017

TABLE OF CONTENTS

1. Introduction

The work hereby presented represents a conceptual framework for the in-line inspection and adaptive correction in the field of high precision manufacturing of turbomachinery freeform shaped components. A wide perspective on the whole concept is firstly presented, then a deep description, comprehensive of study, engineering and validation experiments, is given on a part of the whole concept. This part consists in an on-board correction system aiming at the compensation of positioning errors of freeform shaped parts for their machining via Electro Discharge Machining (EDM). The work has been carried out with the cooperation of SARIX SA (www.sarix.com), a Swiss based company, leader in the micro-EDM high precision machines manufacturing. The work that has been carried out, is nowadays becoming product of the company, as a consequence, some data are not publishable due to confidentiality issues.

1.1. High level objective

The present work envisions the development of a ***novel In-line measurement and correction system***, integrating advanced non-destructive measuring methods and devices, for the realization of micro-scale features in free-form, high-volume, high-added-value functional products. The main objective is to increase the product final performances in terms of efficiency and reliability, and to address the present-day high scrap-rate as well as to increase the overall factory productivity; this, through the promotion of self-adaptiveness to process variations, through monitor and control of every stage of the production with respect to the relative reference models, to successfully address a new generation of zero defects and enhanced performance factories.

The exploitation field lies into one of the most challenging, added-value and advanced industrial sectors in Europe: turbine blades production and machining, where the work pieces are freeform (hard to measure with traditional methods), mainly cast-produced (by definition characterized by large geometrical variations) in high volumes (approximately 50 million pieces in 2016) and the cost of each single work-piece is substantial (from 1.000, up to 10.000€). The global power generation industrial gas turbine market has been estimated at USD 110 billion in 2016 and is projected to grow at a compounded average rate of 3.49% in the next years till 2020. Furthermore, the global aviation gas turbine market has been estimated at USD 49.1 billion in 2016 and is projected to grow at a compounded average growth rate of 5.85% during the forecast period from 2016 to 2020[1,2]. Blades account for a very large percentage of the total cost of each turbine (approximately 40%): it is then a critical success factor to lower the percentages of scrap parts (which account for almost 25-30%[3], just taking into account errors in the machining operations), and to increase the thermo-fluid dynamics performances, currently limited by the geometrical uncertainty of the work piece.

Towards the realization of complex micro-features in free-form products such as turbine blades, the concept (schematized in Figure 1) is related to the development of:

1) an in-line measurement system, based on the exploitation of advanced measurement apparatuses (Computed Tomography scan combined with Laser scan) coupled with novel programming approaches to enhance performances and pace
2) an in-line correction system, based on an adaptive fluid-dynamic model that relates geometrical uncertainty with thermo-fluid dynamic performances, combined with a machining engine that exploits this capability
3) an on-board correction system that eliminates positioning errors on the machine tools

[1]Freedonia Group: FreedoniaFocusWorldCollection

[2]Credence research: Gas turbine electrical power generation market

[3]Manufacturing Engineering Magazine: Cool is Key to Jet Efficiency

4) a strategic PLM module, based on machine learning techniques, that, acting as an extension of existing platforms, integrates in-line measurements into product lifecycle management logics. In the next chapters a more detailed description of each of the objectives is given.

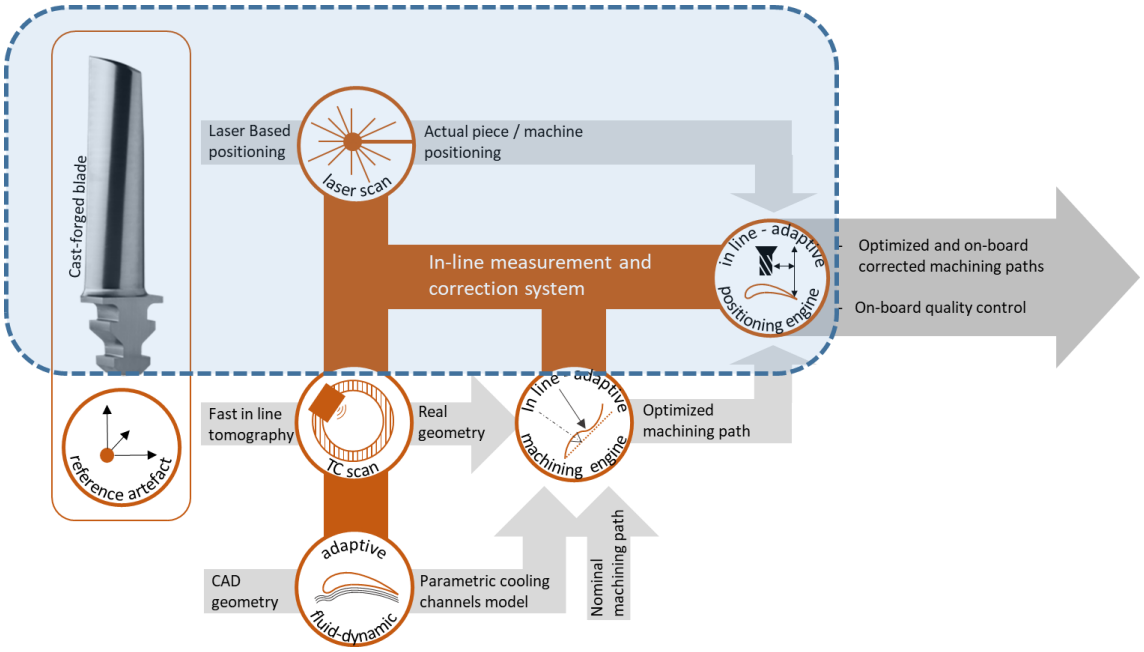

Figure 1: Overall concept conceptual schema; the blue dashed area represents the part of the overall concept that has been carried out in the present thesis

1.2. Motivation and potential impact

1.2.1. Market analysis

Manufacturing remains the main driver of economic wealth: "Manufacturing has a larger multiplier effect than any other major economic activity—a euro spent in manufacturing drives an additional €1.35 in economic activity"[4].

Key elements for enhanced manufacturing competitiveness is the development of high quality, highly productive production processes which justify the rising demand for zero-defects production processes[5], addressing the manufacturing of high-cost products with relevant volumes, requires new approaches. The concept envisioned in the present work empowers such a vision by delivering methods and technologies towards scraps reduction, throughput enhancement and product performance improvement. This through the development of a system level strategy involving an in-line adaptive measurement and correction system, based on advanced non-destructive inspection techniques, interacting with the whole product lifecycle, comprehending its design, manufacturing and maintenance.

One of the key competitive and most relevant sectors in European manufacturing is addressed: the gas turbines industry. As mentioned in , this industry accounts for approximately USD 160 billion in 2016, specifically in the power generation and aviation sectors, which are projected to grow at a

[4]J. P. Holdren, "A National strategic plan for advanced manufacturing," Report of the Interagency working group on Advanced Manufacturing IAM to the National Science and Technology Council NSTC Committee on Technology CoT, Executive Office of the President National Science and Technology Council, Washington, D.C. (2012).
[5]Westkämper, E., and H-J. Warnecke. "Zero-defect manufacturing by means of a learning supervision of process chains." CIRP Annals-Manufacturing Technology 43.1 (1994): 405-408.

compounded average rate of 3.49% and 5.85% in the next years till 2020 respectively[6]. Blades account for a very large percentage of the total cost of each turbine (approximately 40%), air cooling HPT case manifold for another 5%[7]: it is then a critical success factor to lower the percentages of scrap parts (which account for almost 25-30%[8]).

The gas turbines manufacturing for these sectors is also keys to Europe's economic health leading to the direct employment of over 70,000 (power generation) and 32,000 (aviation) people in Europe with a lot more in the supply chain[9].

In detail, the present work addresses specifically the competitiveness of two actors in the turbo-machinery industry: the machine tool manufacturer and the turbines manufacturer, using such a machining system.

Turbomachine components manufacturer

Global turbine blades production is estimated to account for 50 million units per year with a cost for each single piece attested at 1400 euros in average.
To estimate the impact of the introduced approach, we hereby consider the average manufacturer. The average turbine blade manufacturer has a capability of 10.000 blades per year, over 10 production lines. The 25% of this production will be discarded as scrap with a loss of approximately 4.6 million euros. As a consequence, the actual production of the average manufacturer, in order to take into account those scraps, will be approximately of 13.300 units. Moreover, the process of quality control is performed on expensive dedicated machines internally or in outsourcing with an average processing time of 45 minutes per piece. In addition, with current positioning techniques, an average of 15 minutes for each unit has to be taken into account, leading to 60 minutes spent for these processes for each unit, and a total of 13.300 hours yearly for the whole production (1330 hours on each production line).
The introduction of the approach introduced in the present work will be able to reduce the scraps by 50%, leading to a total production of approximately 11.400 units considering the same manufacturer with savings of approximately 2.6 million (approximately 57% with the respect to the first case). The in-line measurement and correction system will account for an average of 60 minutes per unit including both the quality inspection and the positioning procedures; leading to a total of approximately 11.400 hours spent yearly for these processes (1140 hours on each production line), achieving a productivity increase of approximately 15%.
The implementation of the considered approach is estimated in an investment (machinery, sensors, installation and software) of approximately 1.2 million euros, where traditional processes (e.g. Coordinate Measuring Machine, precision mechanical jigs and fixtures etc.) lead to a cost of 300.000 euros. This leads to a differential of 900.000 euros for each production line. Along 10 years of production on 10 lines, the total savings will account for approximately 17 million euros with the break-even point attested at approximately 3.5 years from introduction. Moreover, the technological advancements enabled by the approach introduced allow designers to push forward their solutions, paving the way to further efficiency enhancements. In addition, all the supply chain will take advantage from this approach implementation, such as the machine tool manufacturers and the measurement technology producers.

[6]Prnewswire market research
[7]Defining technologies for the next millennium: GE aircraft engines 2000
[8]Manufacturing Engineering Magazine: Cool is Key to Jet Efficiency
[9]EUTurbines Annual reception 2012

Machine-Tools manufacturer

The turbomachinery industry encompasses mostly two different machining technologies to realize the addressed micro-scale features: EDM and laser based micro-drilling.

In the EDM machines field the key players active both at European and worldwide level are GF-Machining Solutions, Beaumont Machine, Makino, Sarix SA, Knuth Machine Tools USA, AA EDM Corp., CHMER EDM, Ona EDM, AccuteX EDM, Chevalier Machinery and Winbro Group among others. The EDM European (including Switzerland) annual sales value accounts for approximately 500 million euros[10,11]; more than 15% is dedicated to turbomachinery sector.

In the laser processing machines the key players active both at European and worldwide level are Trumpf, Han's Laser, Prima Industrie, Coherent, IPG, Rofin, Cymer and Jenoptik among others. The laser processing machines European annual sales value accounts for approximately 1.2 billion euros[8]; more than 10% is dedicated to turbomachinery sector.

The adoption of the described framework will benefit these industries enabling a more robust, accurate (up to 30%, especially in the case of freeform work pieces) and faster (up to 80% with respect to contact-based methods) work piece positioning embedding on-board also a high precision adaptive inspection instrument for quality control. Moreover, with the adoption of techniques proposed, the mechanical fixtures for the work piece handling can be manufactured with far lower precision requirements, leading to a consistent cost reduction for the whole machine tool (approximately 5%). All of the above empower the competitiveness of the considered sectors which represent, as stated above, crown jewels in the European panorama.

1.2.2. Motivation and main concept pillars

High precision manufacturing processes, such as of turbine blades, suffer for the high number of scraps generated during the whole fabrication process. In particular, an extremely important impact on the final blade performances and reliability originates from micro-features realization, such as the external cooling channels, which put in communication the inner cooling channels (realized within the casting/forging process) with the outer blade surface. Cooling channels are micro-features characterized by small size diameters (i.e. 0.1-0.5 mm) and length up to 30 times the diameter dimension, where positioning tolerances on the blade lays into the micron order of magnitude. To comply with these strict tolerances, and to retain traceability of the measurements, is a complex task, today not fully addressed nor solved, because the surface is freeform and, coming from a casting/forging operation, it is characterized by relatively large geometrical uncertainties, both on surface and internal features. The complexity of such a manufacturing process results in high costs and a high number of scraps. In fact, in modern turbine engines, operating temperatures exceed the melting point of the blades material: these cooling channels have the purpose of delivering fresh air to the blade in order to form a thin, cool, insulating film over the outer blade surface and consequently allowing the blade to operate at those temperatures. Higher operating temperatures translate in a higher overall efficiency of the turbine. As a consequence, increasingly complex manufacturing processes are required to fulfil the needs of modern blades cooling capabilities, which is becoming more and more demanding towards the efficiencies growth.

Similar difficulties can be found in other turbine components, such as air cooling High Pressure Turbine (HPT) case manifolds and combustor liners, where micro-features diameters lay into 0.05/0.3 mm range, lengths up to 10 times the diameter and positioning tolerances in the micron order of magnitude, and, more in general, common to the manufacturing of a wide range of components characterized by functional micro-scale features (e.g. automotive fuel injectors).

[10]Eurostat: statistics on the production of manufactured goods Value ANNUAL 2015

[11]GF Machining Solutions Annual Report 2015

In order to achieve such a goal, the described approach proposes to integrate in the existing manufacturing plant a novel in-line measurement and correction framework, paired with dedicated adaptive fluid dynamic models, that will allow to recalibrate the entire machining process by tailoring it to the specific geometry of each single work piece and, at the same time, allowing to perform inline quality controls.

The research and development work, to achieve the proposed goals, is organized in the following six high level pillars (referred to the overall conceptual schema of Figure 1):

Pillar 1: Reference artefact –This pillar envisions a calibrated artefact to be integrated in the work-piece fixture so that it can be measured together with the work piece and consequently be present in all measurements. In fact, in order to characterize, rely and be able to use a measurement it is necessary to couple and compare it with a standard. This guarantees complete traceability and homogeneity of all involved and following measurements and it also poses as a powerful tool to investigate in the case that a problem related to a specific work-piece occurs later on, as well as to swiftly provide information in case of future repairs. This will allow also a far easier machining setup, especially for other machining processes as well as for the case of repairs, which is a very common practice in turbomachinery products and, in general, in many high value components. The reference artefact will be freeform and it will be developed using the concept of modular freeform gauge[12], this to simulate at best the work piece (i.e. turbine blades) specificities through the use of regular objects such as cubes, spheres, and cones. Materials and surface finish of freeform reference standards will be chosen to fully reflect the work piece produced by end-users involved in the project. A large variety of measurands, such as lengths, diameters, roundness, etc., will be selected on the reference standards and then calibrated using coordinate measuring machines.

In a nutshell:

- Allows the characterization of all measurement systems involved, where today there is a complete lack of standards
- Allows to characterize all measurements performed thanks to the integration in the work piece fixture
- Allows complete traceability of the measurements

Pillar 2: CT scan - The high geometrical uncertainty of casted/forged turbine blades affects both outer and inner surfaces. The only available technology that allows to inspect both is the computed tomography (CT), which today is already in use in turbomachinery industry, but off-line and with the only purpose to detect internal defects such as cracks. This pillar envisions the use of this technology in-line and with the further purpose of localizing internal features with respect to the outer surface. For gas turbine blades, this allows to obtain the complete, accurate 3D model comprehensive of the geometry of the inner cooling channels (an example in Figure 2), which is necessary to characterize the thermo-fluid dynamic performances of each single component (Pillar3). This enables the Adaptive In-line machining engine (Pillar4) to optimize the machining model.

[12] E. Savio, L. De Chiffre, "An artefact for traceable freeform measurements on coordinate measuring machines", Precision Engineering, 26 (2002), 58-68

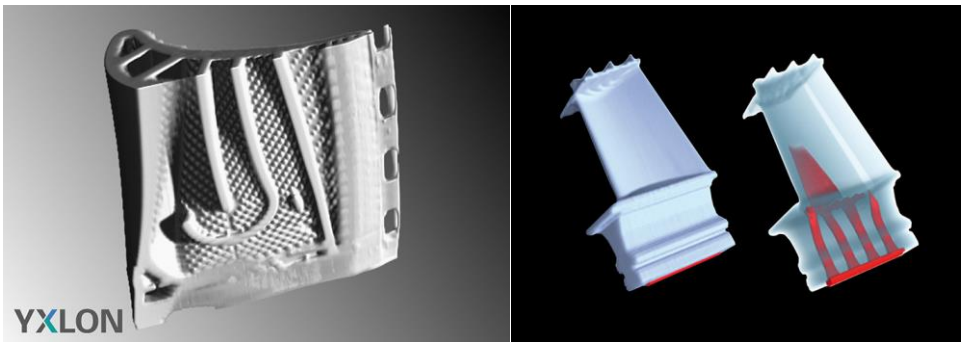

Figure 2: tomography of a turbine blade

Scanning parameters affecting the time such as number of projection images, integration time of projection image acquisition, voxel size, detector pixel binning, operation mode of rotation table, and gain level of the detector will be investigated in order to define an optimum set of parameters ensuring dimensional measurements with accuracy in the micrometre range.

In a nutshell:

- Allows to produce the accurate 3D model of the inner and outer parts of the work-piece
- Fast scan regime allows the computed tomography technology to be used in-line

Pillar 3: Adaptive fluid dynamic model - Film and effusion cooling effects are based on the fresh air flow delivered by the inner cooling channels through the outer ones to the external surface. The flow amount and distribution is greatly influenced by the relative positioning of these micro-features. In real case scenarios this relative positioning is affected by large variability due to the fabrication processes. Today's standard procedure is to trust the actual geometry to be corresponding to the nominal one and thus to machine these micro-features without any further analysis. This pillar envisions the development of an adaptive fluid dynamic model that, considering variations of the nominal geometry, provides the relationship between the geometry of the work piece to its thermo-fluid dynamic performances. The model, in the form of equations or mapping, will relate the micro-scale sensitive geometrical parameters (i.e. the ones of which measurements is enabled by the CT scan, Pillar2) data with their relative impact on the product functionalities, reliability and performances. As a consequence, this model, coupled with Pillar2, enables the In-line adaptive machining engine (Pillar 4) to optimize the machining model accordingly to the real measured geometries and the objective performances. The main advantage of such a model with respect to today standards (e.g. CFD) is its much faster approach to the problem, making the use possible in-line. This is achieved by means of developing an innovative modelling approach dedicated to the representation of the thermo-fluid dynamic effects of the micro-features to be realized on the product performances. In fact, this model does not substitute standard CFD analysis, which are intended for the product design phases, but addresses the need of interpreting the thermo-fluid dynamic impact of geometrical variations of the work piece, to be used only as an in-line correction tool for production.

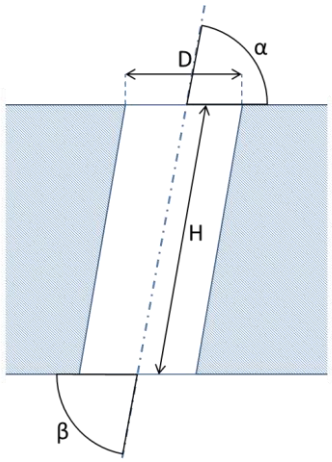

Figure 3: Simplified bi-dimensional example of a micro-feature

The model development will encompass parametric CFD tests together with the investigation of correlations among all the relevant geometrical parameters of each single feature to be machined and their impact on the final thermo-fluid dynamic performances of the component. The in-line adaptive machining engine (Pillar 4) will couple data from this model together with all the geometrical measured data provided by the CT scan (Pillar 2), to optimize the machining model obtaining the desired thermo-fluid dynamic behaviour of each single feature to be realized on each single component.

In a nutshell:

- Adaptive modelling approach to geometrical work piece variations
- Adaptive modelling approach usable in line, characterized by high solving speed

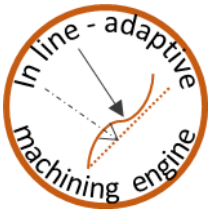

Pillar 4: In line adaptive machining engine - This pillar envisions an engine that has the capability of optimizing the nominal machining model taking into account the work piece geometrical variability. This will be achieved by means of aggregating and elaborating data from the Adaptive fluid dynamic model (Pillar 3), the nominal machining model and the actual work piece real geometry from the CT scan (Pillar 2). Standard machining paths generation does not satisfyingly address the problem of geometrical variability of work pieces, but experience shows that this variability is, in fact, very large and significantly impacting, as detailed in the state of the art section.

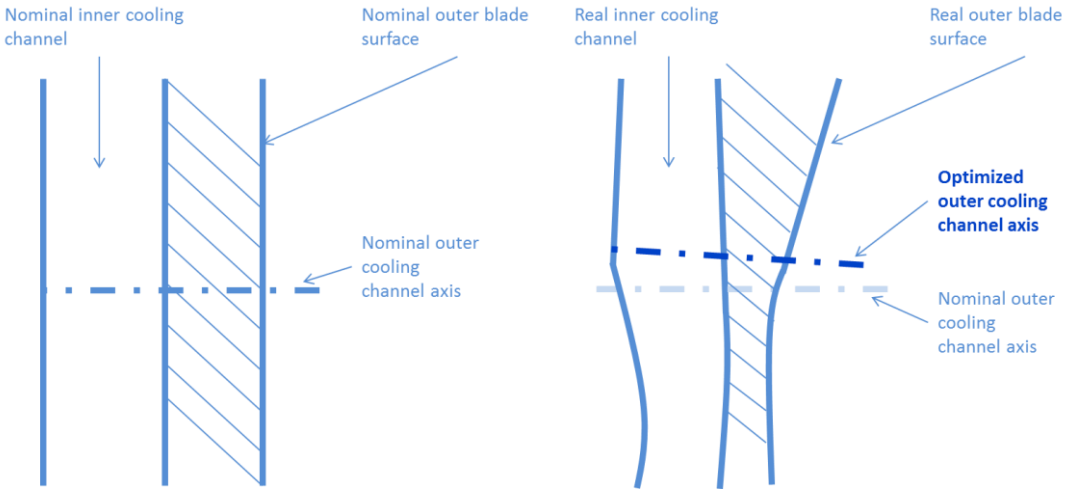

Figure 4: simplified bi-dimensional example of optimization of a cooling hole machining path

The in-line adaptive machining engine simplified procedure is the following:

1. A dedicated algorithm will relate the nominal 3D model (CAD) with the measured 3D data (Pillar2) through iterative surface fitting procedures

2. A dedicated algorithm will extrapolate the measures from the 3D measured data (Pillar2) of all selected geometrical parameters (i.e. identified in Pillar3) relative to each single feature to be machined
3. A dedicated algorithm will solve the model data (Pillar3), modifying the nominal geometrical parameters of the micro-features to be machined, aiming at the optimization of the final fluid-dynamic performances
4. Recalculation of the new machining model for each single work piece based on the new geometrical parameters calculated at the previous step

The optimized machining model is fed to the in-line adaptive positioning engine (Pillar6) on-board the machine-tool.

This approach will pave the way for more complex design solutions, by means of pushing further the production limits in terms of accuracy and expectable performance outcome.

In a nutshell:

- Adaptive tool that tailors manufacturing process to work piece geometrical variability
- Enhanced final product thermo-fluid dynamic efficiency

Pillar 5: Laser scan – On board measurements on freeform shaped parts such as turbine blades are limited today on traditional contact based methods: experience shows that this is not the best approach since those work pieces are freeform and both are characterized by a large geometrical variability, which often translates in poor stability and robustness of the measurement (because contact methods, by definition, must rely on a very small number of data points). This pillar envisions an automatic, contactless and non-destructive laser based system, fully integrated in the machine tool, which will provide an accurate and robust work piece measurement. Since based on the acquisition of millions of data points, this system will be much less sensitive to geometrical variability delivering reliable data to the In-line adaptive positioning engine. In addition, the laser beam can reach narrow areas of the work-piece that are off-limits for touch probes.

The sensor will be completely integrated in the machine-tool workspace by means of a dedicated actuated robotic arm, allowing to move it out of the machine tool workspace when machining operations are being performed. The measuring process are carried out by means of moving the work piece with one of the machine tool own axes while mounted in the machining fixture.

The whole measurement process will take only a few seconds with no risk of collisions with the work-piece, which means that the process is much faster and safer than any traditional contact-based measurement procedure, both during execution as well as in setup. The acquisitions will be triggered by the linear encoder built-in with the machine-tool own axes, meaning that the final resolution in that direction can be tuned to the specific needs by setting the desired acquisition period on the encoder signal.

The system is also an on board inspection tool, enabling to analyse the results of the machining just carried out as well as the work piece itself before the machining process even starts. In Figure 5 is reported an example of an after machining turbine blade inspection.

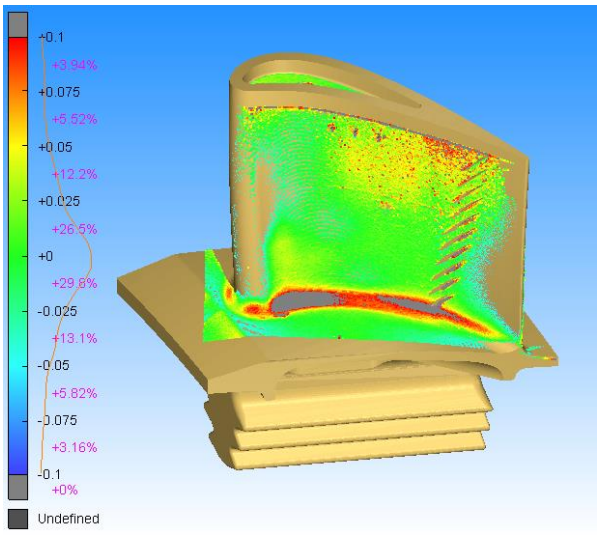

Figure 5: blade shape analysis

This method allows a swift detection of any problem that may occur on the machine-tool, allowing its fast correction and consequently avoid to machine additional defective work-pieces.

In a nutshell:

- Inspection solution completely integrated in the machine-tool
- Drastic robustness enhancement through the acquisition of millions of data points
- Fast and safe process, in opposition to traditional contact-based methods
- Solution enabling on-board quality controls

Pillar 6: In line adaptive positioning engine - This engine consists of an on-board positioning system that enables high precision machining by means of automatically compensating for errors due to imperfect positioning in the machine fixture and to geometrical imperfections of the work piece itself. These problems are particularly difficult to be approached with traditional methods when the work piece is free form, which means that it has no unambiguous reference points, and it becomes even more demanding when the work piece also relatively largely differs from its nominal shape due to previous processes variability, as well represented in turbine blades case study. Furthermore, standard processes are also much slower since relying on contact-based iterative methods, meaning that measurements of all points have to be repeated several times in order, for the procedure, to converge to a satisfactory solution.

In Figure 6 is presented an example showing the large differences between a real casted turbine blade and its nominal CAD model: some areas lay into more than 0.3mm of shape error (the figure represents a cloud point, acquired by means of an optical acquisition sensor, best fitted on its CAD model).

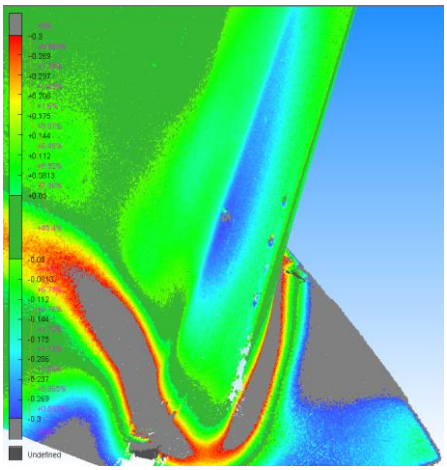

Figure 6: shape differences due to casting

The in-line positioning engine simplified procedure is the following:

1. A dedicated procedure relates the 3D machining model (Pillar4) with the 3D data acquired by the Laser scan (Pillar5) through iterative surface fitting algorithms
2. A dedicated algorithm calculates the actual work-piece position in the machine tool work space
3. A dedicated procedure will re-calculate the nominal machining paths for each single micro-feature to be realized in each single work-piece, compensating for all the positioning and shape errors. The work piece will be ready to be machined with no further steps

The engine is able to compensate any positioning error, allowing to correctly machine work pieces and furthermore to adapt the machining when the shape and dimensional errors are relatively large, which eliminates the need for precise and expensive mechanical fixtures. In addition, the whole process takes only a few seconds, making it much faster than any traditional positioning procedure.

In a nutshell:

- Solution enables accurate positioning regardless of the work piece geometrical variations or fixture imperfections
- Fast process, incomparable to today's standard procedures
- Solution eliminates needs for precise and expensive mechanical fixtures

1.2.3. Factory integration

The introduced concept encompasses different levels of factory integration (see Figure 7), including monitoring and adaptive correction throughout the manufacturing process, and a higher level data gathering promoting strategic PLM logics towards new design solution opportunities, facilitating the work piece repair and factory-level maintenance processes. The first level regards the in-line measurement and correction system proposed, which will inspect every single work piece going through the production line, allowing to constantly monitor the output of previous fabrication stages and stream back valuable feedbacks and predictions allowing to survey and optimize the performances of those processes. If any problem occurs, the system will be able to detect out-of-bound product variations, swiftly recognizing the process responsible and fixing it, avoiding the production of defective work pieces.

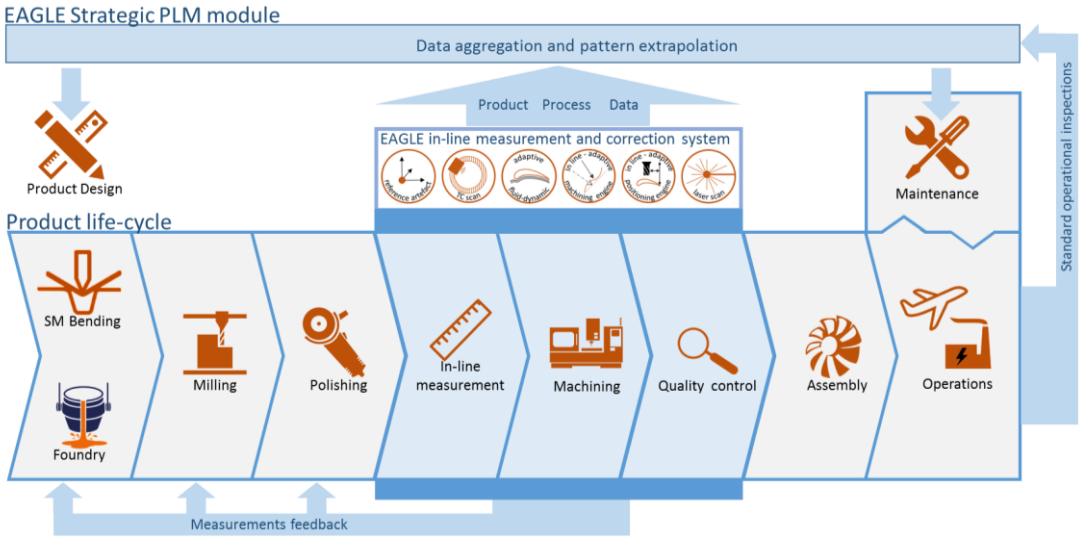

Figure 7: system integration

The second and higher level of factory integration regards the creation of a strategic PLM module, which will manage big data streams generated by in-line inspection and correction system, coupled with data by standard operational inspections, towards their aggregation in a common database. Machine learning techniques will perform analyses towards the extrapolation of patterns regarding recurring defects, production faults and strongpoints, fatigue behaviours, wear factors and, in general, the tendency of any characteristic of interest. This analysis will drive the design processes towards new opportunities and facilitating the work piece repair and factory-level maintenance processes.

2. State of the art

The actual formalization and implementation of a new paradigm of system level measurement and correction system is a complex and challenging activity, requiring to take into account a wide set of internal and external factors enabling the effective definition of a successful strategy. In order to assess the progress beyond the state of the art needed to successfully achieve the goals fostered by the presented vision, an analysis with respect to the topics fostered by the project has been carried out. For each topic, the completely new challenges at RTD level, or the need of adaptation of existent procedures/technologies have been pointed out.

2.1. Progress beyond state of the art

Nowadays, the main application of in-line measurement systems resides in final product quality controls: they are used to check in real time if finished or semi-finished products satisfy pre-defined acceptance criteria with the aim of targeting non-conform pieces and discard them. For this purpose, each industry set its own measurement system, using different technologies with a high standardization level. However, the use of in-line measurement systems for the purpose of adaptively correct the manufacturing process itself it is a quite unexplored field, with no wide adoption in industry. Based on the research and market analysis, the following table summarizes the current limitation in the state of market in the fields of In-line measurements, that are pertinent to the work topics (i.e. applications in the turbomachinery industry).

Topics		**Current State of Market**
Work piece positioning in machine tool workspace		• Most systems rely on precise and expensive mechanics (i.e. grips and fixtures) • A few cases implement a positioning method based on single-points contact methods (i.e. mechanical probe) • Technologies for partial/complete surface reconstruction (i.e. million points data acquired) are used only for after work inspection on dedicated machines at the end of production process. None or limited usage for adaptive positioning correction • The work piece geometry is considered to be perfect such as a CAD model
In-line machining model optimization	**In-line computed tomography**	• CT scan is a very slow process: adopted for off-line measurements • Driving algorithms for CT scan exists for internal defect detection (e.g. cracks), reverse engineering or sample analysis on final quality controls. No localization algorithms are on the market.
	In-line thermo-fluid dynamic analysis	• Fluid dynamic software tool (Computational Fluid Dynamics) are available on the market as design support instruments • No fluid dynamic analysis applications for in-line processes
	Machining paths calculation	• Machining path calculation is based on fixed CAD geometries • Machining path calculation is a very slow process: capable of off-line calculations
Reference standards for measurements traceability		• No standards are defined in the metrology field of optical based devices and x-rays computed tomography at this micro-scale level

2.1.1. *Beyond the state-of-the-art: none or limited knowledge of the work piece real features obtained from previous production stages (e.g. casting, forging) limits the machining capabilities.*

Industrial manufacturing largely uses elementary shapes for production of goods with products that are combination of cylinders, spheres, planes and other simple shapes; this due to the fact that simple geometries are easier to manufacture and less expensive. However, in some application fields, especially when involving interaction with fluids or waves (e.g. fluid dynamics and acoustics), more complex shapes are needed. These shapes lay into the freeform surfaces definition, which may be classified as complex geometrical features. According to ISO 17450-1[13], complex geometrical features have no invariance degree, which is the displacement of the ideal feature for which the feature is kept identical, corresponding to the degree of freedom in kinematics. These freeform shaped parts are of great interest in many industrial applications such as automotive and aerospace; in particular, they become instrumentally important in the design of a turbomachine, for example for both static and rotating components such as turbine vanes and blades. Those components can be realized with many different manufacturing processes[14,15], where high precision casting is the most diffused one with typical tolerances referred to the two dimensional cross-sections in the order of magnitude of $10^{-2} - 10^{-3}$ mm. Positioning of work pieces in the machine tool work space plays a fundamental role in the machining operations effectiveness, and this operation becomes much more challenging in the case of freeform shaped parts. The industry standard, as well as research focus on this topic, mostly regards precise, complex machine fixtures, including smart-modular solutions and self-centering mechanical constructions[16,17,18]. On the market, there exist many producers, specialized in different fields, of these mechanical features such as GF-SYSTEM 3R and EROWA, specialized in wire/sink EDM machine tooling, Christian Dunkel GmbH, specialized in grinding and laser treatment, LANG Werkzeugbau, specialized in five- axis micro-milling. All of them, however, even if they provide accurate and repeatable positioning, do not take into account for the work piece shape variability due to previous production stages. As a consequence, this approach is often not sufficient for the field of micro-scale feature realization in freeform shaped components such as turbine blades/vanes; furthermore, they represent a significant cost for the machine tool. Moreover, a common strategy in high-cost products, such as the turbine blades/vanes, is the product after-work re-manufacturing; in this case the geometrical shape deviations are often completely out of bounds, leading to an even more difficult effective positioning with mechanical fixtures in the parts re-machining.

A few machine tool producers have developed on-board contact based systems: the basic concept of these systems lays into high precision sensing mechanical probe integration in the machine tool to acquire data from the work piece[19]. On the market examples of these systems can be found in WINBRO GROUP, SARIX SA, PRIMA INDUSTRIE and GF-AGIE CHARMILLES. The inspection procedure is typically the following:

1. The work piece is positioned in the machine tool grips,
2. The mechanical probe acquires the coordinates of predefined points on the work piece,
3. A localization algorithm calculates the space position of the work piece based on these points,

---

[13] ISO/TS 17450-1:2005, Geometrical product specifications (GPS) - General concepts - Part 1: Model for geometrical specification and verification.

[14] M. Konter, M. Thumann, "Materials and manufacturing of advanced industrial gas turbine components", Journal of Materials Processing Technology, Volume 117, Issue 3, 23 November 2001, Pages 386–390

[15] S.A.M. Rezavand, A.H. Behravesh, "An experimental investigation on dimensional stability of injected wax patterns of gas turbine blades", Journal of Materials Processing Technology, vol. 182, issues 1–3, 2 February 2007, pp. 580–587

[16] US 6844515 B2, "Method and apparatus for turbine blade machining"

[17] US 7334331 B2, "Methods and apparatus for machining components"

[18] Y. Wang, X. Chen, Q. Liu, N. Gindy "Optimisation of machining fixture layout under multi-constraints", International Journal of Machine Tools and Manufacture", Volume 46, Issues 12–13, October 2006, Pages 1291–1300

[19] Patent US6611731: machining aerofoil components

4. A dedicated correction algorithm provides new machining coordinates based on real space position of the work piece

The mechanical contact probe is nowadays the standard method to estimate the position of a single point in the space, however, especially in some application fields such as the turbine blades manufacturing, the use of this technology leads to lack of robustness and relatively high cycle times. On one hand, the lack of robustness comes from the small number of data points acquired and, as a consequence, the process becomes very sensitive to local shape defects, leading to inaccurate positioning. On the other hand, high cycle times result from the touch probing procedure since, to reach the adequate accuracy, the probe approaching speed must be very low. In general, there is a lack in methods and adopted instruments for on-board positioning of work pieces in machine tool workspace, leading to imprecise machining, high cycle times and a limited knowledge of the real features of work pieces being machined. This leads to the need of a quality control process to after work inspect finished/semi-finished products. In the turbomachinery field, industries such a process is performed by dedicated measurement machines (e.g. CMM and optical inspection machines) and dedicated expertise leading also to high costs of the whole production process.
In order to overcome this problem, the adoption of instruments enabling the acquisition of million high-accuracy data points of the work piece must be investigated. Having the possibility to rely on big data sets representing the whole work piece, enables to compensate for dimensional errors coming from previous manufacturing processes.
In order to acquire big data sets in-line (i.e. thus in relatively short time) several techniques and functioning principles can be considered. An overview is provided by Schwenke et. al.[20]; of particular interest for the scope are the following techniques:

- **Triangulation distance sensors:** the main components are a collimated light source (e.g. a laser diode) and a detector unit consisting of an imaging lens and a position-sensitive detector (e.g. CCD line). The optical axes of the light source and the imaging lens form a fixed angle (i.e. the triangulation angle). The object surface is brought close to the point in which both axes intersect and the diffuse reflection of the light spot on the work piece surface is imaged onto the detector. The position of the image on the detector is function of the distance between the detector and the work piece (see the functioning principle schema in Figure 8). Typical measurement ranges are 2mm to 200mm, providing resolutions down to 10^{-4}. Main uncertainty contributor is the optical characteristic of the work piece surface: very smooth surfaces cannot be accurately measured because of the insufficient diffusely reflected light.

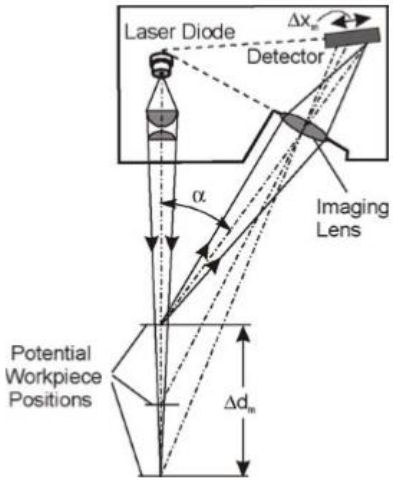

Figure 8: principle of the triangulation sensor

[20] H.Schwenke, U. Neuschafer-Rube, T.Pfeifer, H.Kunzmann "Optical methods for dimensional metrology in production engineering", Keynote paper, Annals of the CIRP, 51/2:685-699

- **Autofocus sensors:** the principle of the autofocus sensor is similar to that of the triangulation sensor, but instead of collimated light being projected the light is focused onto the surface of the specimen. The reflected light is directed to a focus detector by a special beam splitter (see Figure 9). Depending on the position of the surface relative to the focal point, the outer or inner segments of the focus detector are illuminated. Signal processing produces an error signal independent of the reflected intensity. The measurement ranges of typical autofocus sensors are small (up to 250 µm) compared to the triangulation sensor. On the other hand, autofocus sensors can provide a significantly higher accuracy. On cooperative surfaces, relative repeatability in the order of the measurement range can be achieved.

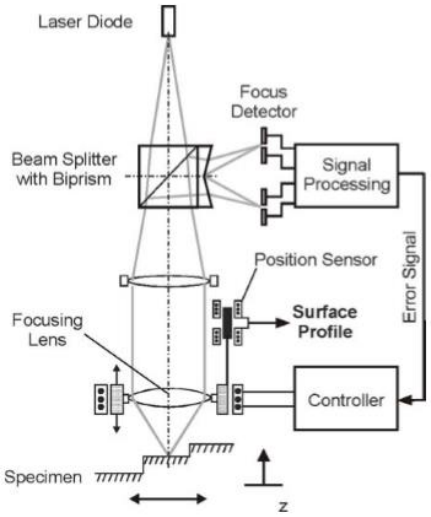

Figure 9: principle of the autofocus sensor

- **Conoscopic holography:** the sensor contains a laser diode that illuminates the specimen by a quasi-monochromatic light beam. The light emitted at the spot on the surface passes through a lens and a circular polariser (see Figure 10) then the circularly polarised light passes through a uniaxial crystal (e.g. calcite). The crystal axis is oriented parallel to the optical axis of the lens. As a result, the incident light hitting the crystal at an angle is split into an ordinary and an extraordinary ray. The ordinary refractive index is constant, while the extraordinary refractive index and so the phase delay between the rays is a function of the direction of propagation relative to the crystal axis. In a first-order approximation, the different refraction angles of the rays can be neglected because the difference between the refractive indices is small. The two rays interfere after having traversed the circular analyser (a second circular polariser) and form interference rings. This pattern is detected by a CCD array. The distance between the rings depends on the distance between sensor and specimen[21]. Typical measurement ranges of conoscopic sensors are between 0.6 mm and 70 mm. The relative accuracy is in the order of 10^{-3} and the repeatability in the order of 10^{-4} of the measurement range.

[21] Sirat, G.Y., 1992, Conoscopic holography. I. Basic principles and physical basics, Journal of the Optical Society of America A, 9, 70-83.

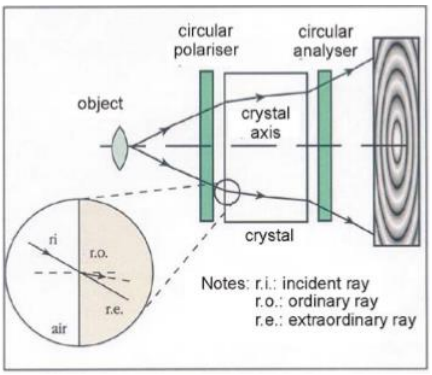

Figure 10: principle of conoscopic holography

- **Photogrammetry and fringe projection systems:** are based on the principle of triangulation. They enable the reconstruction of surfaces by mathematically combining images from different viewpoints. In photogrammetry for large- scale metrology, the measured surface is usually provided with physical markers (e.g. retro-reflective dots) to generate so-called homologous points. These points are recorded by a mobile camera from different perspectives. To measure surfaces without physical markers, two approaches are distinguished[22,23]: the first one is based onto the projection of a pattern on the surface and at least two different camera views. In this case, the pattern only serves to generate homologous points for triangulation within the two or more camera images. The second approach evaluates the deformation of the pattern itself. In this case, the projector of the pattern takes up the role of one camera (see Figure 11). Measuring systems based on fringe projection provide fast acquisition of dense point clouds. A typical measurement volume of structured light systems is in the range of side between 0.1 m and 1 m. These systems provide a relative accuracy of up to 10^{-4} which depends on the phase measuring errors, the pixel and image co-ordinate measuring errors and the lateral structural resolution.

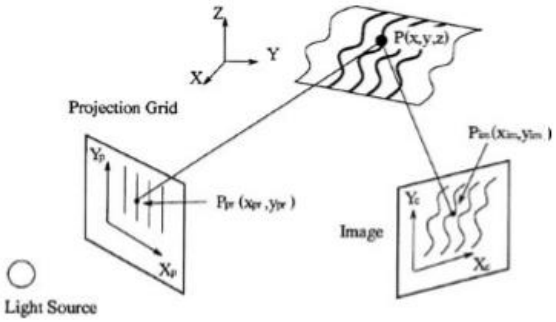

Figure 11: principle of fringe projection

On the market, there exist many commercial sensors that enable this kind of data acquisition as the ones listed above. Manufacturers such as Keyence, Nikon, GOM, MicroEpsilon and COGNEX, among others, provide a wide space of solutions for various applications. In 3.2 a wide set of different sensing technologies that have been considered and tested during the work, is provided.

On the market, most of these tools, as already stated, are nowadays used in most cases for quality after-work inspection integrated in measurements machines such as the case of FARO, KREON and ROMER that produce anthropomorphic arms equipped with laser scanners and touch probes with the purpose of having flexible and portable systems to be used in and off line for quality measurements.

[22] Chen, F. et al., 2000, Overview of three-dimensional shape measurement using optical methods, Optical Engineering, 39/1, 10-22. 68.

[23] Reich, C., et al., 2000, 3-D shape measurements of complex objects by combining photogrammetry and fringe projection, Optical Engineering, Vol. 39, No. 1,224-231

For the same purpose other producers such as WENZEL (i.e. the model ScanTec CORE), BRUKER (i.e. the model Contour CMM), MITUTOYO (i.e. the model AV Active series) have integrated high precision optical acquisition sensors into classical coordinate measuring machines (CMM).

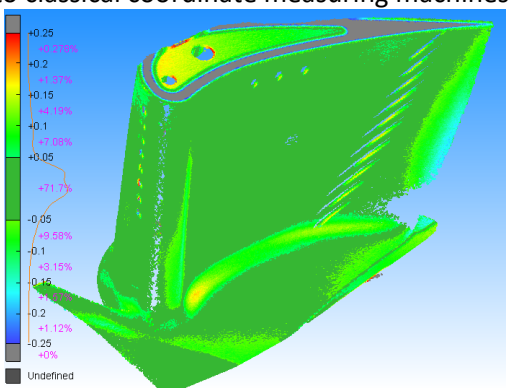

Figure 12: Surface quality analysis done on a turbine blade profile with an high precision 2D laser profilometer (Micro-Epsilon 2960-25).

In Figure 12 is reported an example of a surface quality analysis performed on CMM machine equipped with an high precision 2D laser profilometer; the figure shows, for the entire blade, the distance of each measured point from the nominal CAD model after data (i.e. point cloud) have been best-aligned.
Another typical application is the integration of these tools into additive manufacturing machines such as the case of the 3D printer of Makerbot Replicator, that, by means of integrating a 3D laser scanner into the machine, has enabled the reverse engineering and direct replication, via additive manufacturing, of spare parts.
No commercial application of these technologies has been noticed in terms of integrating them directly in machine tools to enable, other than the on-board inspection, the work piece positioning automatic correction in micro-scale accuracy field.
In order to handle the million points data coming from these systems specific software tools and complex algorithms need to be used. In this field there already exist on the market various software packages and algorithms for surface reconstruction/modelling, measurements and automatic compare instruments for inspecting work pieces with the respect to their nominal CAD model. Such software packages include HEXAGON METROLGY 3D Reshaper, 3DSYSTEMS Geomagic, MVTec Halcon, COGNEX VisionPro and MATLAB. None of them have been noticed in terms of data aggregation and elaboration to provide automatic positioning correction.
Therefore, the direct integration of optical acquisition sensors in industrial machine tools with the purpose of work piece positioning, such as for example micro-EDM, micro-laser drilling and micro-milling machines, from both hardware and software side, is a quite unexplored field. The benefits of this challenge are expected to be found not only in the fact of enabling the development of a process that includes both work piece positioning and after-work inspection, but, above all, in the enhancement of the machining process performances in terms of accuracy, robustness and reduced cycle time.

Proposed improvement in a nutshell– On board positioning and inspection laser based system
The development of an adaptive in-line positioning system capable of rapidly and accurately, at micro-scale level, position the work piece in the machine tool workspace by means of elaborating million points data-set coming from an optical non-destructive acquisition sensor integrated in the machine tool. Furthermore, once the work piece has been machined, the accuracy of the machining operations done on the outer surface will be directly verified on board through traceable measurements, eliminating the needs of further quality controls with dedicated machines. Thanks to the development of a machine tool integrated positioning method, including both algorithms and hardware advancements, realization of complex micro-scale features in freeform work pieces will be enabled, benefiting machining process performances, quality control processes and machine tool cycle time.

2.1.2. *Beyond the state-of-the-art: machining path calculations are performed on nominal CAD model not considering geometrical variations caused by previous production stages (e.g. casting, forging, milling).*

An in-depth analysis has been conducted on the specific problems and limitations encountered in turbomachinery industry about the impact of micro-scale uncertainties in manufacturing on the final performances of gas turbines.

The thermal efficiency and specific power output of a gas turbine are primarily dependent on two major cycle parameters: the pressure ratio and the turbine inlet temperature. The increase of these two main parameters allows the overall performances to rise. Over the past years, there has been a continuous growth in the turbine entry temperature TET. Blade materials moved from normal casting alloy, passing by directionally solidified materials, ending up with single crystal materials, which represent the state-of-the-art for this component. Moreover, with the continuous increase in TET and overall pressure ratio to have higher thermal efficiency and, therefore, lower specific fuel consumption, the cooling demand for a specific turbine blade has continuously increased, leading to an even more sophisticated request for cooling technology (e.g. film cooling). Nowadays, TET exceeds the melting temperature of the blade metal, therefore, a continuous implementation in the technology level should be performed.

Film cooling is a fundamental component of the overall cooling of turbine airfoils. Film cooling protects the airfoil surface by way of a thin layer of air ejected from the inside the blade towards the outside surface. The cooling air is taken from the compressor outlet, and the temperature can be higher than ambient temperature, depending on the bleeding points, however, if compared to the TET, there is a sensible gap which can allow for the heat removal. Since the coolant gas is at a lower temperature than the mainstream gas, the heat transfer towards the airfoil is reduced. Film cooling also removes heat from blade surface through the film hole by internal convection[24]. At the leading edge of the vane, the heat transfer coefficients are very high, and as the flow splits and travels along the vane, the heat flux decreases. Along the suction side of the vane, the flow immediate transitions from laminar to turbulent, and the heat transfer coefficients increase. As the flow accelerates along the pressure surface, the heat transfer coefficients also increase[25].

Basically, film cooling removes heat by decreasing the gas temperature near the wall. Nevertheless, as the coolant flows, it mixes downstream with the mainstream gas: this will result in a progressive decay of the cooling performance due to the increased temperature of the coolant[26]. Bunker[27] studied the effects of manufacturing, considering the design of an HPT airfoil and the relative tolerances allowed in the finished product. Seven different manufacturing factors are taken into consideration and are showed in Figure 13, along with the relative tolerance considered.

Film hole diameter (effective)	±10%
Film hole L/D	±6%
Film hole angle to surface tangent	±5 deg
Film hole orientation to external flow	±5 deg
Film hole orientation to internal flow	±5 deg
Film hole P/D	±10%
Film hole shaped exit spec	±30%

[24] S. V. Ekkad and J.-C. Han, "A Review of Hole Geometry and Coolant Density Effect on Film Cooling," in Frontiers in Heat and Mass Transfer, 2013.

[25] J.-C. Han and L. M. Wright, "Enhanced Internal Cooling for Turbine Blades and Vanes, Ch. 4.2.2.2," in The Gas Turbine Handbook, U.S. DOE-National Energy Technology Laboratory (NETL), 2006, pp. 321-354.

[26] D. G. Bogard, "Airfoil Film Cooling, Ch. 4.2.2.1," in The Gas Turbine Handbook, U.S. DOE-National Energy Technology Laboratory (NETL), 2006, pp. 309-321.

[27] R. S. Bunker, "The Effect of Manufacturing Tolerances on Gas Turbine Cooling," Journal of Turbomachinery, vol. 131, pp. 1-11, October 2009.

Figure 13 - Manufacturing Factors[9]

For each one, the influence on parameters such as the external heat transfer and the adiabatic film effectiveness has been evaluated. However, for simplicity, results are only expressed through a qualitative analysis. According to Bunker, parameters with the huger impact on both the adiabatic film effectiveness and the external heat transfer coefficient are the film hole diameter, the film hole angle to surface angle, the film hole orientation to external flow, the film hole pitch-to-diameter P/D, and the film hole shaped exit spec (shaping). Film hole length-to-diameter L/D and film hole orientation to internal flow have a lower impact on the previous cooling design parameters. Moreover, each of the previous parameters is affected by the positioning tolerances of the holes, which have a direct influence especially if the holes are shaped. Lee et al.[28] focused that certain manufacturing factors may appear in a coupled manner for real geometry. For example, the film hole orientation to the flow could change the hole angle to surface tangent and the exit shape of the hole itself, as well as the hole length. As far as their study is concerned, only two separate manufacturing factors are taken into consideration: the injection angle (iAng) and the scaling factor (SF). Based on five design variables, a Kriging surrogate model and a Monte Carlo Simulation with descriptive sampling method was coupled with the design optimization process using Genetic Algorithm to find out, through an optimization process, the best hole configuration in order to reach high performance. Furthermore, it has been also confirmed that the tolerance of the holes near the leading edge is more influential to the cooling performance, rather than the holes on the trailing edge. A study conducted by Montomoli et al.[29] examines an innovative design to increase the film cooling performance over a blade, called DBFS (Figure 14).

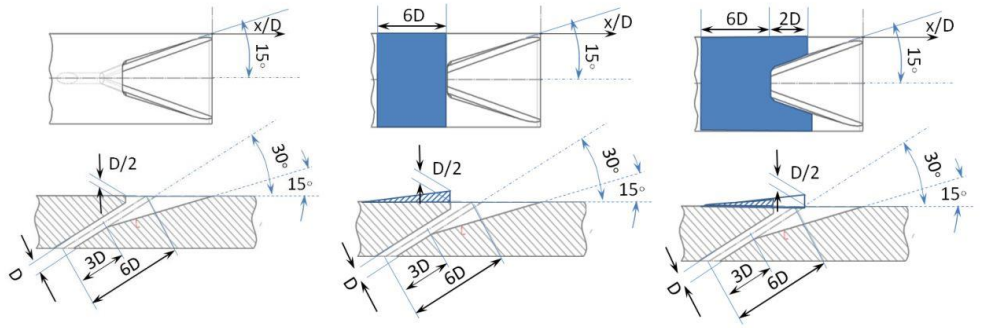

Figure 14 - Film cooling geometry[11]

Besides, the authors considered a stochastic distribution for the free stream Mach number and, especially, the coolant blowing ratio M. Results have proved a minimum gain of 30% in the coolant adiabatic effectiveness until 20 diameters downstream.

An additional proof of the importance of the size and shape of the cooling holes comes from a research made by D. Bohn and R. Krewinkel[30]. Concerning the effusion cooling holes, they considered a plate with seven rows of holes having a diameter of 0.2 mm each one and investigated about the cooling performance with and without oxidation. The Oxide layer Al_2O_3 grows from the CMSX-4 substrate into the cooling holes, forming a 20 µm layer and, therefore, reducing the available space for the coolant. Several analyses have been conducted with two separate blowing ratios, M: $M_1 = 0.28$ and $M_2 = 0.48$. What is relevant from their simulation results is that the oxidation layer significantly affects the flow field around the holes, however cooling effectiveness does not differ sensibly from the clean case

[28] S.Lee, D.-H. Rhee and K. Yee, "Optimal Arrangement Of The Film Cooling Holes Considering The Manufacturing Tolerance For High Pressure Turbine Nozzle," in ASME Turbo Expo 2016: Turbomachinery Technical Conference and Exposition, Seoul, South Corea, 2016.

[29] F. Montomoli, A. D'Ammaro and S. Uchida, "Numerical and Experimental Investigation of a New Film Cooling Geometry with High P/D Ration," International Journal of Heat and Mass Transfer, vol. 66, pp. 366-375, 2013.

[30] D. Bohn and R. Krewinkel, "Conjugate Simulation of the Effects of Oxide Formation in Effusion Cooling Holes on Cooling Effectiveness," in Proceedings of ASME Turbo Expo 2009: Power for Land, Sea and Air, Orlando, Florida, 2009.

(around 0.5% variation in the substrate layer). Flow field, on the other hand, is highly affected by the corrosion, and the results can be observed in Figure 15.

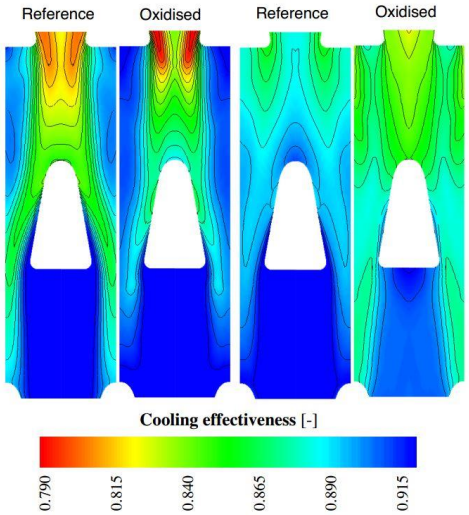

Figure 15 Cooling Effectiveness for M=0.28 (left) and M=0.48 (right)[12]

Changes are more relevant for the case of M=0.48, for which a higher discrepancy between the clean case and the oxidized one, especially upstream the hole, is evident. As a consequence of this analysis it is clear that micro-scale level uncertainty in manufacturing micro features (e.g. shaped holes) in turbine blades has a direct and tremendous impact on the final performance of the gas turbine.

As already underlined, the progressive increase in Turbine Inlet Temperature (TIT) and Overall Pressure Ratio (OPR) has led to a continuous growth in thermal efficiency, especially for aero engines. Turbine blade cooling represents one of the most important elements in gas turbine research and development, along with the combustion chamber; of particular interest, regarding the combustion chamber, are the flame containment walls (liner): a high-efficiency liner cooling system can lead to a sensible limitation of pollutant emissions. In order to meet the high-efficiency requirement, both an enhanced cooling and a reduced heat flux from the hot gasses toward the component wall have to be performed. The effusion cooling is one of the most promising techniques for improving cooling performance. It can be considered a compromise between the film cooling (widely used in nozzle and turbine blade) and the transpiration cooling[31]. The effusion cooling consists of a high number of cooling holes, usually made by high precision drilling techniques, with a diameter in the order of microns. The smaller the angle, the better: usually the angle is around 30°, however, angles up to 10° – 11° can be reached, in order to perform a better wall protection of the film[32]. Enhancing the number of holes increases the surface heat transfer, hence, higher overall effectiveness levels can be reached. Moreover, the presence of holes with elevated length to diameter ratio allows to remove a high amount of heat inside the holes by convection: this phenomenon is usually called heat sink effect[13].

The physics of the flow developed in the effusion cooling zone is determined by the interaction of the cold jets, coming out from the holes, with the mainstream hot flow. This interaction creates, immediately downstream of the jets, a flow field characterized by an array of large-scale swirling structures. Realizing small diameter holes, from 5 µm to 10 µm, allows to limit the structural weakening due to the presence of discontinuities in the material and to create a geometry with a uniform covering: it is possible to achieve a more effective film coverage of the surface. However, the use of too small diameter holes is limited by the hole occlusion caused by the deposition of particulates and/or by the metal oxidation inside the holes. This phenomenon would lead to a quick decay of the cooling performance due to the formation of hot spots. It is important to underline that, with the effusion cooling technique, it is possible to realize high values of L/D ratios (up to 10 in air cooling HPT

[31] J. Han, S. Dutta and S. Ekkad, Gas Turbine Heat Transfer And Cooling Technology, Boca Raton: CRC Press, 2012.

[32] C. A. McNally, I. R. Pashby and J. Flokes, "Laser drilling of cooling holes in aero-engines: State of the art and future challenges," Materials Science and Technology, no. 20(7), 2004.

case manifolds): that plays an important role in the increasing of the overall effectiveness thanks to the raising of the heat transfer surface dimension and hence improving the amount of heat removed by convection by the coolant flowing through the plate. Additionally, shaped end section can be adopted both lengthwise and sideways (Figure 16): the first allow for a better contact between the jet-flow and the liner wall, the latter increases lateral dispersion.

Figure 16 - Fan-shaped hole

Tolerances and manufacturing techniques play a really important role. Several different manufacturing techniques can be adopted, spacing among EDM hole drilling, laser and electron beam drilling. Such techniques have to perform holes with high aspect ratio (up to 10); for this reason, the more accurate and precise the method, the better the final geometry in terms of cooling efficiency. Today's manufacturing technology for gas turbines includes typically some casting/forging, sheet metal bending and welding processes that are by definition characterized by high geometrical uncertainty.
In opposition, today's machining path calculation relies on fixed nominal geometry obtained from CAD model of the work piece mounted in the machine tool workspace by means of mechanical fixtures. The tool that is nowadays typically used for generating machining paths from CAD models is the Computer Aided Manufacturing (CAM), which is a well-established throughout multi-axis numerical control machine tool field, with also commercial software that includes both CAD-CAM packages such as UG NX, TopSolid and ZW3D. However, these tools have clearly limitations because they cannot adapt machining paths calculations for each different work piece to be machined throughout a production line and so compensating for previous manufacturing processes uncertainty.
In order to implement the concept of adaptability an adaptive thermo-fluid dynamic model coupled with the real geometrical data of each single work piece are needed. The first will enable to pair the manufacturing uncertainties with the relative impact on the final work piece performance, the second will enable the fluid dynamic model to be supported with the uncertainty parameters of each single work piece. The whole system will enable the recalculation of the machining paths maximizing the product performances disregarding of previous processes variability. Moreover, as clearly stated from the previous analysis, for the purpose of implementing the measurement process to the turbomachinery industry and, in general all highly integrated production processes, both information of the real outer surface and inner geometries are needed.

The only technology available to measure inner and outer geometries at the same time, with sufficient accuracy, resides in the X-rays usage. X-ray computer tomography (CT) so far primarily used for medical diagnostics has became an increasingly promising tool for dimensional metrology on engineering parts. The visible contrast in CT is produced by the X- ray absorption of the material and therefore is a function of the local electron density of the object under study. So far, the main aspects of interest for the industrial application of CT scanning are the non-destructive analysis of faults (like cracks, flaws, shrink holes) and the material composition inside the volume. Increasingly, users want to quantitatively measure internal and external geometrical features. The object to be scanned is located on a rotary table (see Figure 17). Depending whether a line (ID) or an area (2D) detector is used, CT systems are capable of measuring 2D or 3D information with one revolution of the part. Up to now, resolution and repeatability aspects have been studied and laid down in standards (see e.g. ASTM E 1441-001). One limit for the spatial resolution in CT is the size and the shape of the X-ray focus. For X-ray tubes the minimum focus size increases with tube power and tube voltage. For larger parts, tubes of higher voltage have to be employed. Therefore, the achievable resolution decreases with the size of the object scanned. Typical parameters are in the order of 250 µm resolution with a 450 kV tube for

an aluminium object up to 150 mm, or 10 µm resolution with a 225 kV micro focus tube for an aluminium object up to 10 mm in size. The quantities mainly influencing the measurement uncertainty are also the relative distances of source, object and detector, the geometry of the object, the lateral resolution of the detector and the geometrical deviation of the mechanical axes.

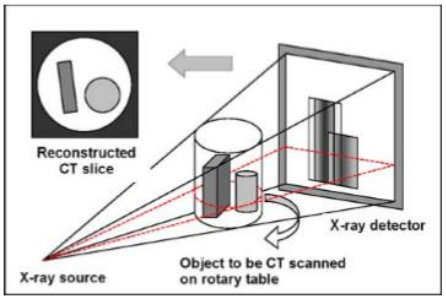

Figure 17: principle of x-ray tomography

These machines are well developed in the market and successfully employed in turbomachinery industry with the only purpose, as already stated, of detecting micro-scale defects such as cracks in the turbine blade and combustor components. Among the main producers there are GE MEASUREMENTS with the Nanotom CT machine and also turbine blade's dedicated machines such as blade|line CT Aircraft Turbine Blade machine, NIKON METROLOGY with the XT-H Series, YXLON with the FF and Precision Series and WERTH MESSTECHNIK with the TomoScope machine. All of the above fulfil the technical requirements in terms of X-ray source energy amount (i.e. they are able to penetrate high density nickel based alloys such as Inconel) and accuracy (i.e. 0.1-10µm); however, none of them, at the actual state of the art, can be employed in-line with the production since the scanning time for maintaining the aforementioned accuracy performances is too high (i.e. more than 2.5 hours to scan an average sized turbine blade). Moreover, none of them provide algorithms and acquisition routines with the purpose of localizing the internal structures of work pieces with the respect to outer surfaces. This leading to a lack in commercial available technologies to fulfil the requirements of an in-line adaptive inspection and correction system.

Concerning the thermo-fluid dynamics, studies are typically performed in the design phase of the product. Many commercial tools capable of supporting the designer in the aerothermal analysis; basically, three ways can be adopted as a design process:

- An experimental approach: relatively expensive and capable of reproducing only a small amount of cases.
- A correlative approach: this method is widely used for industrial purposes and it is based on correlations derived from experimental campaigns. The most important and influential ones can be found in the open literature, whereas each manufacturer tailors the technique using corrections coming from field data and specific component tests.
- CFD approach: CFD aims at the design validation of the previous test and it is broadly used for evaluating new design solutions and geometries. The valuable aspect is the possibility to run many different virtual experiments with small changes from one to another, in order to evaluate the differences in terms of output and to find an optimal geometry for each particular case.

CFD solves partial differential equations (Navier-Stokes equations) describing fluid motion and heat exchange in mechanical systems. The analytical solution of these equations is possible only in very simple cases, whereas for industrial applications an approximated numerical approach is necessary. These numerical methods at the base of CFD tools include different solution strategies:

- Direct Numerical Simulation (DNS): it is based on the direct numerical solution of the NS equations, resolving the entire turbulence spectrum thanks to an appropriate spatial and time discretization. This allows to achieve very accurate results, but unaffordable computational cost for realistic applications.

- Large Eddy Simulations (LES): it is based on the resolution of roughly the 80% of the largest turbulent scales, the filtering the remaining small scales of the turbulence spectrum This method allows the computational time shortening relative to a DNS simulation; however, especially for very complicated geometries such as film cooled blades, it still involves a significant cost. It is nowadays under continuous development but is gaining more and more interest in the industry.
- Reynolds Averaged Navier-Stokes (RANS): it is based on the assumption that the fluid dynamic quantities can be separated in mean and instantaneous values. Only the mean flow field is solved, whereas additional equations are introduced to model the effect of turbulence. This method allows a further reduction in the computational cost, but its accuracy relies on the turbulence models used. It is a robust approach and represents the state-of-the-art in design validation for industrial applications.

The most widely used commercial software packages, using the aforementioned techniques, include CAD-integrated solutions such as DASSAULT SYSTEM, SolidWorks, and AUTODESK Inventor, which target product designers who are primarily seeking to solve steady-state, single-phase, non-reacting flow problems with a focus on ease of use. More specialized solutions that allow for more complicated and comprehensive analysis include ANSYS Fluent and SIEMENS Star CCM+, representing the actual state-of-the-art in terms of capabilities and market share; Fluent seems to capture more market share in electronic and industrial product markets and Star-CCM+ in the aerospace, automotive and energy industries. There exist also open-source solutions such as Open-FOAM; in order to make open-source more user-friendly, developers have wrapped codes such as Open-FOAM into more user-friendly GUI environments bundled with additional software such as pre- and post-processors. Examples are Visual-CFD, Caedium, HELYX and simFlow. An interesting recent twist on this concept is that of web browser based simulation, as provided, for example, by SimScale.
All of these software packages, as already stated, are used in the design and verification phases, however the computational time required for their adoption as in-line instruments is far too high.

Improvement – In-line adaptive machining model optimization based on an adaptive thermo-fluid dynamic model coupled with tomographic in-line measurements
The development of an adaptive machining system capable of optimizing the nominal machining model taking into account the work piece geometrical variability together with its thermo-fluid dynamic performance. This will be achieved by means of successfully develop an adaptive thermo-fluid dynamic model and a fast in-line computed tomography machine. The data acquired will be aggregated together and used in-line in order to recalculate, for each single work piece, the optimal machining model. Furthermore, the system will enable the immediate evaluation of previous manufacturing errors that are too large to be compensated with any system, leading to an immediate discharge of the work piece, avoiding waste of further expensive machining operations. Thanks to the development of an adaptive machining model optimization method, based on both algorithms and hardware advancements in the field of tomographic measurements and thermo-fluid dynamics, the realization of complex micro-scale features, optimized for each single free-form work piece for compensating previous manufacturing process errors, will be enabled. This benefiting the final performances of the final integrated product, the quality control processes and the whole production scrap reduction.

2.1.3. Beyond the state-of-the-art: lack of standards for reference models for optical and tomographic based measurement systems.

The common practice for evaluating the performances of a measuring system, and at the same time enable the measurements traceability throughout a complex multi-stage process, is to rely on measurements performed on common standardized reference artefacts of well-known characteristics. From measurements performed on these artefacts, the measurement system uncertainty can be certified according to various standards such as the ISO 10360.

Procedures and artefacts to be used are very well established and clarified in the ISO 10360 regarding the use of contact probing in Coordinate Measurement Machines (CMMs). In this field, the most widespread test artefact is the Ball Bar: a ball bar consists of two precision spheres mounted at either end of a long rigid bar. They are available in a range of lengths and may be adjustable. The distance between the two ball centre is measured by the touch-probe several times and compared with the nominal one; from this test accuracy and repeatability of the system can be established and certified.
However, the same level of standardization and acceptance is not yet reached in the optical acquisition sensors field and, above all, in computed tomography.
In the field of laser based acquisition sensors, several authors proposed algorithms and artefacts for the calibration of laser line scanners[33,34,35]. However today, there are almost no publications about performance evaluation tests and artefacts for laser line scanners mounted on CMMs. Some possible reference artefacts have been proposed by[36] and are illustrated in Figure 18: single sphere, steps, single or multiple edges, sphere-plane combinations, faceted sphere and double-curved surfaces.

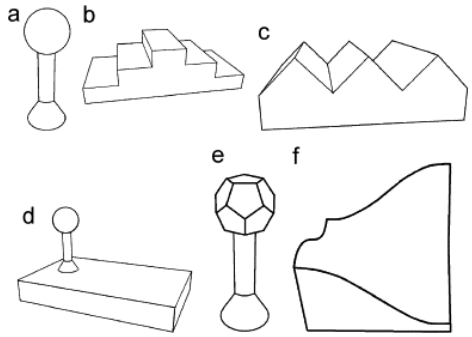

Figure 18: Possible artefacts for verification of laser line scanners: sphere (a), steps (b), edges (c), sphere–plane combination (d), faceted sphere (e) and double-curved surface (f).[18]

In the field of computed tomography, no standards have been defined yet; a current topic is creating a future part of ISO 10360 for CMSs using dimensional computed tomography (CT). In Figure 19 are reported a few reference artefact that have been tested for an ISO survey for the purpose of investigating future standardization in this field[37].

Figure 19: Mandatory reference standards inside the ISO test survey (left): PTB hole plate Al2 size 48 mm × 48 mm × 8 mm with 28 holes of 4 mm in diameter and NMIJ step cylinder SC1 with maximum outer diameter of 50 mm and central hole 8 mm in diameter inside PMM[19].

[33] Y. L. H.-Y. F. F. Xi, "Error compensation for three-dimensional line laser scanning data," The International Journal of Advanced Manufacturing Technology, vol. 18, p. 211–216, 2001.
[34] J. N. C. Che, "A ball-target-based extrinsic calibration technique for high-accuracy 3-D metrology using off-the-shelf laser-stripe sensors," Precision engineering, vol. 24, p. 210–219, 2000.
[35] B. Z. X. L. Z. H. P. R. G. Wang, "Modelling and calibration of the laser beam-scanning triangulation measurement system," Robotics and autonomous systems, vol. 40, p. 267–277, 2002.
[36] S. C. P. B. J.-P. K. Nick Van Gestel, "A performance evaluation test for laser line scanners on CMMs," Optics and Lasers in Engineering, p. 336– 342, 2009.
[37] J. I. U. N.-R. Markus Bartscher, "ISO test survey on material influence in dimensional computed tomography," in Case Studies in Nondestructive Testing and Evaluation, Elsevier, 2016.

From the aforementioned considerations it is clear that there is a lack of standards for reference artefact implementation in both fields of optical acquisition sensors and in computed tomography field of metrology. Moreover, there is no standard neither scientific reviews on the development of an artefact able to fulfil at the same time both the requirements from the two different measurement systems so that it can be used in an in-line measurement system such as the one hereby proposed.

Improvement – Development of a reference artefact fulfilling requirements for laser based acquisition sensors and tomographic inspection, leading to traceability of measurement throughout the whole production process and the whole product lifecycle.
The development of a calibrated artefact to be integrated in the work-piece fixture so that it can be measured together with the work-piece; consequently, the reference itself is present from all the measuring devices involved in the system (i.e. the laser based devices and the x-rays tomography). This leading to complete traceability and homogeneity of all involved and following measurements that can be used along the whole production process as well as along the whole product lifecycle.

3. Laser scan/Positioning engine pillars development and implementation

As introduced in the very beginning of the document, a wide conceptual framework has been presented, then hereby is descripted the study, engineering and validation experiments of a part of the whole concept. This part consists in an on-board correction system aiming at the compensation of positioning errors of freeform shaped parts for their machining via Electro Discharge Machining (i.e. the Laser scan and Positioning engine pillars). Firstly, the machine tool used for the experiment is described, then a wide perspective on various sensors suitable for the application that have been tested, is given, then the solution for the sensing equipment integration on board the machine tool is described. Secondly, the calibration procedure of the system is described together with two different approaches for positioning. The method is generally described and is valid for the implementation among different machine tools. The various measurement error sources, relative to the specific equipment used but extensible to other use cases, are evaluated and reported. At the end the experimental tests performed on the specific SARIX micro-EDM machine tool, are reported.

3.1. Machine tool and process specifications

3.1.1. Electro Discharge Machining (EDM), generalities

Electrical discharge machining (EDM) is one of the most extensively used non-conventional material removal processes. Its unique feature of using thermal energy to machine electrically conductive parts regardless of hardness has been its distinctive advantage in the manufacture of mold, die, automotive, aerospace and surgical components. In addition, EDM does not make direct contact between the electrode and the work piece eliminating mechanical stresses, chatter and vibration problems during machining. The basis of EDM can be traced as far back as 1770, when English chemist Joseph Priestly discovered the erosive effect of electrical discharges or sparks[38]. However, it was only in 1943 at the Moscow University where Lazarenko[39] exploited the destructive properties of electrical discharges for constructive use. They developed a controlled process of machining difficult-to-machine metals by vaporizing material from the surface of metal. The Lazarenko EDM system used resistance–capacitance type of power supply, which was widely used at the EDM machine in the 1950s and later served as the model for successive development in EDM[40]. It was only in the 1980s with the advent of computer numerical control (CNC) in EDM that brought about tremendous advances in improving the efficiency of the machining operation. CNC has facilitated total EDM, which implied an automatic and unattended machining from inserting the electrodes in the tool changer to a finished polished cavity or cavities[41]. The material erosion mechanism primarily makes use of electrical energy and turns it into thermal energy through a series of discrete electrical discharges occurring between the electrode and work piece immersed in a dielectric fluid[42].

[38] S. Webzell, “That first step into EDM, in: Machinery”, 159, (4040) Findlay Publications Ltd, Kent, UK, November 2001, p. 41

[39] Anonymous, History and development, in: “The Techniques and Practice of Spark Erosion Machining”, Sparcatron Limited, Gloucester, UK, 1965, p. 6.

[40] A.L. Livshits, Introduction, in: “Electro-erosion Machining of Metals”, Department of Scientific & Industrial Research, Butterworth & Co., London, 1960, p. x

[41] L. Houman, Total EDM, in: E.C. Jameson (Ed.), “Electrical Discharge Machining: Tooling, Methods and Applications”, Society of Manufacturing Engineers, Dearbern, Michigan, 1983, pp. 5– 19.

[42] H.C. Tsai, B.H. Yan, F.Y. Huang, “EDM performance of Cr/Cu based composite electrodes”, Int. J. Mach. Tools Manuf. 43 (3) (2003) 245–252.

The thermal energy generates a channel of plasma between the cathode and anode[43] at a temperature in the range of 8000 to 12,000°C or as high as 20,000°C[44] initializing a substantial amount of heating and melting of material at the surface of each pole. When the pulsating direct current supply occurring at the rate of approximately 20,000–30,000 Hz [45] is turned off, the plasma channel breaks down. This causes a sudden reduction in the temperature allowing the circulating dielectric fluid to implore the plasma channel and flush the molten material from the pole surfaces in the form of microscopic debris. This process of melting and evaporating material from the work piece surface is in complete contrast to the conventional machining processes, as chips are not mechanically produced. The volume of material removed per discharge is typically in the range of 10^{-6} – 10^{-4} mm3 and the material removal rate (MRR) is usually between 2 and 400 mm3/min[46] depending on specific application. Since the shaped electrode defines the area in which the spark erosion will occur, the accuracy of the part produced after EDM is fairly high.

Traditionally there are two basics implementation strategies for the EDM based machine tools:

- **Die-sink EDM:** in the case of die-sinking EDM, the required shape is formed negatively in the metal with a three-dimensional electrode that has been formed prior to the process. By superimposed movements in the main axes x, y, c, z, the most varied shapes, indentations and cavities are created, such as cannot in part be achieved by any other machining system.
- **Wire-cut EDM:** wire cut EDM discharges the electrified current by means of a taut thin wire, which acts as the cathode and is guided alongside the desired cutting path, or kerf. With Wire-cut EDM also electrodes for Die-sink EDM can be manufactured.

The recent trend in reducing the size of products has given micro-EDM a significant amount of research attention. Micro-EDM is capable of machining not only micro-holes and micro-shafts as small as 5 µm in diameter but also complex three-dimensional (3D) micro-cavities[47]. This is unlike mechanical drilling, which can produce holes just up to 70 µm, or the micro-fabrication process such as laser machining, which can only create holes of 40 µm[48]. In addition, a feasibility study of applying micro-EDM as an alternative method for producing photo-masks used in the integrated circuit (IC) industry has been conducted[49]. Other applications include the general interest in developing trajectory EDM to solve the machining problems of water-cooling channels used in molds or manifolds, or the air-cooling channels used in turbine blades, that often involves the need for complex shaped parts. Ishida and Takeuchi[50] proposed a trajectory EDM technique facilitating the electrode to move along a smooth trajectory, while performing EDM eliminating the conventional drilling or boring operation required. Other attempts have also been made on trajectory EDM with special apparatus and complex control mechanism is needed to develop the trajectory motion of electrode. The micro-EDM machine tool used for the developments hereby presented belong to this family, using Computer Aided

[43] E.I. Shobert, “What happens in EDM”, in: E.C. Jameson (Ed.), Electrical Discharge Machining: Tooling, Methods and Applications, Society of Manufacturing Engineers, Dearbern, Michigan, 1983, pp. 3–4

[44] G. Boothroyd, A.K. Winston, “Non-conventional machining processes”, in: Fundamentals of Machining and Machine Tools, Marcel Dekker, Inc, New York, 1989, p. 491.

[45] S.F. Krar, A.F. Check, “Electrical discharge machining”, in: Technology of Machine Tools, Glencoe/McGraw-Hill, New York, 1997, p. 800.

[46] S. Kalpajian, S.R. Schmid, “Material removal processes: abrasive, chemical, electrical and high-energy beam”, in: Manufacturing Processes for Engineering Materials, Prentice Hall, New Jersey, 2003, p. 541.

[47] K.P. Rajurkar, Z.Y. Yu, “3D micro-EDM using CAD/CAM”, Ann. CIRP 49 (1) (2000) 127–130.

[48] T. Masuzawa, “State of the art of micromachining”, Ann. CIRP 49 (2) (2000) 473–488.

[49] S.H. Yeo, G.G. Yap, “A feasibility study on the micro electro discharge machining process for photomask fabrication”, Int. J. Adv. Manuf. Technol. 18 (1) (2001) 7–11.

[50] I. Ishida, Y. Takeuchi, “L-shaped curved hole creation by means of electrical discharge machining and an electrode curved motion generator”, Int. J. Adv. Manuf. Technol. 19 (4) (2002) 260–265.

Manufacturing (CAM) for the generation of complex three dimensional trajectories similarly to a CNC micro-milling approach.

3.1.2. Micro-EDM machine tool specifications

In particular, as introduced in the beginning of the document, the machine tool used for the experimentation is a SARIX SX200 Aero (Figure 20), a micro-EDM milling machine especially designed for the realization of micro-sized features (down to 8 µm diameters) in aerospace components. It is characterized by six axes:

- 4 linear axes (X,Y,Z,W)
- 2 rotary axes (A,B)

In Table 1 are listed the main technical specifications.

MACHINE TOOL		
Work Table	700x300	[mm]
Travel X axis	350	[mm]
Travel Y axis	200	[mm]
Travel Z axis	200	[mm]
Travel W axis	150	[mm]
Z axis feed rate	600 max	[mm/min]
X-Y axis feed rate	600 max	[mm/min]
Linear axes resolution	0.1	[µm]
Rotary axes resolution	0.005	[deg°]
Table load	50	[kg]
Net weight	450	[kg]
Dimensions [mm]	950x850x1300	[mm]
GENERATOR		
Free run voltage	60÷255	[V]
Frequency	1÷250	Pos
Current pulse	1÷200	Pos
Dimensions	135x110x500	[mm]
CONTROL UNIT		
Power supply	230V/50Hz	[V/Hz]
Nominal power	650	[VA]
Dimensions	450x400x690	[mm]
DIELECTRIC UNIT		
Capacity	25	[l]
Dielectric	Deionized water or oil	-
Dimensions	500x780x680	[mm]

Table 1: SARIX SX-200 Aero main specifications

The electrodes used by the machine are always cylindrical with different diameters, and are used like milling tools, driven by complex trajectories generated by CAM software.
An additional feature of this machine tool is that the electrode can act as a mechanical touch probe allowing to acquire single data points coordinates of work pieces in the machine tool workspace with a probing accuracy of ±1µm.

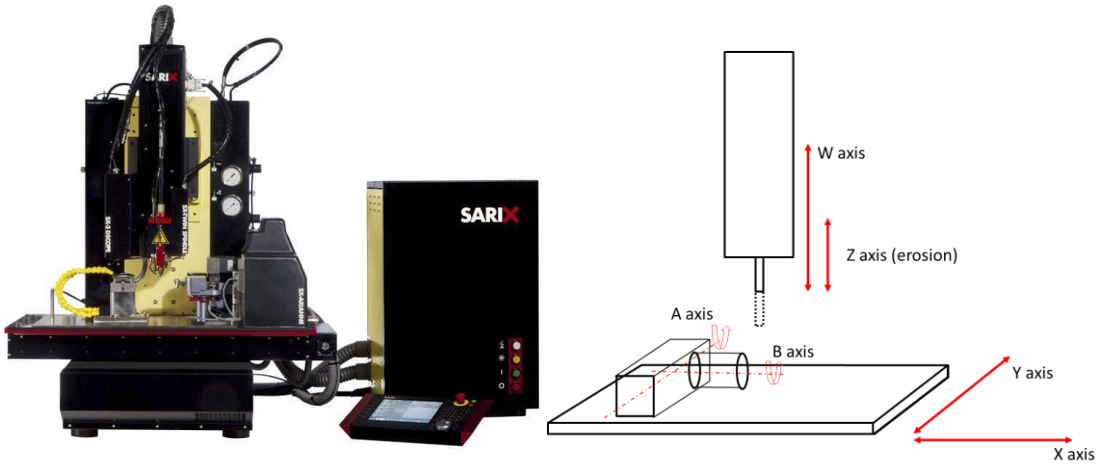

Figure 20: SARIX SX200 Aero

3.1.3. Kinematic chain characterization

The machine tool linear axes have not been characterized, since their resolution lay into more than one order of magnitude less than the required one, for the specific application.

The rotary axes (i.e. A and B of Figure 20), on the other hand, have been characterized in order to consider their impact in the overall kinematic chain for the measurement system characterization, since their resolution lay into the same order of magnitude of the required one. To do so, a high resolution analogic encoder has been mounted on A and B axes (in Figure 21 a picture of the test bed); the encoder provides 3600 pulses per turn, thus 14400 digital steps, which are interpolated at 1:128 obtaining 1843200 pulses per turn corresponding to 0.0001953° per step.

On the other hand, the internal encoder resolution of the A-B axes is 0.0005° per step.

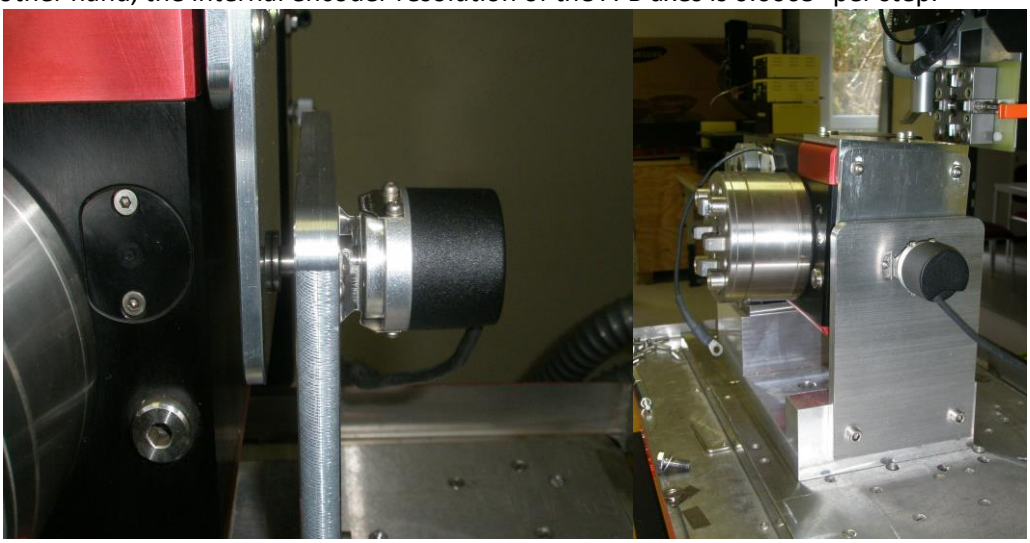

Figure 21: high resolution analogic encoder test bed

The two axes are moved from -10° to 370° and back, while the encoder acquires data. In Figure 22 is reported the obtained graph of the full movement forward and backward of A-axis; in light blue is represented the absorbed current; in red (i.e. in mdegrees) is represented the measured error from the external encoder; in dark blue (i.e. in degrees) is represented the axis position.

A not perfectly constant value of the current is due to a non-uniform friction distribution along the complete motor turn; the periodic component of the measured error is due to the screw-nut mechanism of the gearbox, quantifiable in ca. 0.006°.

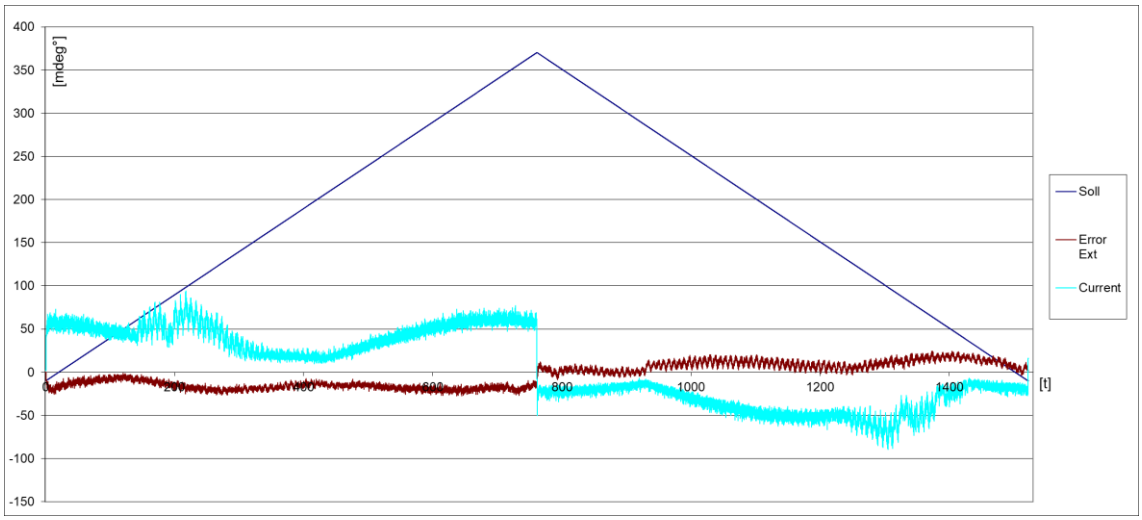

Figure 22: A axis analysis with high precision analogic encoder. The axis is moved from -10° to 370° and back. In light blue the absorbed current; in red the measured angle; in blue the position profile

In Figure 23 are reported the values of the measured error in the two directions (i.e. forward and backward) along the whole rotation angle. The distance between the two curves representing the forward and backward movements, represents the axis inversion error quantifiable in ca. 0.015°. The maximum measured absolute error corresponds to approximately ±0.023°.

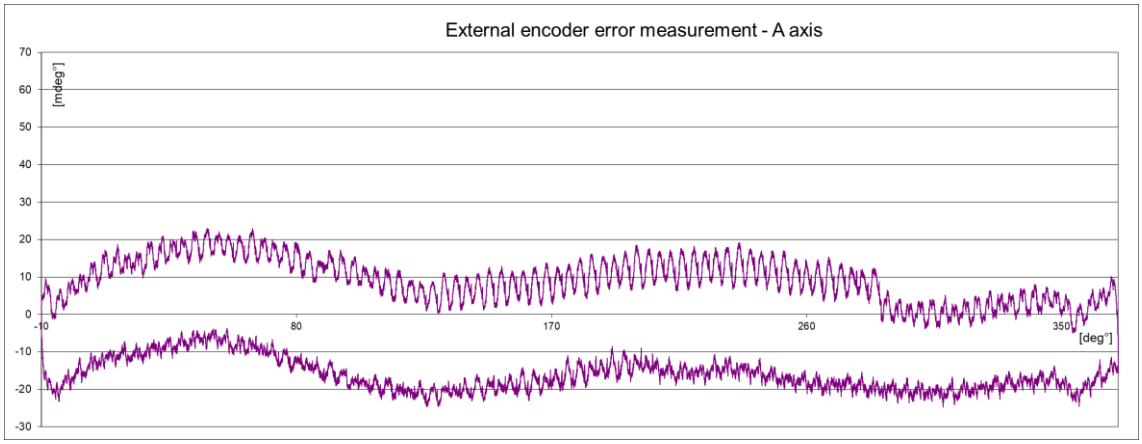

Figure 23: A axis analysis with high precision encoder. The axis is moved from -10° to 370° and back. In purple the error compared to the angular position. The displacement between the two lines represents the motor inversion error, quantifiable in ca. 0.015°.

The same analyses have been performed on B axis, of which results are reported in Figure 24 and Figure 25. In this case, the axis inversion error results in 0.005°, the hysteresis cycle due to the screw-nut mechanism in 0.003° and the maximum position error in ±0.015°.

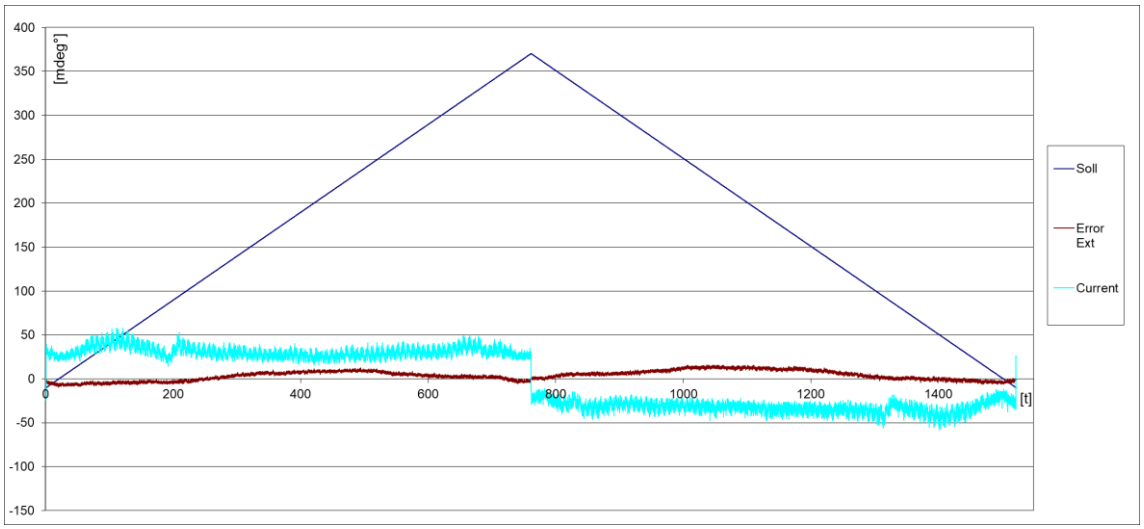

Figure 24: B axis analysis with high precision analogic encoder. The axis is moved from -10° to 370° and back. In light blue the absorbed current; in red the measured angle; in blue the position profile

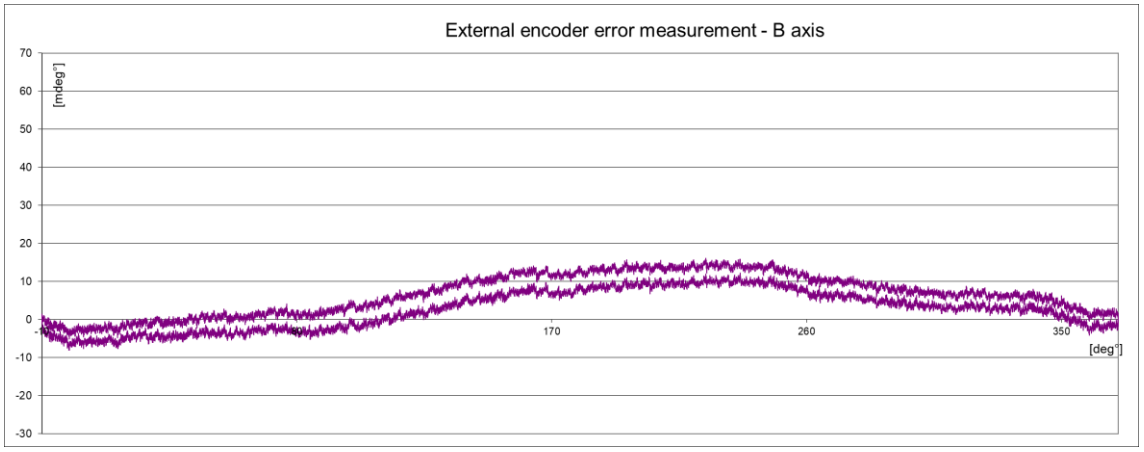

Figure 25: B axis analysis with high precision encoder. The axis is moved from -10° to 370° and back. In purple the error compared to the angular position. The displacement between the two lines represents the motor inversion error, quantifiable in ca. 0.005°.

These uncertainties will finally result in work piece positioning errors, and thus must be considered as an error source for the system. In particular, in order to point out the order of magnitude of the final error along the X-Y-Z directions the following calculation can be considered:

$$error = 2 * distance * \sin\left(\frac{\alpha}{2}\right) \qquad (1)$$

For example, solving the (1) for a distance of 200mm and an error angle of 0.02°, will give an error of approximately 70µm.

3.2. Sensing equipment choice and tests

3.2.1. General requirements and choice drivers

In order to successfully choose the sensor among the various technologies available on the market, that have been extensively described in 2.1.1, some basic requirements for the specific application are hereby listed:

- **Accuracy:** the overall positioning tolerances that must be achieved lie into the range of ±30µm, as a consequence the instrument must allow for a probing accuracy of at least an order of magnitude less
- **Ease of integration:** the system has to be installed on-machine, therefore dimensions must be compatible with the space available on the machine tool
- **Compactness:** exclusion of systems provided inside as external measuring systems or mounted on robotic arms.
- **Measurement speed:** the frequencies of data acquisition must be compatible with machining operation time. A measurement of an average work piece of dimensions 50x100x150 mm must stay into a few minutes' order of magnitude
- **Measurable object size:** on the same machine tool many different work pieces with different dimensions and aspect ratios can be machined; turbine blades, which represent the typical application for this machine tool lie in the range of 20x40x80 mm up to 100x100x300 mm
- **Working distance:** the sensor working distance must be compatible with the physical dimensions of the machine and the work pieces
- **Weight:** the weight of the sensor must be compatible with the machine tool axes load capability without affecting their precision and speed
- **Price:** being this project part of the industrial development of SARIX SA, the sensor choice must also undergo some commercial considerations: together with SARIX SA, has been targeted a price of 15'000 Euros for the sensing equipment.
- **Sensibility to highly reflective surfaces:** turbine blades and, more in general, aerospace components are often highly reflective; the sensor must be capable of measure accurately these kind of surfaces
- **Sensibility to environment conditions:** the machine tool can be used in very different environments at the customer production plant, especially regarding light conditions and temperature; the sensing equipment must be able to operate in most of these conditions

These requirements are strictly related to the specific application targeted in the present work thesis, and to the commercial developments of SARIX machine tool.
Considering the aforementioned requirements, a wide research on commercial solutions has been carried out; the list of the equipment potentially able to fulfil the requirements listed above is reported in Table 2, together with their main characteristics.

MANUFACTURER	PRODUCT NAME	INSPECTION TECHNIQUE	MEASURABLE OBJECT SIZE	FIELD OF VIEW	STAND-OFF DISTANCE	RESOLUTION or POINT SPACING	ACQUISITION TIME	ACCURACY	WEIGHT
AICON3D	MoveInspect HR	Fringe projection	1000x100mm^2 (max in one single shot)	Variable with work piece size, and aspect ratio	Variable with work piece measurable size	5MP	Variable with work piece measurable size (up to 30Hz)	1m^3: 20µm	8.5kg
	MoveInspect HR	Fringe projection	1000x100mm^2 (max in one single shot)	Variable with work piece size and aspect ratio	Variable with work piece measurable size	1.3MP	Variable with work piece measurable size (up to 1KHz)	1m^3: 100µm	7kg
Nikon Metrology	L100	Laser triangulation	Variable (moving sensor/work piece); 105mm (line length)	60mm	105mm	X: 42µm Y: dependant from motion system resolution	200Hz	Z: 6.5µm	300g
	LC15Dx	Laser triangulation	Variable (moving sensor/work piece); 18mm (line length)	15mm	60mm	X: 22 µm Y: dependant from motion system resolution	70Hz	Z: 1.9µm	370g
	XC65Dx	Laser triangulation	Variable (moving sensor/work piece); 3x65mm (line length)	3x65mm	75mm	X: 45 µm Y: dependant from motion system resolution	75Hz	Z: 12µm	440g
	XC65Dx-LS	Laser triangulation	Variable (moving sensor/work piece);	3x65mm	170mm	X: 80 µm Y: dependant from motion system resolution	75Hz	Z: 15µm	480g

			3x65mm (line length)						
GOM	ATOS Compact Scan	Fringe projection	1000x35mm^2 (max in one single shot)	Variable with work piece size, and aspect ratio	Variable with work piece measurable size(min 450, max1200mm)	2MP	n/d	Variable with work piece measurable size (up to 21µm)	4kg
	ATOS Core Series	Fringe projection	From 45x30mm^2 (max in one single shot), up to 500x380mm^2(max in one single shot)	Variable with work piece size, and aspect ratio	Variable with work piece measurable size(From 170, up to 440mm)	5MP	n/d	Variable with work piece measurable size (From 20, up to 190µm)	2.9kg
	ATOS Triple Scan	Fringe projection	850x170mm^2 (max in one single shot)	Variable with work piece size, and aspect ratio	Variable with work piece measurable size (min 490, max830mm)	12MP	n/d	Variable with work piece measurable size (up to 40µm)	5.5kg
	ATOS II Triple Scan	Fringe projection	1500x38mm^2 (max in one single shot)	Variable with work piece size, and aspect ratio	Variable with work piece measurable size (min 490, max2000mm)	5MP	n/d	Variable with work piece measurable size (up to 20µm)	5.5kg
	ATOS III Triple Scan	Fringe projection	1500x38mm^2 (max in one single shot)	Variable with work piece size, and aspect ratio	Variable with work piece measurable size (min 490, max2000mm)	8MP	n/d	Variable with work piece measurable size (up to 10µm)	5.5kg

COGNEX	DS Series	Laser triangulation	Variable (moving sensor/work piece); From 76 up to 725mm (line length)	From 79 up to 410mm	From 87 up to 180mm	X: from 59 to 457µm Y: dependant from motion system resolution	10KHz	Z: from 4 to 265µm	700g
KEYENCE	LJ-V Series	Laser triangulation	Variable (moving sensor/work piece); From 14 up to 180mm (line length)	From 15 up to 290mm	From 54.6 up to 300mm	X: from 5 to 60µm Y: dependant from motion system resolution	62.5KHz	Z: from 0.4 to 5µm	From 450 to 1000g
	LJ-G Series	Laser triangulation	Variable (moving sensor/work piece); From 7 up to 62mm (line length)	From 5 up to 96mm	From 15 up to 200mm	X: from 2.5 to 20µm Y: dependant from motion system resolution	62.5KHz	Z: from 0.2 to 2µm	From 260 to 480g
KREON 3D	Aquilon	Laser triangulation	Variable (moving sensor/work piece); 50mm (line length)	30mm	75mm	X: 25µm Y: dependant from motion system resolution	1KHz	Z: 5µm	450g
	Zephir II	Laser triangulation	Variable (moving sensor/work piece); 70mm (line length)	75mm	75mm	X: 50µm Y: dependant from motion system resolution	250Hz	Z: 10µm	370g
SHAPEDRIVE	G3 Series	Fringe projection	500x316mm^2 (max in one single shot)	Variable with work piece size, and aspect ratio	Variable with work piece measurable size	5MP	Variable with work piece measurable	Variable with work piece measurable size (up to	1.55kg

							size (up to 22Hz)	2µm with objet size of 30x19mm^2)	
	G2 Series	Fringe projection	360x198mm^2 (max in one single shot)	Variable with work piece size, and aspect ratio	Variable with work piece measurable size (from 100 up to 450mm)	2.3MP	Variable with work piece measurable size (up to 22Hz)	Variable with work piece measurable size (up to 10µm with objet size of 20x10mm^2)	900g
Alicona	Infinite Focus	Autofocus	5.63x5.63mm^2 (max in one single shot) – variable with zoom rate	Variable with zoom rate and work area (from 4 up to 36mm)	Variable with zoom rate and work area (from 4.5 up to 37mm)	Variable with zoom rate and work area (XY: from 0.41 up to 4.35µm)	n/d	Variable with zoom rate and work area (from 2.3 µm up to 10nm)	
Optimet	ConoLine-100	Conoscopic Holography	Variable (moving sensor/work piece); 18mm(line length)	30mm	50mm	X: 90µm Y: dependant from motion system resolution	20KHz	Z: 20µm	2.1kg
Laser Design	XLP Series	Laser triangulation	Variable (moving sensor/work piece); From 23 up to 144mm (line length)	From 26 up to 265mm	From 53 up to 390mm	X: from 19 to 78µm Y: dependant from motion system resolution	100Hz	Z: from 6 to 24µm	500g

Micro Epsilon	scanControl Series	Laser triangulation	Variable (moving sensor/work piece); From 9.4 up to 120.8mm (line length)	From 8 up to 265mm	From 52.5 up to 390mm	X: from 19 to 78µm Y: dependant from motion system resolution	Up to 2KHz	Z: from 1 to 12µm	440g

Table 2: commercial sensing equipment list

From Table 2 some considerations have been done prior to perform any test in working conditions; this in order to narrow the choice among a selected shortlist. Note that these considerations have been done in order to ensure the compatibility with the specific application of SARIX machine tool; as a consequence, also industrial drivers have been considered.

In particular, all the sensors using the fringe projection as measurement principle, have been discarded for their weight and their volumetric occupancy: this would limit too much the on-board integration strategies. In fact, the only option available for these kind of sensors is to use them stand-alone, introducing the problem of having an unknown (and difficult to be measured and fixed) displacement of the sensor and the machine tool reference frame, which is not an issue for the quality inspection purpose, but at the same time not acceptable for the on-board positioning correction purpose. The only tested sensor using fringe projection technology is the Shapedrive G3 series, which seemed to be less problematic from this point of view.

Also the sensors using conoscopic holography as measurement principle have been discarded, because the maximum achievable resolution in the direct measurement direction (Z in Table 2), is limited to 20µm which lays in the same order of magnitude of the targeted final requirements.

Finally, also the sensors using autofocus as measurement principle have been discarded because the measurable area in a single measurement shot is far too narrow making the measurement time required for a typical work piece (i.e. turbine blades) too high. Moreover, the stand-off distance of this kind of sensor is very short and strictly linked with the technology used (thus not scalable with simple optics change as for other sensing principles such as laser triangulation) for the purpose of the project, making difficult to measure some areas of freeform shaped parts because of their physical reachability.

Among the sensors based on laser triangulation technology, the Kreon Acquilon and ZephirII have been discarded for the same reason (rated accuracy in Z direction not sufficient for positioning purposes), as well as Laser Design and Cognex equipment (the available models start with a too large measurement ranges, which make the sensor less accurate in X-Y direction). Keyence sensors have been discarded because their need for an external controller, which translates in major problems in its integration within the machine tool. Keyence however provides a far higher acquisition frequency, that translates into higher achievable measurement speed, but up to certain values, it does not represent an instrumental issue for this work application purpose. Finally, Nikon sensors have been discarded for commercial reasons: even if they provide a potentially valid solution, they have been considered too expensive if compared with the machine tool market price.

3.2.2. Sensing equipment test

Some tests have been performed on the selected (see 3.2.1) sensors in order to verify their performances in the working conditions. A calibrated specimen (see Figure 26) has been used in order to verify the repeatability of the measurements.

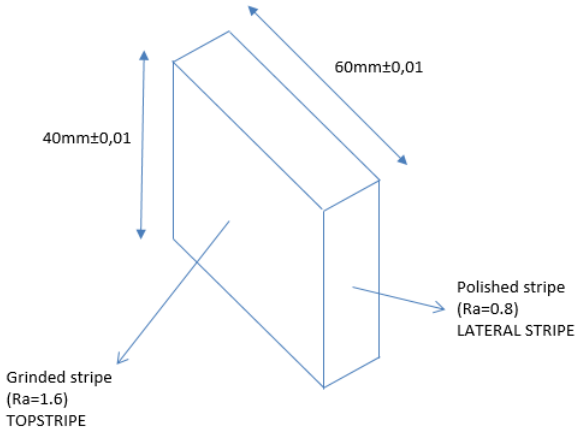

Figure 26: calibrated specimen characteristics

For the laser triangulation sensor (MicroEpsilon 2960-25), in order to acquire a surface, the sensor itself must be moved along an axis; this has been achieved through its integration into a certified CMM (DEA Scirocco), as reported in Figure 27.

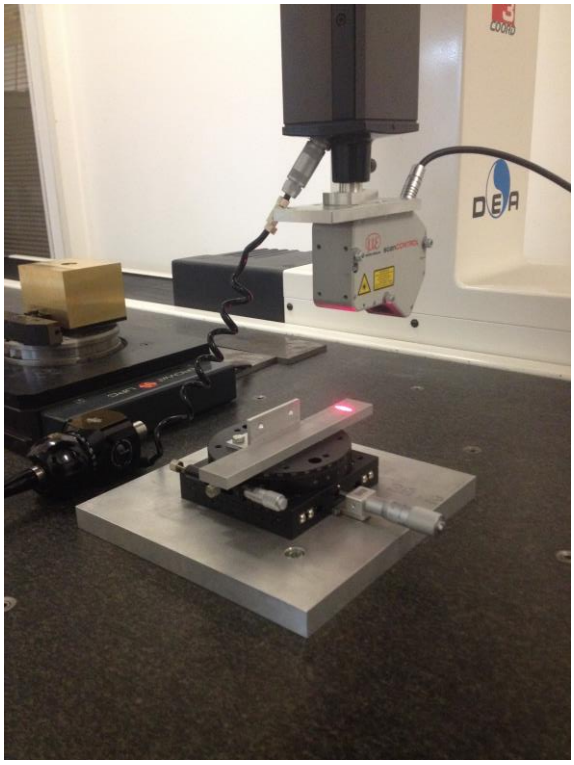

Figure 27: MicroEpsilon 2960-25 mounted on a CMM (DEA Scriocco)

The sensor acquisition is triggered by the linear encoder of the CMM with a resolution of 1µm each 25 steps (25µm of line spacing); the maximum sensor acquisition frequency is 140Hz. For this experiment, the CMM speed has been set to 2mm/s, thus the acquisition frequency results in 80Hz. With this setup, the lateral stripe of the specimen has been acquired 70 times consequently in the same conditions, resulting in a 70 times superposed complete reconstruction of the specimen lateral stripe surface (see Figure 28). Then a cross section, obtained in the midrange of the specimen, of the superposed point clouds has been gathered, resulting in a median oscillation of the Z measured coordinates of ca. ±2µm. The inclination of the data, observable in Figure 28, is due to the imperfection in the sensor mounting on the CMM, however, this does not interfere with the measures object of this test; the issues related to the alignment of the sensor with the machine tool reference frame, will be treated in the next chapters.

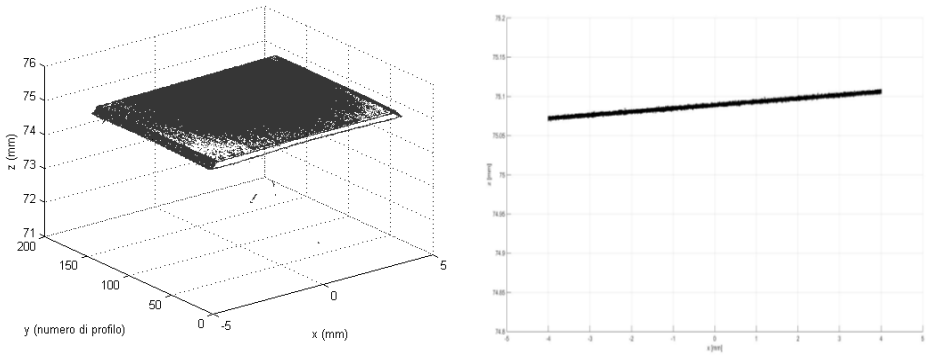

Figure 28: MicroEpsilon 2960-25 mounted on certified CMM (DEA Scirocco). 70 superposed acquisitions performed at 2mm/s on the calibration polished rectilinear surface (Ra=0.8): LATERAL STRIPE of specimen of Figure 26. On the right a cross-section view of the image on the left. Median oscillation≈±2µm

The fringe projection sensor (Shapedrive G3 Series) has been similarly mounted on the same CMM, and the same experimental setup has been used. The lateral stripe of the specimen has been acquired 70 times consequently in one single shot (i.e. the fringe projection technology, as specified in the previous paragraphs, does not require the sensor to be moved for a single-shot surface acquisition) in the same conditions and, from the resulting point cloud, a cross section, obtained in the midrange of the specimen, has been analysed and reported in Figure 30. The median oscillation of the measured Z coordinate of the surface resulted in ±23µm

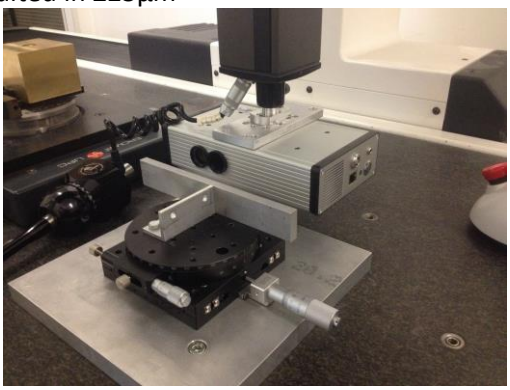

Figure 29:Shapedrive G3 mounted on a CMM (DEA Sciocco)

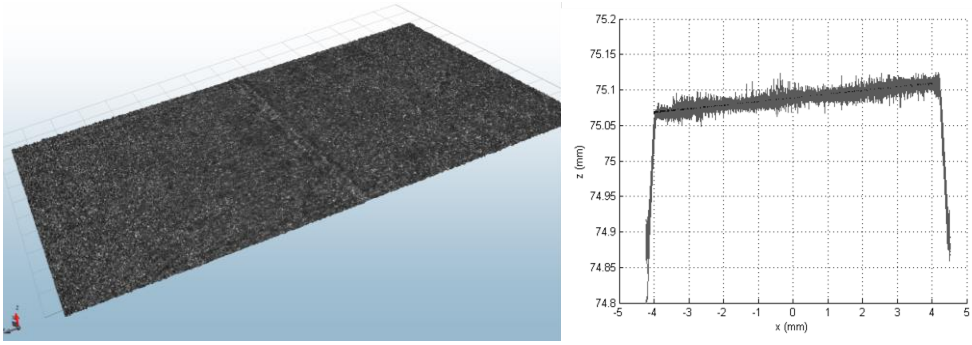

Figure 30: Shapedrive G3 series. 70 superposed single-shot acquisitions on the calibration polished rectilinear surface (Ra=0.8): LATERAL STRIPE of specimen of Figure 26. On the right a cross-section view of the image on the left. Median oscillation≈±23µm

As a consequence of the performed tests, and considerations for the specific purpose, a list of pros and cons for the two tested sensors is reported in Table 3.

	MicroEpsilon 2960-25 (laser triangulation)	**Shapedrive G3 (fringe projection)**
PROS/CONS	Higher accuracy and repeatability Lower dimensions Low sensitivity to ambient conditions and work piece aspect ratio Lower price Higher scalability with work piece dimensions (by changing optics, it changes the scanning line length and stand-off distance so that bigger work pieces can be measured with slightly lower accuracy)	Higher speed for acquisition of an entire work piece No need for sensor motion Lower sensibility to misalignment with the machine tool

Table 3: comparison of pros and cons among the two tested sensors

From the considerations of Table 3, and in agreement with SARIX SA as industrial committer, MicroEpsilon 2960-25 has been chosen for the purpose of the project. In Table 4 the full specifications are reported.

Z-axis	Standard measuring range	Start of measuring range	53.5mm	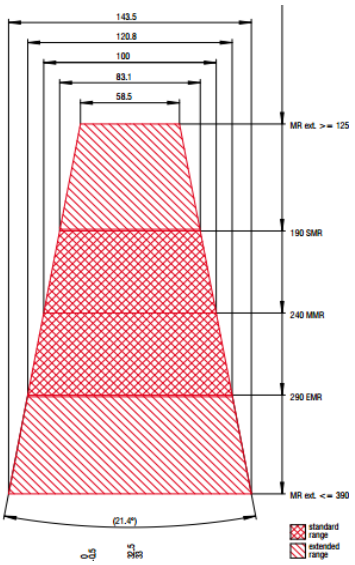
		Midrange	66mm	
		End of measuring range	78.5mm	
		Height of measuring range	25mm	
	Extended measuring range	Start of measuring range	53mm	
		End of measuring range	79mm	
	Linearity	2sigma	±0.1%FSO	
	Reference resolution	2µm		
X-axis	Standard measuring range	Start of measuring range	23.4mm	
		Midrange	25mm	
		End of measuring range	29.1mm	
	Extended measuring range	Start of measuring range	23.2mm	
		End of measuring range	29.3mm	
	Resolution	1280points/profile		
Profile frequency		Up to 300Hz		
Light source		Semiconductor laser 405nm		
Aperture angle laser line		20°		
Laser power		Class 2M		
Protection class		IP65		
Weight		380g		

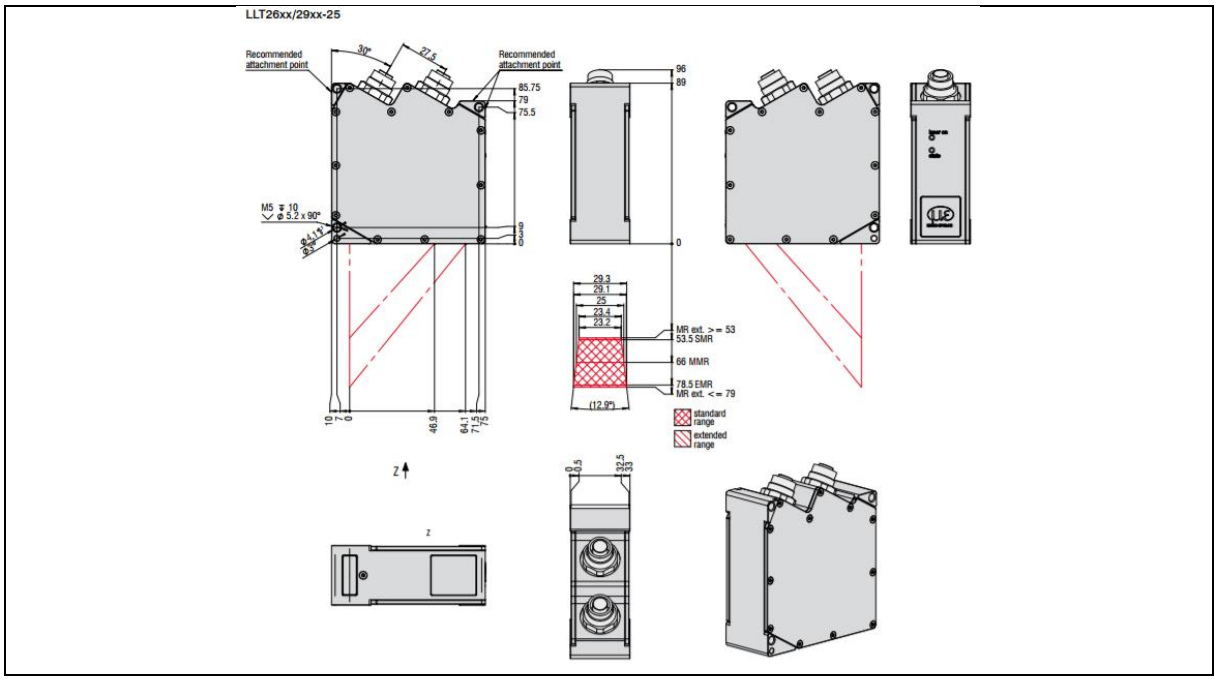

Table 4: MicroEpsilon 2960-25 full documentation

3.3. On board integration

3.3.1. General considerations and requirements

In modern machine tools is possible to achieve large benefits in terms of machining precision and time reduction in both operations and setup by integrating in the machine tool itself an automatic measurement unit[51]. The basic concept resides into the idea of having machining unit and measurement unit sharing the same precision axes. Since this integration largely affects the process effectiveness, four main factors have been targeted as instrumental to be taken into account:

1. The minimization of machine tool workspace loss, in fact the final workspace available result in the intersection among the tool and sensor workspaces (in Figure 31 a schema is reported), this because measurable and machinable points have to coincide
2. The measurement repeatability
3. The need of maintaining the machine tool head free from impediment during machining operations
4. The need of having the possibility of changing the positioning of the sensor according to the work piece specifications

In principle the measurement sensor could be left in a fixed position with respect to the machine tool head, which avoids problems 2 and 3, but on the other hand the distance increases (problem 1) and the flexibility of the system decreases (problem 4).
In particular, in an automatic machine tool a basic and instrumental characteristic is the machine available workspace, which is defined as the volume reachable by the tool (Figure 31). This parameter defines the maximum allowable dimensions for the work piece to be machined and consequently part of the economic value of that specific machine tool.
Since the measurement sensor and the tool share the same axes, the available workspace gets reduced on each axis by a length equal to twice the distance between the measurement sensor and the tool. If, for example, we consider a punching machine with a worktable that travels along the X and Y axes and where the tools travel along the Z axis, we obtain the situation represented in Figure 31. Many other setups share the same problems, so a smart solution for minimizing this loss is required.

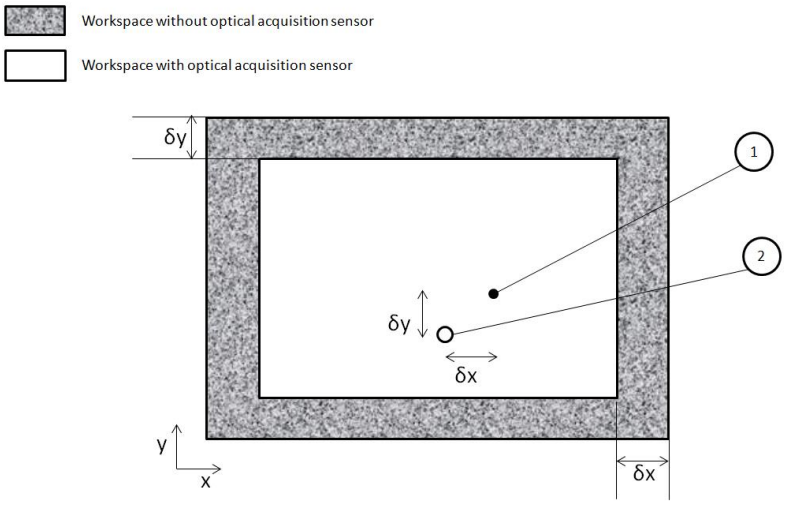

Figure 31: machine tool workspace loss due to sensor integration; 1: optical acquisition sensor, 2: machine tool end-effector

[51] F. Zhao, X. Xu, S.Q. Xie, "Computer-Aided Inspection Planning - The state of the art", Computer in Industry, No. 60, pp. 453-466, 2009

3.3.2. *Integration solution design and development*

A mechanical actuated arm, of which a schema is reported in Figure 32, has been developed in order to satisfy all requirements. The sensor is moved in and out of the workspace thanks to a rotary actuator. The arm geometry and position are adjustable so to adapt to different machine heads, work pieces and machine tool configurations. During measuring operations the rotary movement allows to minimize the distance between sensor and tool head and consequently to minimize the workspace loss, while during machining operations allows to move the sensor out of the way and so to free of any impediment the machine tool (i.e. in Figure 33 a schema is reported). The repeatability of the movement is guaranteed by a precision conical adjustable jig mounted on the arm; tests have been done and reported in 3.3.3.

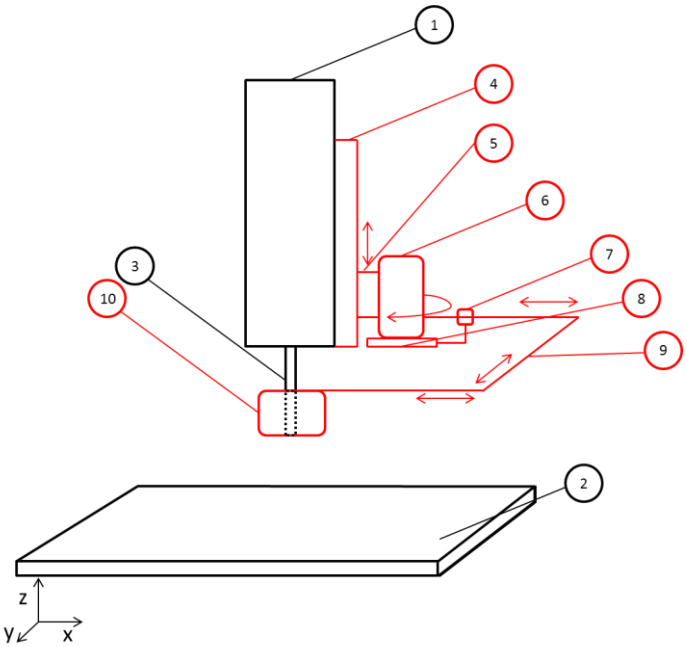

Figure 32: Mechanical sensor integration schema: point 1 represents the machine tool Z axis, point 2 represents the machine tool work plate, point 3 represents the machine tool end effector, point 4 represents a rail which is directly fixed on the machine tool axis, point 5 represents the slider which is able to move along the aforementioned rail, point 6 represents a pneumatic rotating actuator which is capable of move the connected arm around its rotational axis, point 7 represents a mechanical conical adjustable jig able to ensure the motion accuracy and repeatability, point 8 represents the fixed plate on which the fixed part of the jig is mounted, point 9 represents the mechanical arm that carries the sensor and point 10 represents an optical acquisition sensor able to acquire data on any work piece being machined.

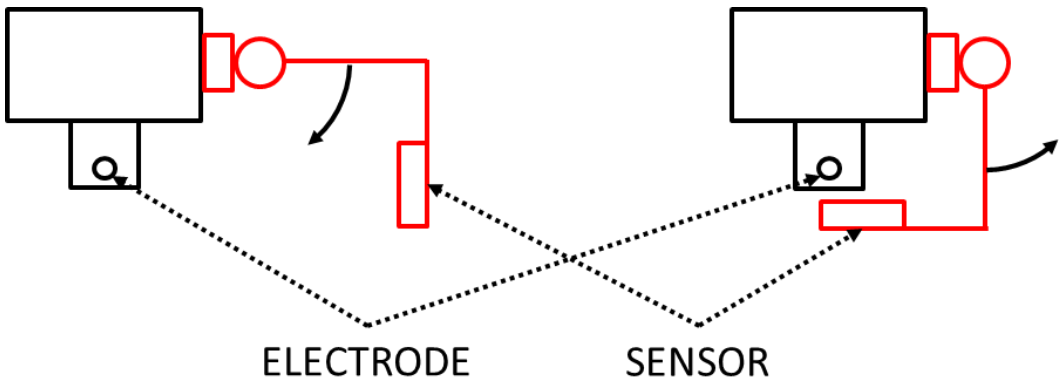

Figure 33: actuated arm positions

Since the chosen laser triangulation sensor measurements are affected by vibrations in the range of 20-500Hz, the rotating arm must be designed in order to be rigid enough not to transmit these ranges of vibrations in the steady state (i.e. in the measuring position, once the complete movement is done).

Component	Manufacturer	Item code
Manual rectilinear guide	Igus	TK-01-30-1, 350 HKA
Linear actuator	SMC	CD85RAY8-30-B
Roteting actuator	SMC	MDSUB20-90D-S7PLS
Aluminum profiles	Kanya	LIGHTWEIGHT EXTRUSION 50x50 TYPE A02-1
Connectors	Kanya	A20-60
Connectors	Kanya	C30-30
Connectors (rail)	Kanya	A32-63
Precision conical jig	Misumi	TPCAT S25

Table 5: list of commercial components used for the first prototype development

For the first prototype (see Figure 34) the commercial components listed in Table 5 have been used for the development of the rotating arm.

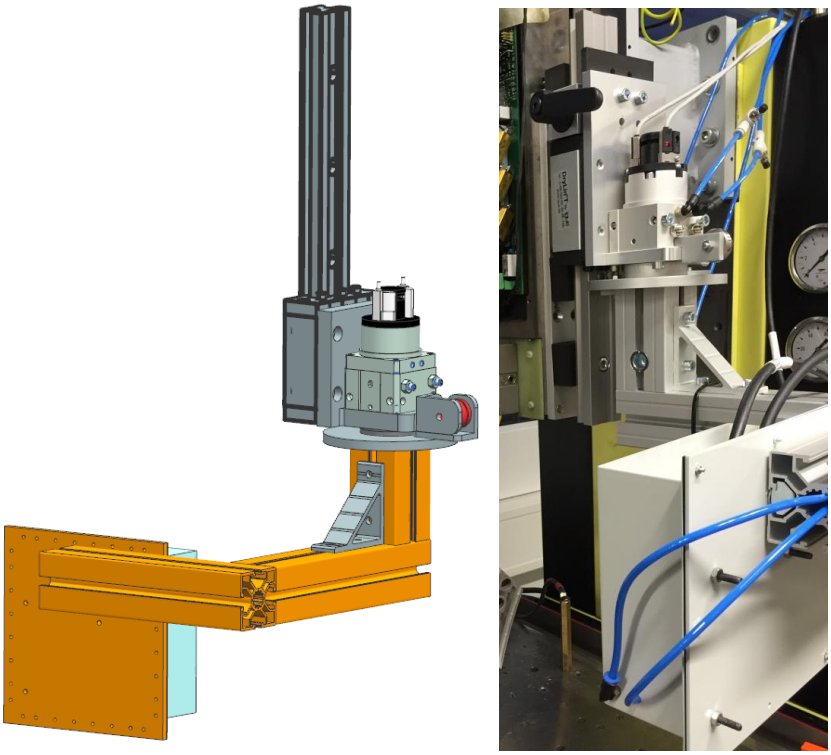

Figure 34: on the left, the CAD representation of the designed actuated arm; on the right, a picture taken from the first prototype of the designed actuated arm

3.3.3. Integration solution testing

In order to measure the effectiveness of the integration solution, a repeatability test has been performed; the calibration artefact (i.e. details are extensively treated in the next chapters) has been acquired 15 consecutive times by means of opening and closing the actuated arm among the two positions (i.e. Figure 33). Then the acquired data are best-fitted (i.e. the procedure is extensively explained in the next chapters) with respect to the first data acquired that functions as a reference. From this best-fit procedure, the deviations, in terms of displacement and inclinations, have been extracted.

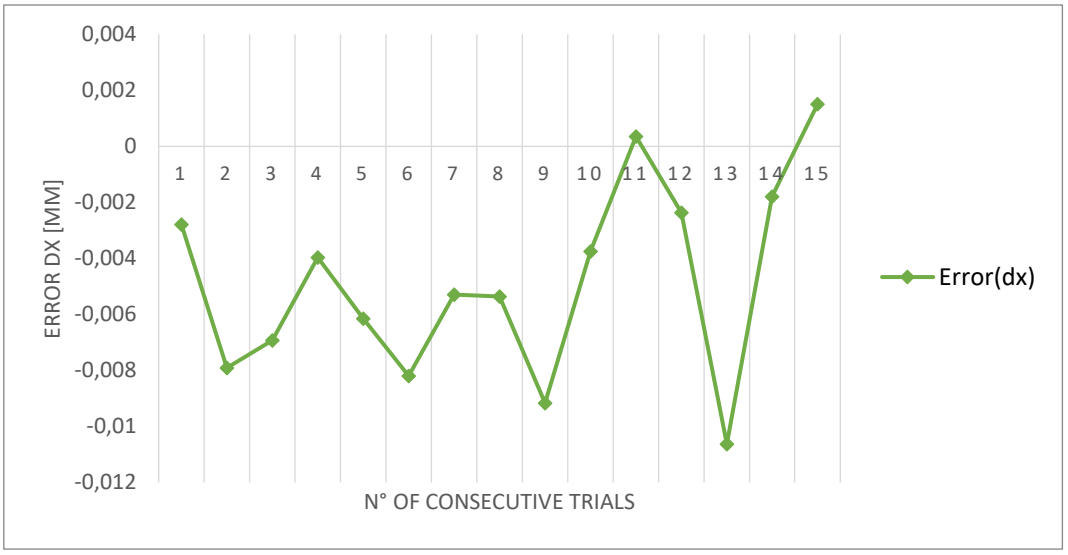

Figure 35: measured error in X direction due to integration solution imperfection

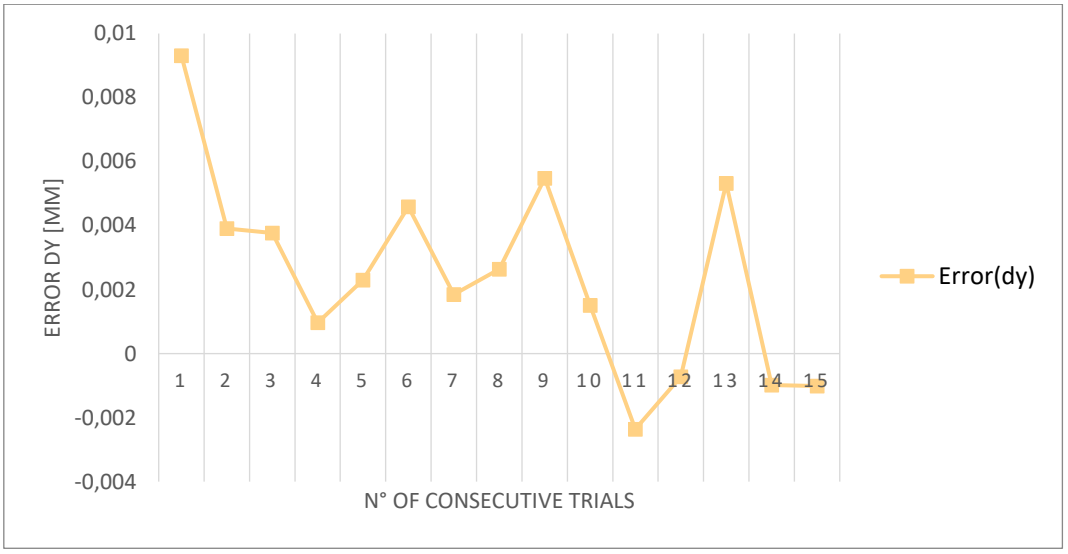

Figure 36: measured error in Y direction due to integration solution imperfection

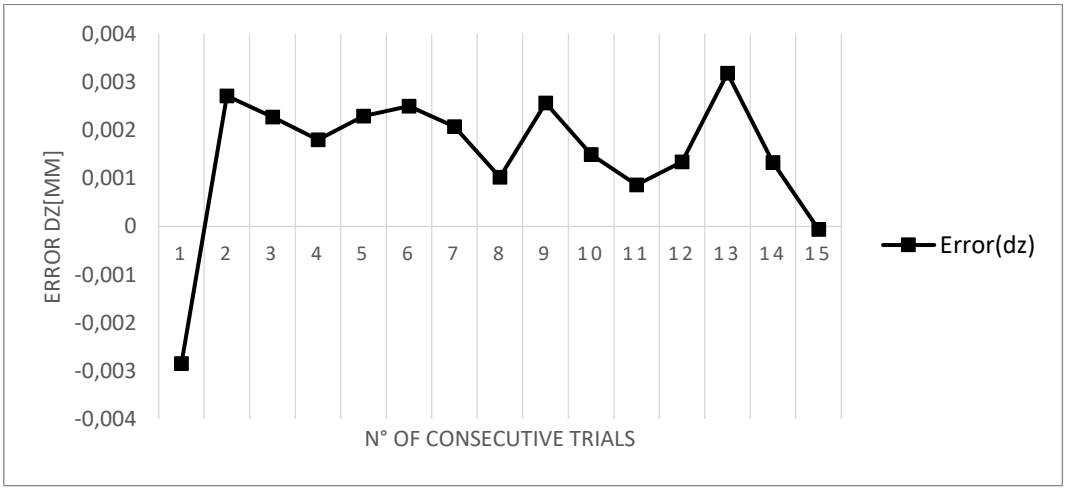

Figure 37: measured error in Z direction due to integration solution imperfection

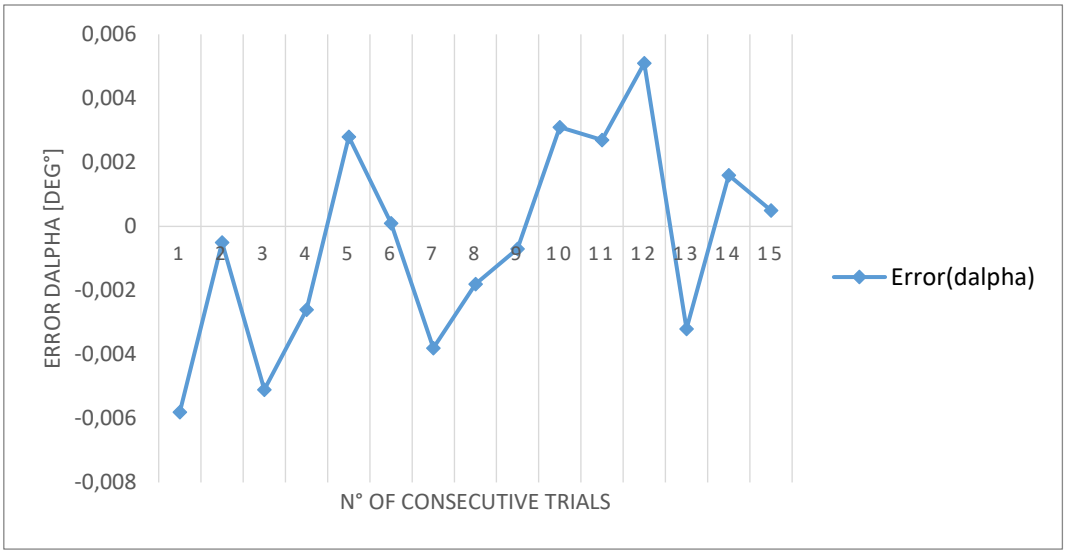

Figure 38: measured error in α angle (inclination around the X axis) due to integration solution imperfection

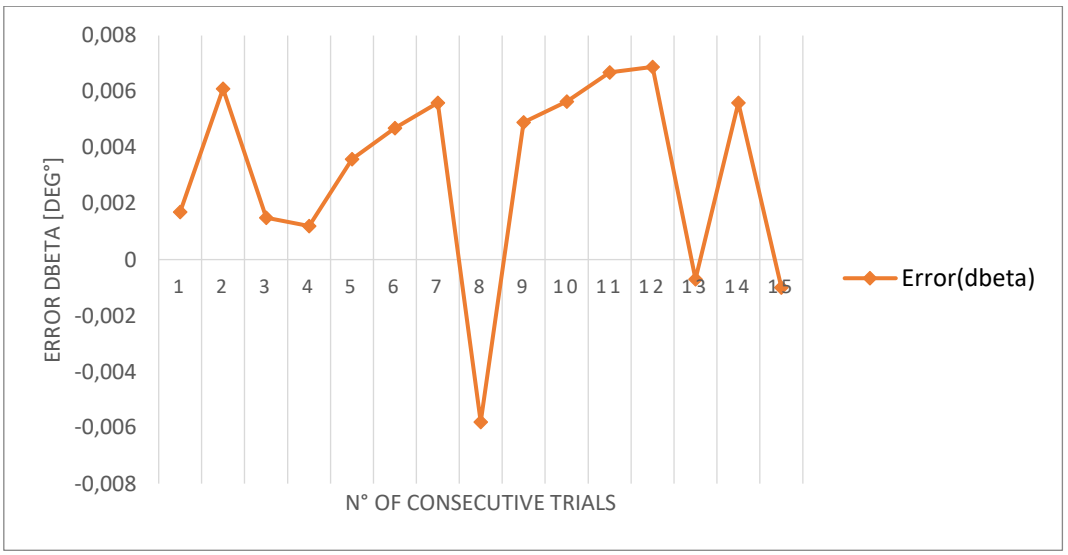

Figure 39: measured error in β angle (inclination around the Y axis) due to integration solution imperfection

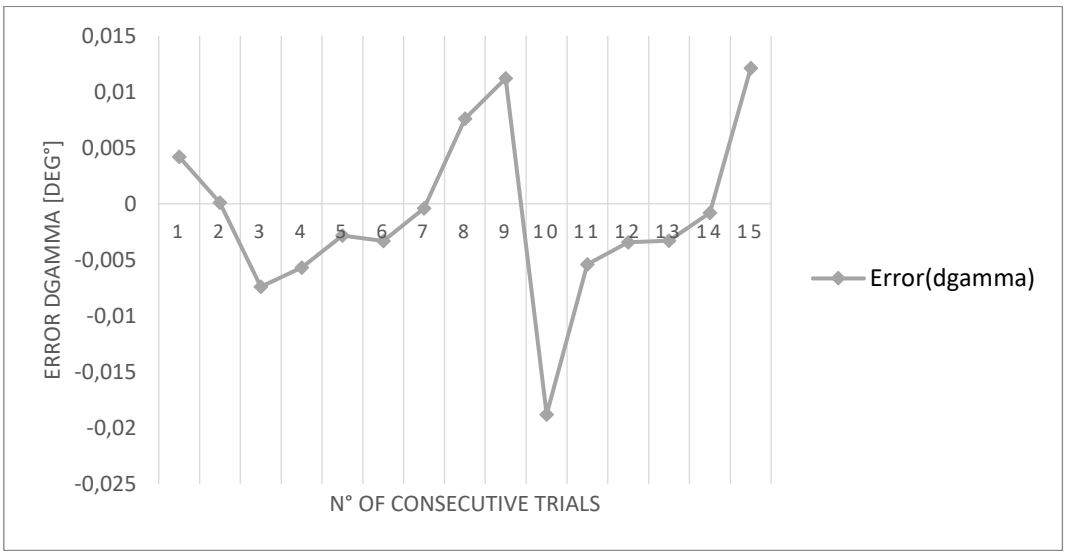

Figure 40: measured error in γ angle (inclination around the Z axis) due to integration solution imperfection

In Figure 35, Figure 36, Figure 37, Figure 38, Figure 39 and Figure 40 are reported the results of the 15 consecutive trials; those results demonstrate the repeatability of the integration solution mechanics, that lays into the a satisfactory range for the required application.

	Min	Max	Average
Dx [mm]	-0,01063	0,001505	-0,00483
Dy [mm]	-0,00236	0,00931	0,002439
Dz [mm]	-0,00285	0,00318	0,001501
dAlpha [deg°]	-0,0058	0,0051	-0,00051
dBeta [deg°]	-0,0058	0,00688	0,003107
dGamma[deg°]	-0,0188	0,0121	-0,00108

Table 6: integration solution repeatability test summary table

In Table 6 are summarized the results of the performed test. The test demonstrates the repeatability of the specific actuated arm prototype developed for SARIX machine tool; however, generalizing the concept, any adopted solution for the on-board integration in any machine tool, must be tested towards the repeatability characterization, since these values represent an error source for the final work piece positioning.

3.3.4. Work piece specimen for experiments

The considered case study for the system experimentation is a dummy turbine blade (its model is reported in Figure 41), realized in metal additive manufacturing and replicating the geometrical characteristics of a production blade airfoil. Many tests have already been conducted on real production turbine blades, although these are not publishable due to confidentiality issues. The micro-features to be realized are the blade cooling holes, which have been designed in order to reproduce real scenarios in terms of size, positioning and geometry.

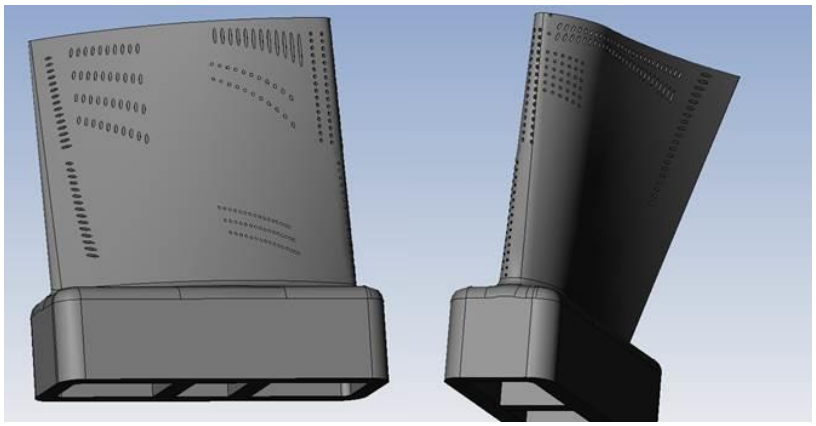

Figure 41: dummy turbine blade

3.3.5. Data post processing software environment

In order to handle the point cloud data specific software tools and complex algorithms need to be used. In this field there are many existing software packages for surface reconstruction/modelling, measurements and for the automatic comparison of the work pieces with respect to their nominal CAD model. The software package used for this experimentation is HEXAGON METROLOGY 3D Reshaper, however there exist many others like 3DSYSTEMS Geomagic, MVTec Halcon, COGNEX VisionPro and MATLAB. All the conducted experimental work can be easily migrated to any of these software packages.

3.4. System calibration

A system calibration procedure is necessary to express the measurements performed by the sensor into the machine tool reference frame. This requires to define the transformation matrixes between the sensor and the machine tool reference systems in terms of offset angles and translations.

3.4.1. Calibration artefact

In order to allow the calculation of the aforementioned matrix, a calibrated artefact has been developed (in Figure 42 is reported its CAD model); this is specifically designed to allow the extraction of reference points with both measurement systems: tactile (using the machine tool electrode as pointed out in 3.3.4) and optical (with the integrated laser triangulation sensor as described in Table 4). The former requires regular fine grinded geometries and a highly electrically conductive material, while the latter sufficiently large reference surfaces and adequately reflective material and surface finish. In the state of the art section (see Figure 18) have been reported some standard artefacts for the calibration of laser based measurements system; however, due to the fact that the same reference standard need to be measured by two different systems, a totally new design have been done.

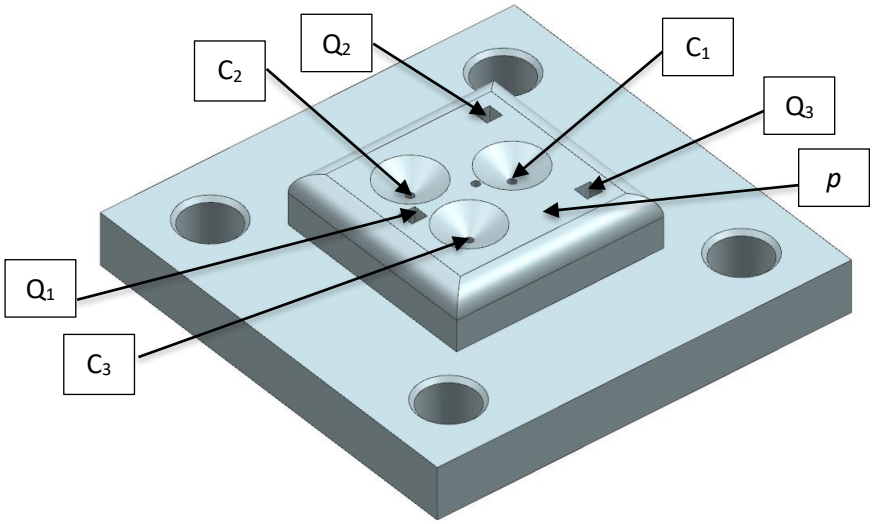

Figure 42: calibrated artefact

In Figure 43 is reported also the bi-dimensional working drawing together with the related dimensions and tolerances. The machining of the artefact is performed with a SARIX machine tool via micro-EDM process in order to achieve the requested accuracy.

The calibrated artefact is directly mounted on the machine tool plate in a fixed position via four fasteners, so that it can be reached, in terms of physical access, to both the machine tool end-effector (electrode) and the laser triangulation sensor.

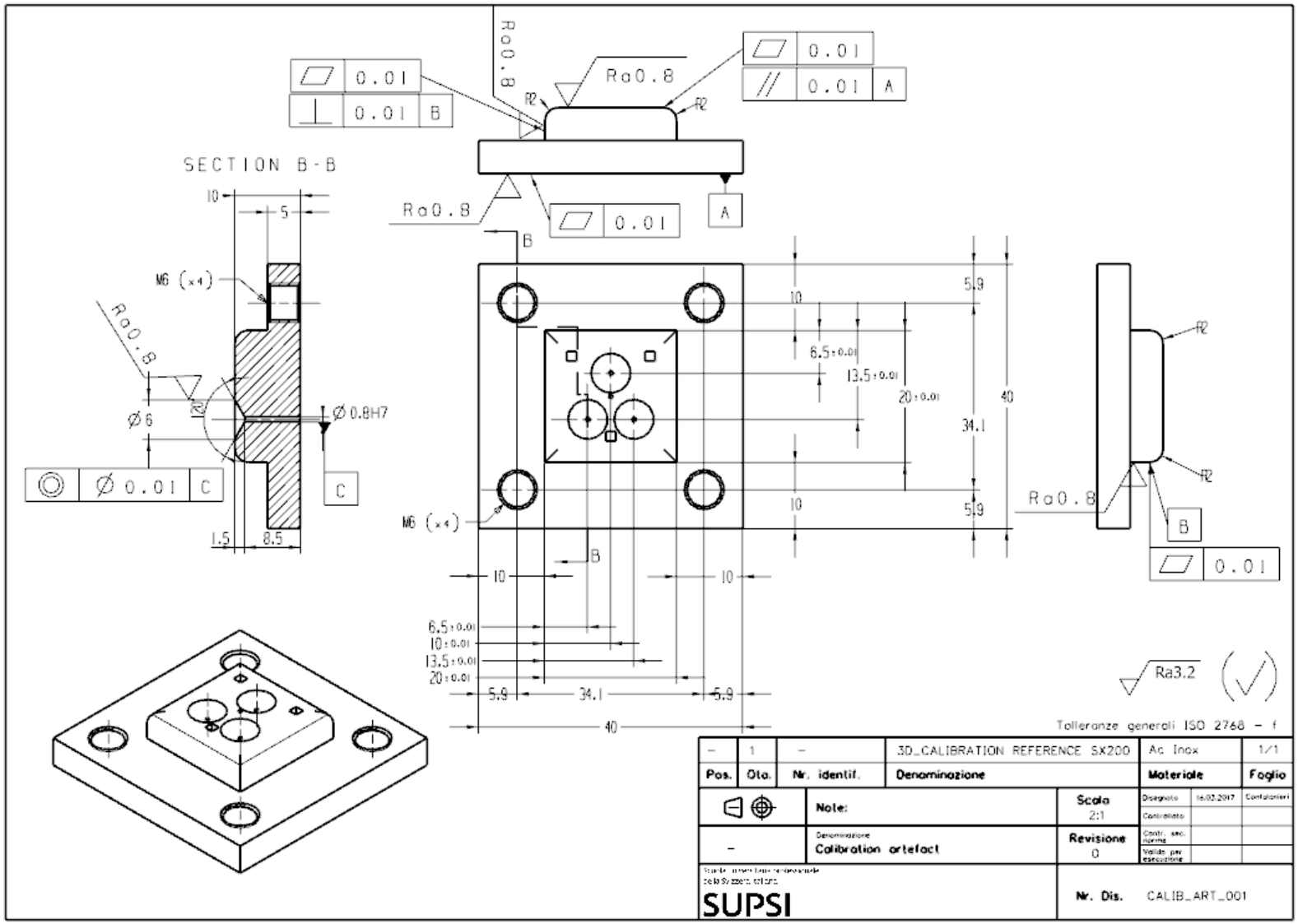

Figure 43: calibrated artefact dimensional drawing

The artefact satisfies all the aforementioned requirements allowing the accurate measurement of specific references such as the cones centre (C_1, C_2, C_3), squares centre (Q_1, Q_2, Q_3) used as a final test feature, and the versor of the plane p. The aforementioned measurements allow to define the transformation matrix between the sensor and the machine tool reference systems in terms of offset angles and translations. In 3.4.2 the full calibration procedure developed is pointed out, and in 4.1 the experimental results are reported.

3.4.2. Calibration procedure development

The artefact is mounted on the machine tool work plate, and the reference points are measured by both systems. The transformation matrixes are then calculated by comparing the coordinates of these reference points in the two reference systems. Specifically, the cones/holes centres are used to measure the translation vector (T_{sm}) that expresses the translation between the machine tool end effector and the laser triangulation sensor reference frame, while the inclinations of the calibrated planes are used to calculate the rotation matrix (R_{sm}) that expresses the rotation between the two reference systems. Squares slot centres (Q_1, Q_2, Q_3) are used as reference at the end of the process to double-check the calculated transformation matrixes.

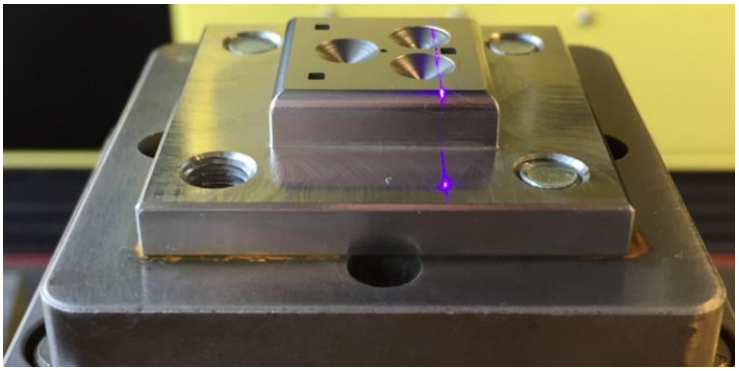

Figure 44: acquisition of the calibration artefact

The laser triangulation sensor scans the artefact (in Figure 44 is reported an example of the acquisition procedure of the calibration artefact; in Figure 45 is reported an example of the laser triangulation sensor measurement of the calibration artefact) and the necessary data is obtained by means of extracting (i.e. by means of a surface best-fitting procedure) the three cones (C_1, C_2, C_3) and the plane p, while the machine tool electrode (i.e. via touch probing procedure) measures the same parameters by means of finding the centre of the three calibrated holes and by measuring the coordinates of several points on the upper and lateral surfaces.

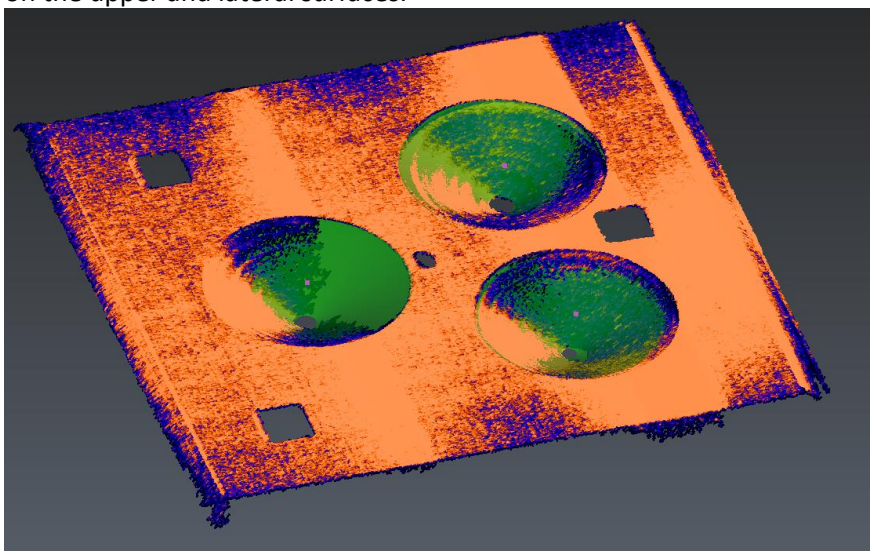

Figure 45: best fitted cones C1, C2 and C3 and plane *p* from the laser triangulation sensor point cloud data acquired

Additionally, in order to correctly calculate the translation vector it is necessary to subtract the machine coordinates of the starting point of the scan ($\boldsymbol{V_0}$); in fact, these coincide with the origin of the laser scanner reference frame for each specific scan, which varies depending on the needs of each measurement position throughout the machine tool workspace. In Figure 46 is reported a simplified schema of the displacements of the machine tool and the laser triangulation sensor reference frames.

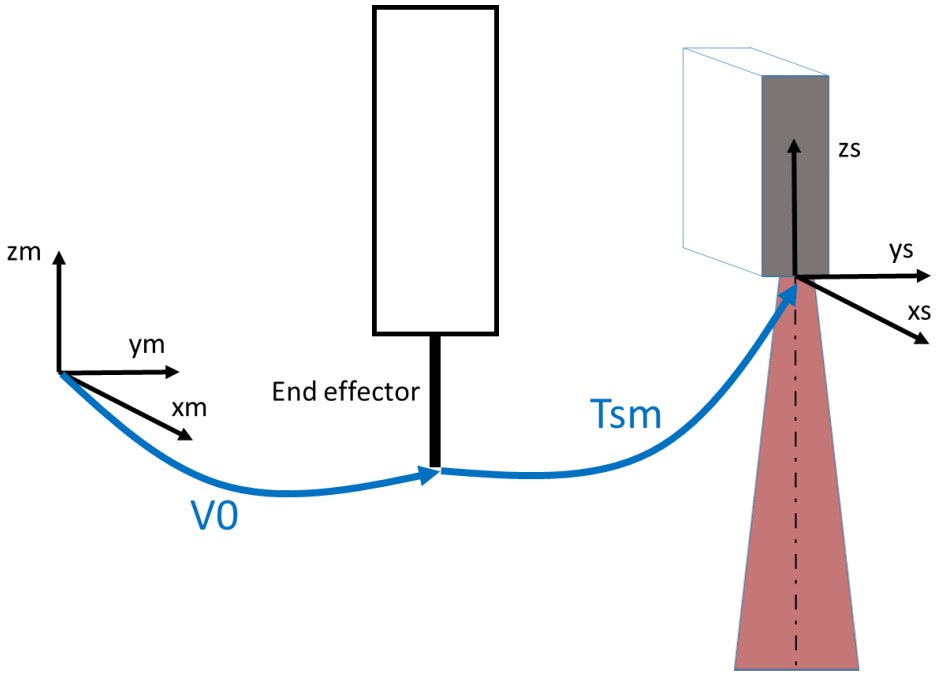

Figure 46: simplified schema of displacements of machine tool and laser triangulation sensor reference frames

Hereby are reported the governing equations of the calibration problem; the inclinations measured by the machine tool electrode (i.e. extrapolated from the plane *p* versor) and expressed with respect to the machine tool reference frame are required so to consider the mounting of the calibration target on the machine plate as well:

$$\alpha = r_{x\,m} - r_{x\,s} \quad \beta = r_{y\,m} - r_{y\,s} \quad \gamma = r_{z\,m} - r_{z\,s} \tag{2}$$

$$\mathrm{R}_{x\alpha} = \begin{bmatrix} 1 & 0 & 0 \\ 0 & cos\,\alpha & -sin\,\alpha \\ 0 & sin\,\alpha & cos\,\alpha \end{bmatrix};\ \mathrm{R}_{y\beta} = \begin{bmatrix} cos\,\beta & 0 & sin\,\beta \\ 0 & 1 & 0 \\ -sin\,\beta & 0 & cos\,\beta \end{bmatrix};\ \mathrm{R}_{z\gamma} = \begin{bmatrix} cos\,\gamma & -sin\,\gamma & 0 \\ sin\,\gamma & cos\,\gamma & 0 \\ 0 & 0 & 1 \end{bmatrix} \tag{3}$$

$$R_{sm} = \mathrm{R}_{z\gamma}\mathrm{R}_{y\beta}\mathrm{R}_{x\alpha} \tag{4}$$

$$T_{sm} = \begin{vmatrix} x_m - x_s - x_{V0} \\ y_m - y_s - y_{V0} \\ z_m - z_s - z_{V0} \end{vmatrix} \tag{5}$$

The calculated transformation matrixes ($\boldsymbol{R_{sm}}$ and $\boldsymbol{T_{sm}}$) are then applied, together with the additional translation vector representing the starting point of each scan ($\boldsymbol{V_0}$), to each measurement performed allowing to calculate the points coordinates in the machine tool workspace ($\boldsymbol{P_m}$) starting from the coordinates in the sensor reference frame ($\boldsymbol{P_s}$).

$$P_m = R_{sm}(P_s - V_0) + T_{sm} \tag{6}$$

Equation (6) represents the general rule valid for transforming each point acquired with the laser triangulation sensor in its reference frame, into the same point expressed in the machine tool reference frame.

However, this does not take into account for measurements deformations due to mounting misalignment of the laser triangulation sensor. In fact, mounting misalignments angles α, β and γ shown in Figure 47, produce a slightly deformed acquisition due to the fact that the axis used for the sensor motion are not exactly parallel with the sensor ones, due to mounting imperfections.

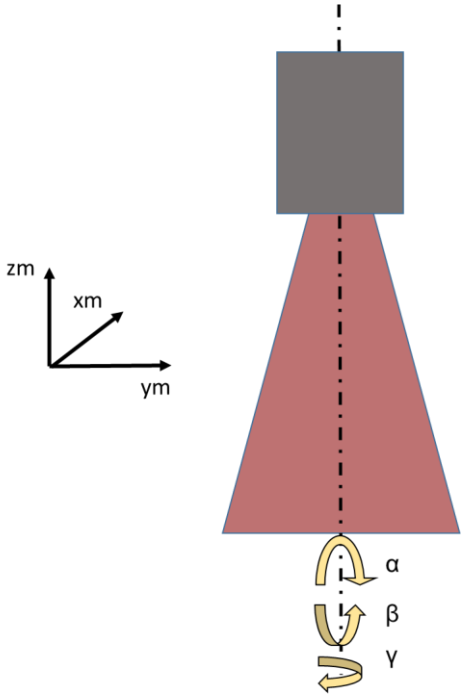

Figure 47: laser triangulation sensor angle mounting misalignments

This leading to the need of an iterative procedure in order to firstly measure α, β and γ, then compensate for the deformation (i.e. by means of repositioning each of the points acquired by the laser sensor; the full method is described in the next paragraphs), re-measure α, β and γ, until the difference between two subsequent measurements lays below the desired threshold. Once the final values of α, β and γ are defined, the deformation compensation algorithm needs to run for each of the acquisitions performed by the sensor. In this way, the laser triangulation sensor does need only an initial coarse mechanical alignment during mounting; the fine alignment will be compensated by the aforementioned algorithm.

3.4.3. Angles α and γ measurement

In order to measure α and γ angles, the following procedure has been followed:

The α_m seen from the machine tool (i.e. via touch probing procedure) and α_s, seen from the laser sensor are calculated:

$$\alpha_m = \arctan[(C_{3mz} - C_{2mz})/(C_{3my} - C_{2my})] \quad (7)$$

$$\alpha_s = \arctan[(C_{3sz} - C_{2sz})/(C_{3sy} - C_{2sy})] \quad (8)$$

The γ_m seen from the machine tool (i.e. via touch probing procedure) and γ_s, seen from the laser sensor are calculated:

$$\gamma_m = \arctan[(C_{2mx} - C_{3mx})/(C_{2my} - C_{3my})] \quad (9)$$

$$\gamma_s = \arctan[(C_{2sx} - C_{3sx})/(C_{2sy} - C_{2sy})] \quad (10)$$

3.4.4. Angle β measurement

The angle β has to be treated differently, since misalignments, from the laser sensor point of view, are more difficult to be measured. In fact, a β angle does not produce a direct effect on the calibrated artefact inclination, but, instead, it produces a variation in x and z coordinates. In order to measure this effect, as shown in Figure 48, the calibration artefact is measured two times at two different known machine tool Z coordinates (i.e. Z_m) allowing the extrapolation of the angle β, equation (11).

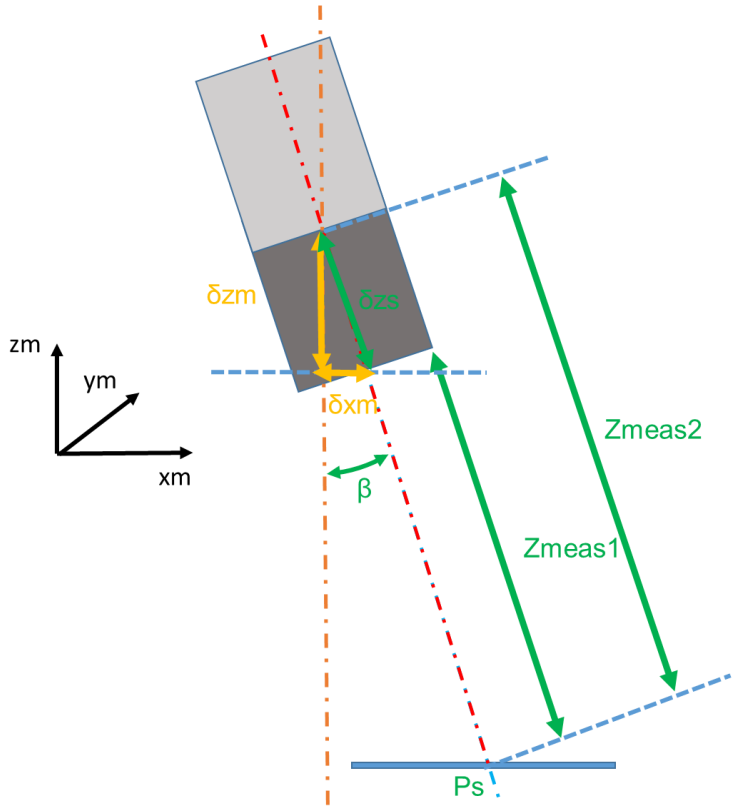

Figure 48: double shot acquisition procedure to measure β misalignment

$$\beta_s = \arcsin[\delta xm/(20 + \delta dzs)] \quad (11)$$

In this case the measurement of the machine tool electrode is not required, since the inclination of the calibration artefact mounting does not affect the measurement.

3.4.5. Final calibration equations and alignment testing

As introduced in 3.4.2, the measurements performed with the laser triangulation sensor are affected by a deformation due to the misalignments between the sensor and the machine tool reference frames originated by the imperfect mounting. As a consequence, equation (6) has to be corrected into the (12), and the input values for the angles α, β and γ need to be calculated as pointed out in 3.4.3 and 3.4.4.

$$P_m = R_{sm}(P_s - V_{si}) - V_0 + V_{si} + T_{sm} \quad (12)$$

Where:

$$V_{si} = \begin{vmatrix} x_{si} \\ 0 \\ 0 \end{vmatrix} \quad (13)$$

Where x_{si} represents the X coordinate of each single laser line (i.e. values correspond to the sensor trigger gathered from machine tool X axis linear encoder) expressed in the sensor reference frame. This because, being the effect of the misalignment resulting in a deformation of the measured point cloud, this cannot be treated as a rigid body; instead each point has to be corrected singularly.

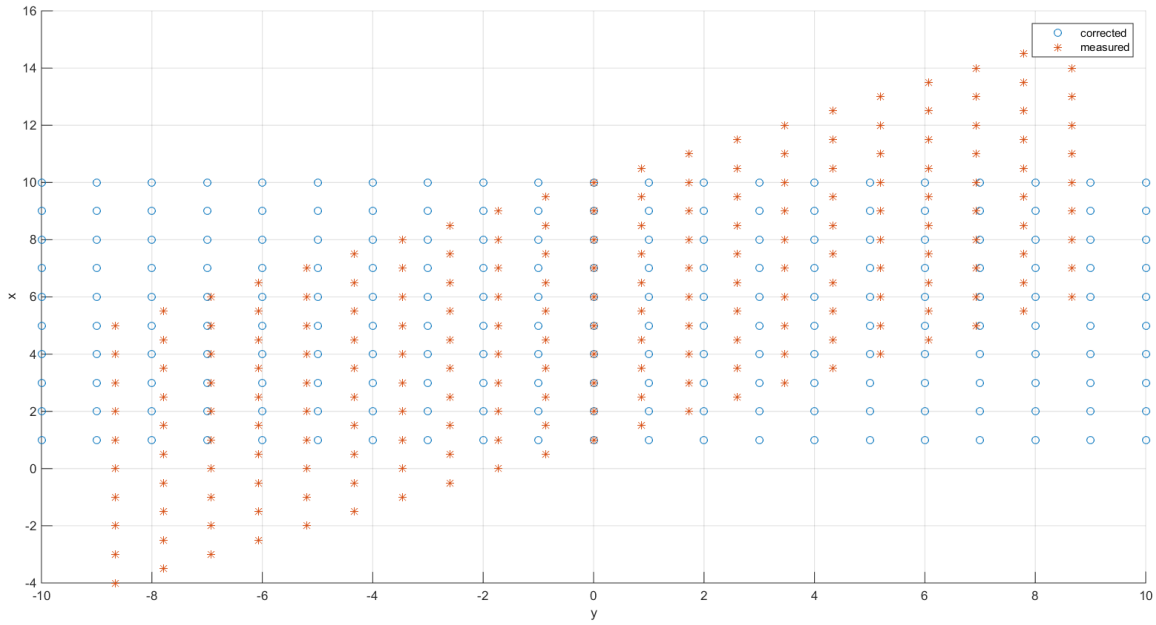

Figure 49: example of deformation correction due to a sensor misalignment in γ

In Figure 49 is reported a simplified example with exaggerated value of misalignment of γ, showing the effect of the correction just described.

3.4.6. Angles measurement results

In Figure 50 are reported 17 consecutive trials of the complete measurement procedure of misalignment angles α, β and γ. The standard deviation relative to these trials is respectively 0.0028, 0.0220 and 0.0234. This result is perfectly compatible with the expected repeatability required for the scope of the activity.

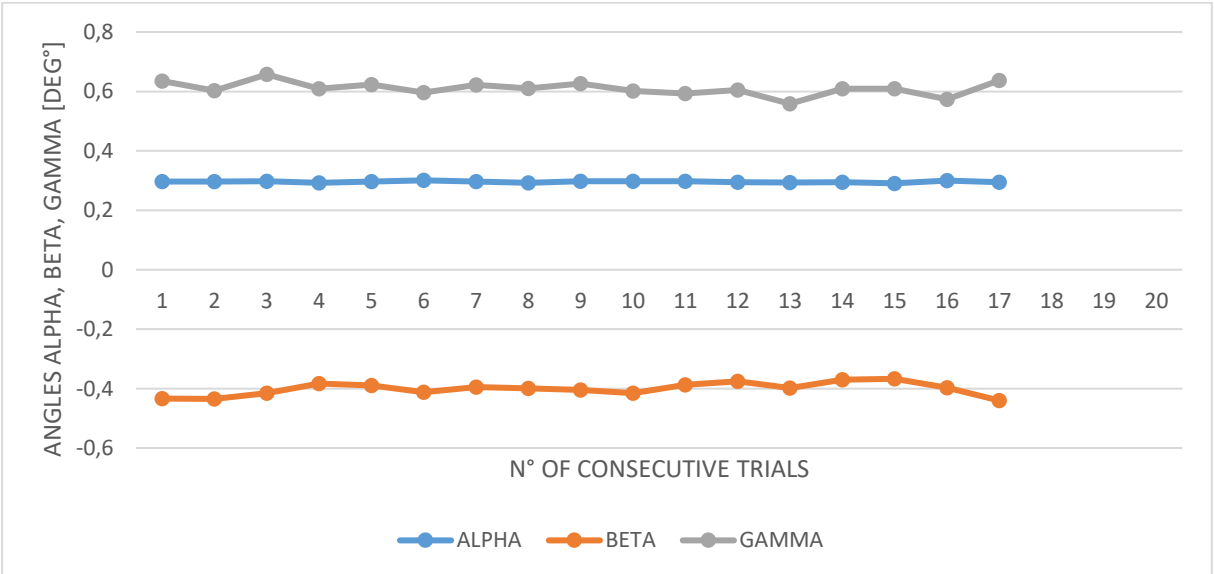

Figure 50: measurement of misalignment angles α, β and γ in 17 consecutive trials

As stated in 3.4.2, the misalignment angles α, β and γ cause the laser sensor acquisition to be deformed; this leading to the need of an iterative procedure in order to calculate a sufficiently accurate

value of the three angles. At every iteration the angles are re-calculated with a dataset compensated with the angles calculated at the previous step.

In the following graphs (Figure 51, Figure 52, Figure 53) are reported the trends of α, β and γ values calculated at five algorithm iterations.

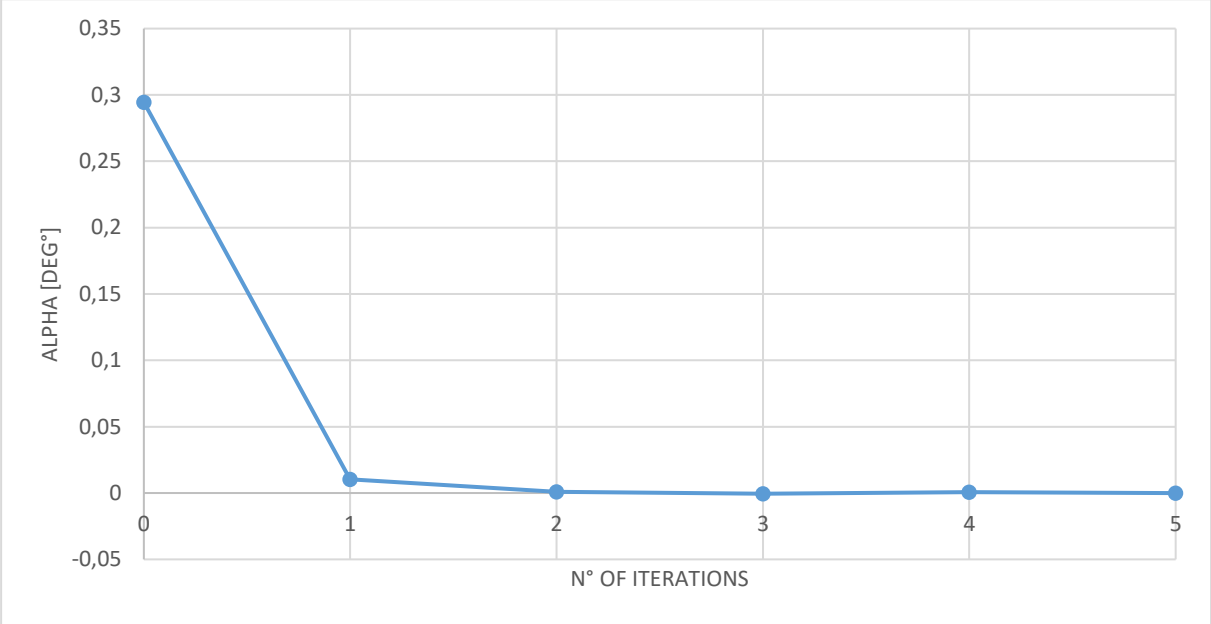

Figure 51: 5 iterations of the misalignment correction procedure of α angle

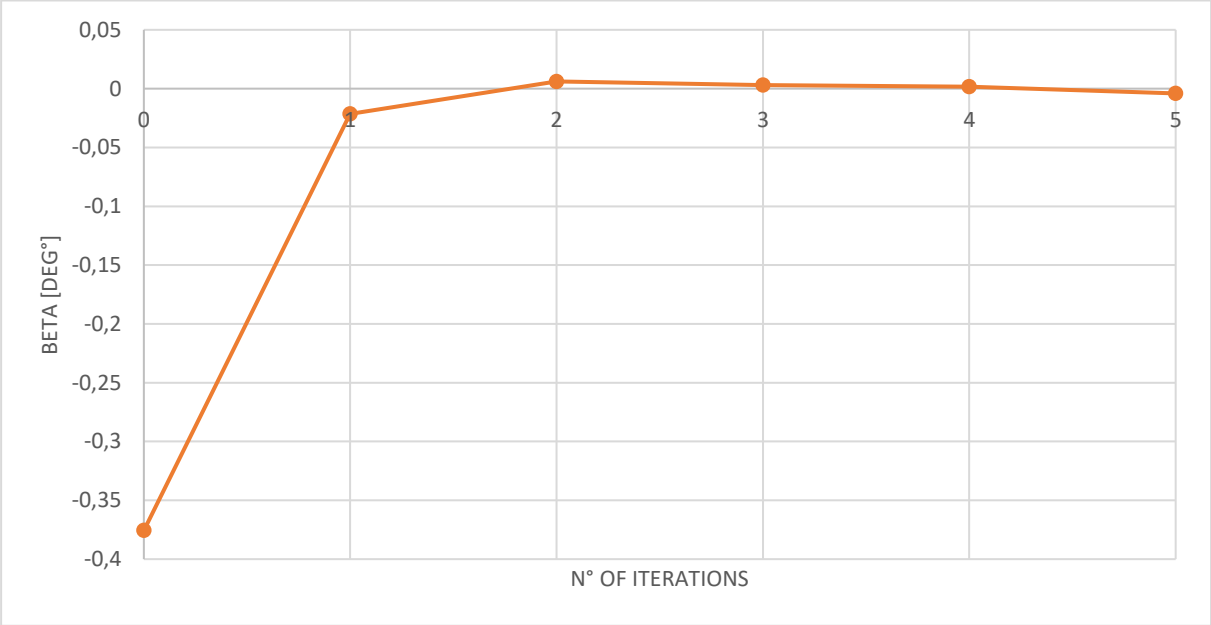

Figure 52: 5 iterations of the misalignment correction procedure of β angle

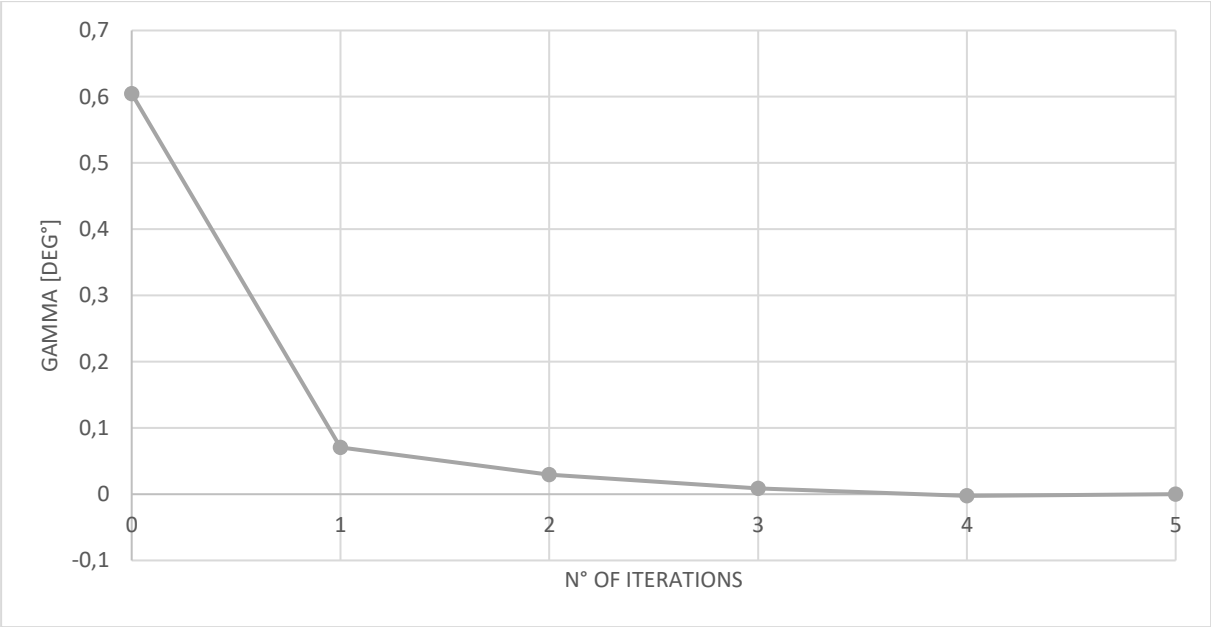

Figure 53: 5 iterations of the misalignment correction procedure of γ angle

Since from the first iteration, the values of the angles are sufficiently close to zero for the scope of the work, just this first iteration will be included in the final procedure allowing also to save time in production.

As a consequence equation (4) is corrected into the following:

$$R_{sm} = \mathrm{R}_{z\gamma 1}\mathrm{R}_{y\beta 1}\mathrm{R}_{x\alpha 1}\mathrm{R}_{z\gamma 0}\mathrm{R}_{y\beta 0}\mathrm{R}_{x\alpha 0} \qquad (14)$$

3.5. Positioning procedure

3.5.1. Positioning procedure development – local adaptive method

In order to correct the position of the blade on board the machine tool a dedicated positioning procedure has been developed. The procedure is carried out by means of scanning the work-piece, translating the measured data into the machine tool reference frame through the use of the parameters calculated in the calibration procedure and finally solving dedicated algorithms in order to calculate the corrected position with respect to the nominal CAM data.
The first step is the acquisition of a portion of the actual work-piece mounted into the machine tool. The portion to be acquired is chosen so to include the area to be machined (the one in which cooling holes have to be realized) by means of properly setting the position ($\boldsymbol{V_0}$) of the linear axes and the angular position ($\boldsymbol{A_0}, \boldsymbol{B_0}$) of the work piece through the rotating axes A and B.
The acquisition is carried out by means of moving the work piece below the sensor with the machine axis paired to the sensor, which triggers the process. The sensor produces a point cloud dataset, which is then elaborated and transferred to the machine tool reference frame by means of applying formula (12). Moreover, a further translation vector is applied to the whole dataset in order to position the machine tool coordinate system into the point representing the centre of rotation of the A and B axes (in Figure 54 is reported as point C). All the following procedures have to be considered referred to this coordinate system.

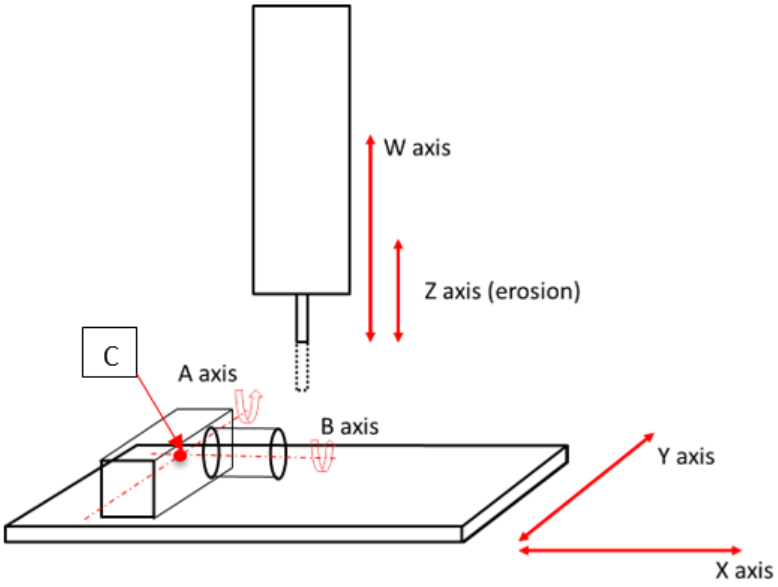

Figure 54: kinematic structure of SARIX SX200 Aero. Point C represents the center of rotation of A and B axes

The dataset is now located in its acquisition position and has to be transferred in its nominal machining position; this is done by means of applying (15) and (16) in sequence to the entire dataset itself.

$$\mathrm{R}_0 = \mathrm{R}_{\mathrm{x}(-B_0)}\,\mathrm{R}_{\mathrm{y}(-A_0)} \qquad (15)$$

$$\mathrm{R}_1 = \mathrm{R}_{\mathrm{y}(A_{wn})}\mathrm{R}_{\mathrm{x}(B_{wn})} \qquad (16)$$

Where A_{wn} and B_{wn} represent the nominal machining angles relative to the set of cooling holes to be machined with that inclinations of A and B axes.
This rotations sequence is necessary due to the machine tool kinematics structure detailed in 3.1.2, and thus represents a specific configuration made for SARIX machine tool; however a migration to any kinematic structure can be done easily, and this specificity does not affect the generality of the proposed approach.

At this point the CAD file of the work-piece in the nominal machining position is also loaded in the scene together with all points and lines, gathered from CAM system, representing the axes and the position on the blade of the cooling holes to be machined; the CAD file coupled with these information is referred as machining model hereafter (an example is provided in Figure 55).

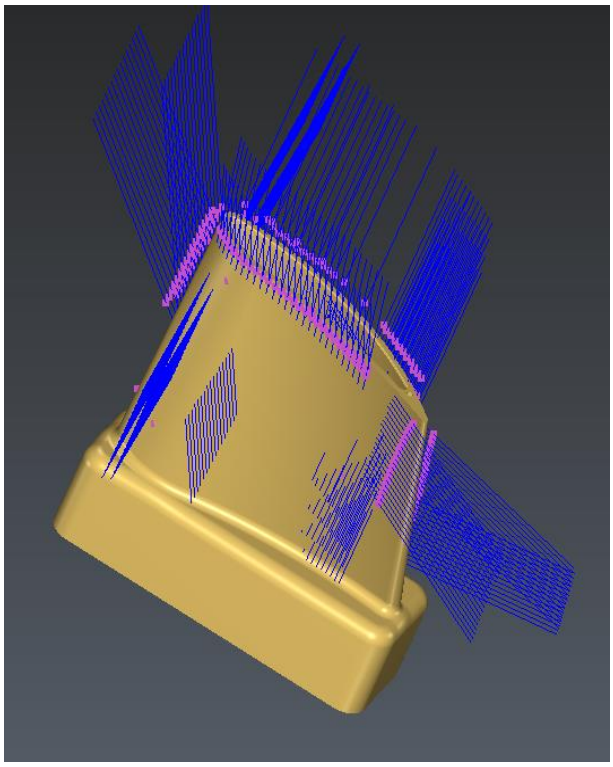

Figure 55: machining model example

In the nominal machining position, the versors representing the axes of the set of cooling holes to be machined are all parallel to the machine tool Z axis.
Then, the nominal CAD model surface is best fitted, through an ICP algorithm (i.e. best fit means the transformation that minimizes the distance with other objects in a least squares sense. The working method is based on ICP-Iterative Closest Point, and the overall algorithm is proprietary of the commercial software used: Hexagon Metrology 3D-Reshaper), to the acquired dataset, allowing the correction of its nominal positioning along all the six degrees of freedom. At this point the CAD model position coincides with the actual position of the work piece in the machine tool workspace, both in terms of translations and inclinations, and so the machining starting points coordinates differ from the nominal ones and the versors of the cooling holes' axes are not anymore parallel to the machine tool Z axis (17), accounting in fact for a difference equal to the positioning correction applied.

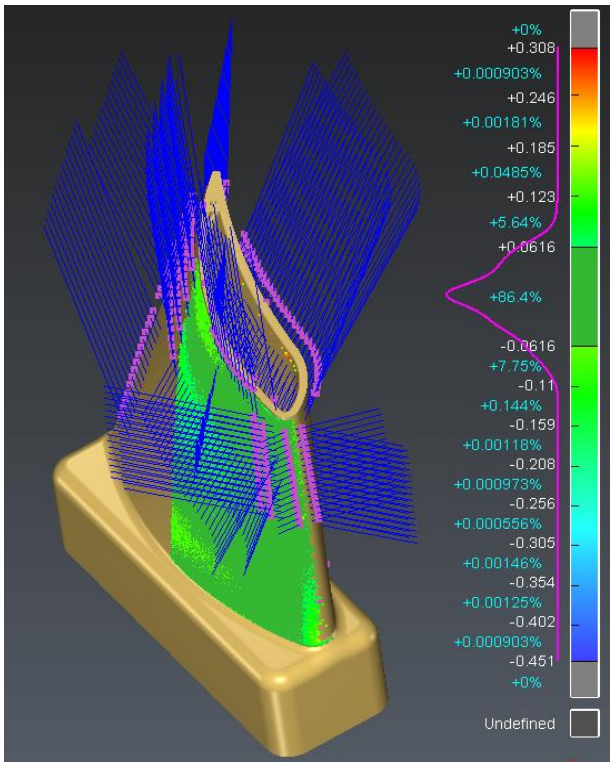

Figure 56 Best fit ICP algorithm result example

The final step is the calculation of the corrected machining position by means of calculating the angle values of A and B that bring the versors direction back to be parallel with the machine tool Z axis. This is achieved by means of applying (18) to the machining model and then solving (19).

$$V_{hole} = \begin{vmatrix} V_x \\ V_y \\ V_z \end{vmatrix} \quad (17)$$

$$\mathrm{R}_2 = \mathrm{R}_{\mathrm{x}(-B_{wn})}\mathrm{R}_{\mathrm{y}(-A_{wn})} \quad (18)$$

$$\mathrm{R}_{\mathrm{y}(A_{wc})}\mathrm{R}_{\mathrm{x}(B_{wc})}V_{hole} = \begin{vmatrix} 0 \\ 0 \\ 1 \end{vmatrix} \quad (19)$$

$$\mathrm{R}_3 = \mathrm{R}_{\mathrm{y}(A_{wc})}\mathrm{R}_{\mathrm{x}(B_{wc})} \quad (20)$$

Where A_{wc} and B_{wc} represent the corrected machining angles relative to the set of cooling holes to be machined.
Finally, (20) is applied to the machining model, obtaining the corrected coordinates of the cooling holes to be machined both in terms of translations and inclinations.

3.5.2. Alternative method for positioning – six points constrained method

Often, as stated in the state of the art section, the turbine blade producers refer all the machining operations performed on the blades, to a predefined coordinate system positioned with respect to six points collocated on the airfoil surface and defined with respect to the turbine rotating shaft. The method described in 3.5.1, does not take into account for this industrial constraint; as a consequence an alternative method is hereby presented, and it has been developed, together with SARIX SA, in order to be able to make the system compliant with this standard as well if needed.

This method and the relative equations are identical to the ones expressed in 3.5.1, the only difference resides into the best fit algorithm needed to make the CAD model position coincide with the actual position of the work piece in the machine tool workspace, and thus accounting for corrections. In this case the best fit operation is constrained to firstly minimize the distance of the six points in the CAD and the same six points on the acquired dataset. The main issue is then related to the correct identification of these six points on the dataset itself.

The identification procedure starts with the acquisition of many portions of the blade (i.e. the number depends by the physical dimensions of the blade with respect to the measuring range of the sensor, Table 4), so to be able to reconstruct its entire geometry.
To each of the dataset representing each of the portions of the blade acquired, (12), (15) and (16) are thus applied in sequence in order to reposition all the acquired datasets in the nominal machining position.

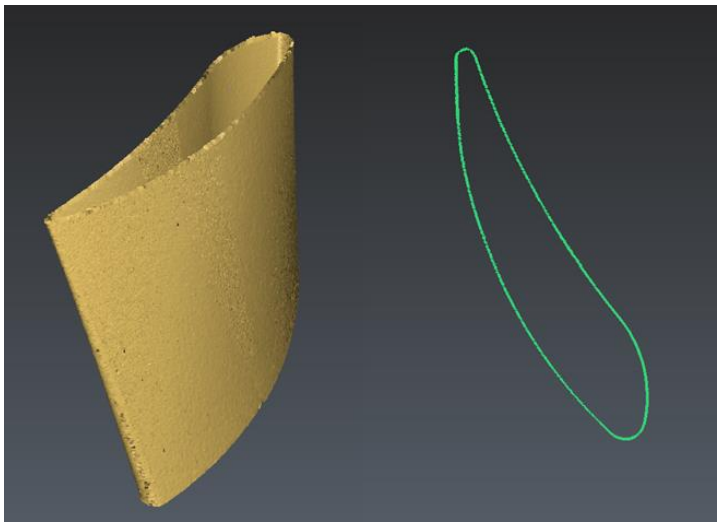

Figure 57: on the left: example of reconstruction of the entire airfoil surface, on the right: a cross-section of the blade reconstruction on the left

At this stage, the acquisition portions are merged together so to consider them as a whole rigid body (in Figure 57 is reported an example of a complete reconstruction of the airfoil of the considered specimen - Figure 41). Then the ICP surface best-fit algorithm is applied and the whole reconstructed airfoil is fitted on its CAD model which contains the aforementioned six points in the nominal position. At this stage the corresponding points on the reconstructed geometry can be identified (in Figure 58 is reported an example, where the points are easily identifiable with blue spheres constructed on them) by means of finding the points at the minimum distance with the nominal ones.

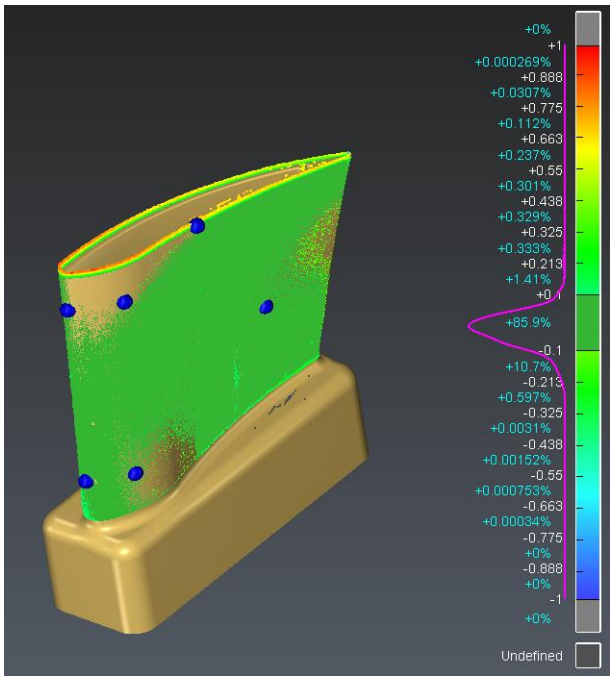

Figure 58: the six airfoil nominal points identified on the reconstructed blade geometry best fitted with its CAD model

Once these points have been identified, a second best fit algorithm is applied minimizing the distance between the identified points and the correspondents on the machining model. This second best fit replaces the one described in 3.5.1, and provides the actual positioning of the turbine blade on the machine tool used for completing the positioning procedure. In Figure 59, is reported an example of the best fit operation with the machining model; in pink are highlighted the six pairs of points (i.e. pertaining respectively to the acquired dataset and to the machining model) of which relative distance has been minimized.

Both the proposed methods account for specific equations describing the specific machine tool kinematic structure, however, the method is easily extensible to any different machine tool with a different kinematic disposition.

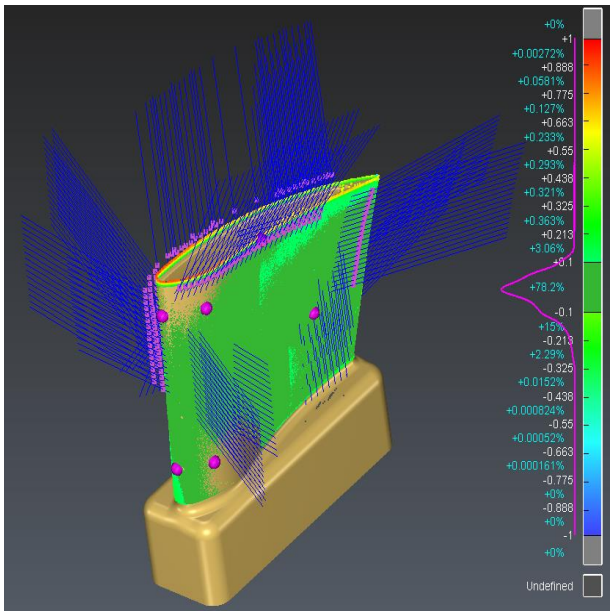

Figure 59: example of results of alternative, six points based, best fit procedure

As it can be seen from the comparison between Figure 58 and Figure 59, the best fit results are slightly different; this is due to different procedures just presented and, as expected, the six points based one, presents a slightly higher deviation.

3.5.3. A-B axes centre of rotation localization

In paragraph 3.5.1 has been introduced the A-B axes centre of rotation (i.e. named Point C in Figure 54), which represents the datum point of the reference system for the calculations performed in the whole positioning procedure, with both the presented methods. As a consequence, the localization of this point largely affects the accuracy of the whole procedure. In order to localize this point, a high precision measuring gauge (a picture is reported in Figure 60) provided by the fixturing system producer (i.e. Erowa system solutions) has been used; the gauge is constituted by a precision cylinder with calibrated surfaces on top and a calibrated hole in the middle.

Figure 60: Erowa system solutions precision measuring gauge

First of all, the A-B axes have to be fine aligned with respect to the machine tool reference system; this is done thanks to a mechanical level dial gauge used on the aforementioned precision measuring gauge surfaces fixtured on B axis.

Then, the standard procedure for rotation centre localization includes the measurement, via touch probing, of the centre of the calibrated hole in the A axis vertical position obtaining thus the X-Y coordinates of Point C (i.e. see Figure 61 on the left for reference), and the measurement, always via touch probing, of multiple points (which are averaged and from which is subtracted the calibrated distance from the hole centre) along the calibrated surface, in order to gather the Z coordinate of Point C (i.e. see Figure 61 on the right for reference).

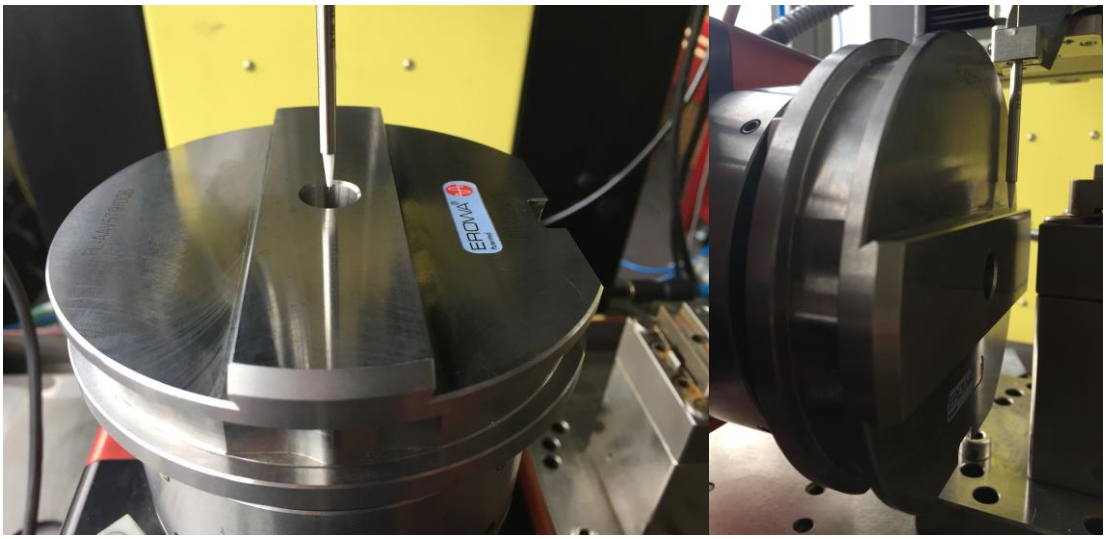

Figure 61: standard rotation centre (i.e. Point C) localization procedure, via touch probing

Following the aforementioned standard procedure, leads to the determination of Point C coordinates in the SARIX machine tool; different methods can be used for different machine tools kinematic disposition. However, during the experimental trials, some limitations on this procedure emerged resulting in a non-optimal localization of the rotation centre (i.e. Point C). In particular, this causes an erroneous parametrization of the machine tool kinematic structure: the real centre of rotation differs from the one parametrized in the algorithms (i.e. both with traditional machining procedures and with the ones proposed in the present work thesis). In fact, this point is used to recalculate the positions of any point on the work piece in all the different machining positions, which of course are characterized by different A-B axes values, as a consequence, an imprecise estimation of the point leads to a wrong estimation of these positions resulting in a difference between the nominal CAM generated and the real world coordinates.

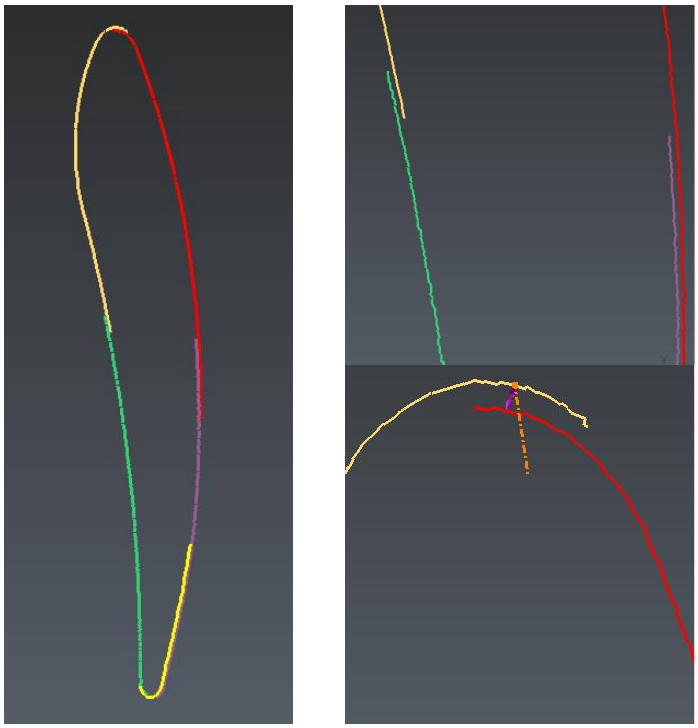

Figure 62: qualitative image representing the reconstruction of an entire blade airfoil with the procedure pointed out in 3.5.2 leading to a reconstruction error caused by the uncertainty of Point C localization. In yellow, orange, green, purple and red are represented the different blade airfoil acquisitions made necessarily with different A-B axes values; the distances among these portions lay into the 0.03 and 0.08 mm range.

A qualitative example showing this effect, is reported in Figure 62, where the blade complete reconstruction algorithm described in 3.5.2, has been applied and the acquisitions of the reconstructed blade are not correctly overlapping with a point to point spatial distance laying into the 0.07-0.18mm range.

In Figure 63 is reported a simplified bi-dimensional schema, representing the effect of an error in the localization of the rotation centre (i.e. Point C) resulting from the movement of A-axis.

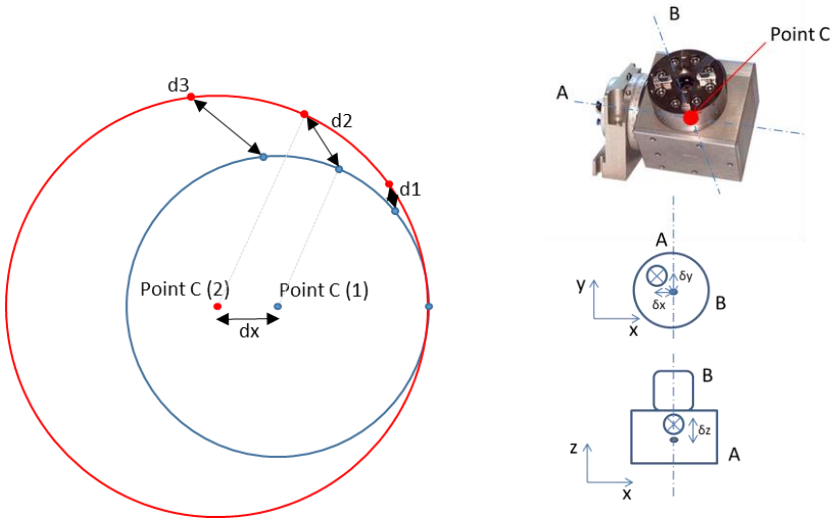

Figure 63: simplified bi-dimensional schema representing an error in X coordinate localization of the rotation centre (Point C) together with its effect along the whole axis rotation. D1, D2 and D3 represent an example of how the point-to-point distances varies along the whole rotation angle. On the right the complete schema reporting the error along the three directions

Considering only an error on X coordinate and the only A-axis rotating along the whole 360° circumference, in the ideal case, the error trend is reported in Figure 64, in percentage with respect to the error in X coordinate estimation.

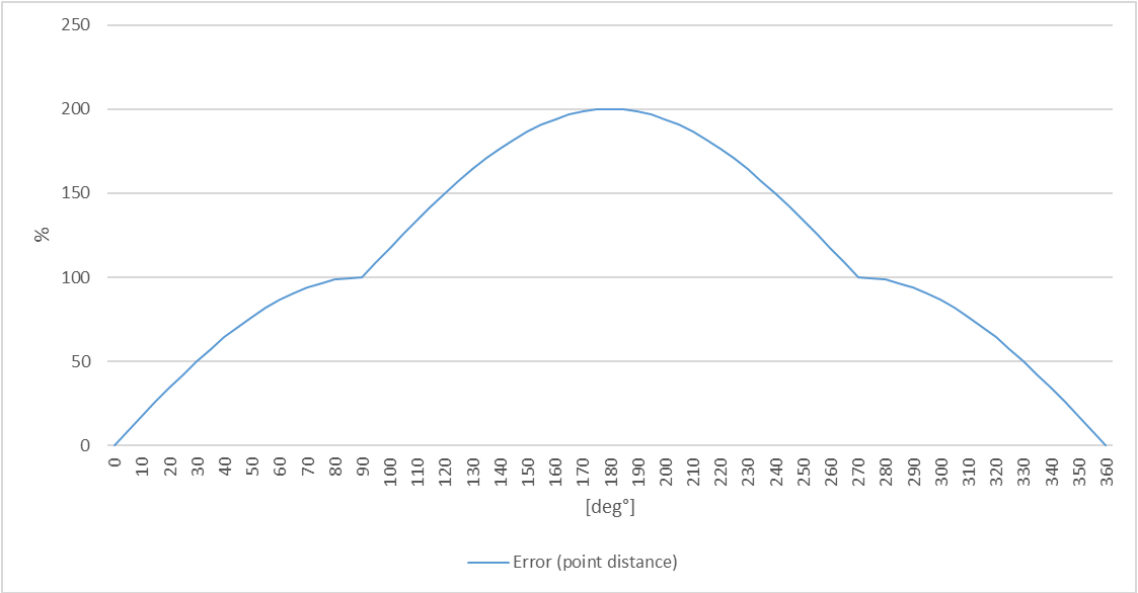

Figure 64: simplified bi-dimensional diagram reporting an error in one coordinate localization of the rotation centre (Point C) together with its effect along the whole axis rotation in %

The combined effect of localization errors in X, Y and Z coordinates of the rotation centre is not easy to be graphically represented; furthermore, complicating the problem, the two rotation axis of A and B axes do not intersect in a real case scenario, due to fabrication imperfections (see Figure 63).

As a consequence, a calibrated sphere has been mounted on the Erowa system measuring gauge screwed in the threaded hole already manufactured (blue circle in Figure 60) in order to perform point measurements on the actual axes in different A-B positions with the touch probing method.

The error estimation procedure is the following:

1. A first point (calibrated sphere centre coordinates) is measured with $A=A_1$ and $B=B_1$ angles and used as the reference point
2. A second point (calibrated sphere centre coordinates) is measured with $A=A_2$ and $B=B_2$ angles
3. The reference point coordinates are rotated around Point C so to set $A=A_2$ and $B=B_2$
4. The error corresponds to the spatial distance between the reference point (as rotated in point 3.) and the second point

In Figure 65 is reported an example of application of this procedure repeated for 36 measured points along the 0°-180° range of motion for A and B axes together. The first point, of which coordinates have been acquired at A=0° and B=0°, is used to carry out the procedure as reference point.

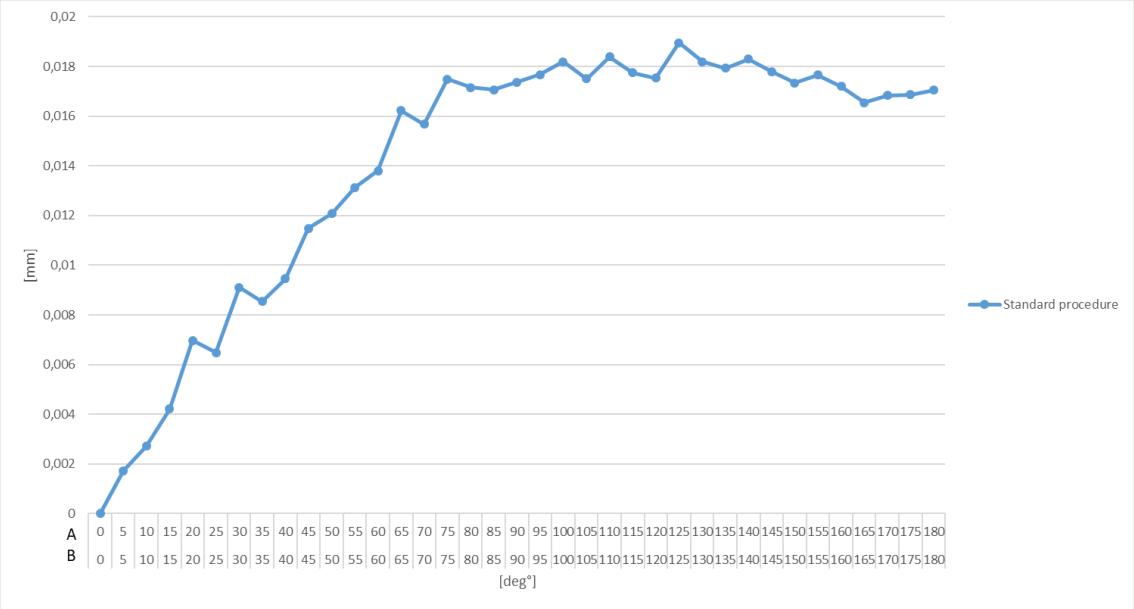

Figure 65: error (point distance) estimation for different values of A-B axes with the standard localization method of the rotation centre (i.e. Point C)

In this case the maximum error is gathered at A and B values equal to ca. 125° and corresponds to approximately 0.0185mm.

In order to minimize this effect, a different approach has been followed, based on an iterative procedure. This approach involves the usage of a solver (i.e. the GRG non-linear solving method), which is asked for iterate the aforementioned process while changing the rotation centre coordinates so to minimize the error in the estimation of its spatial coordinates. In this case the standard procedure used for the estimation of the rotation centre point coordinates is used as a first approximation value.

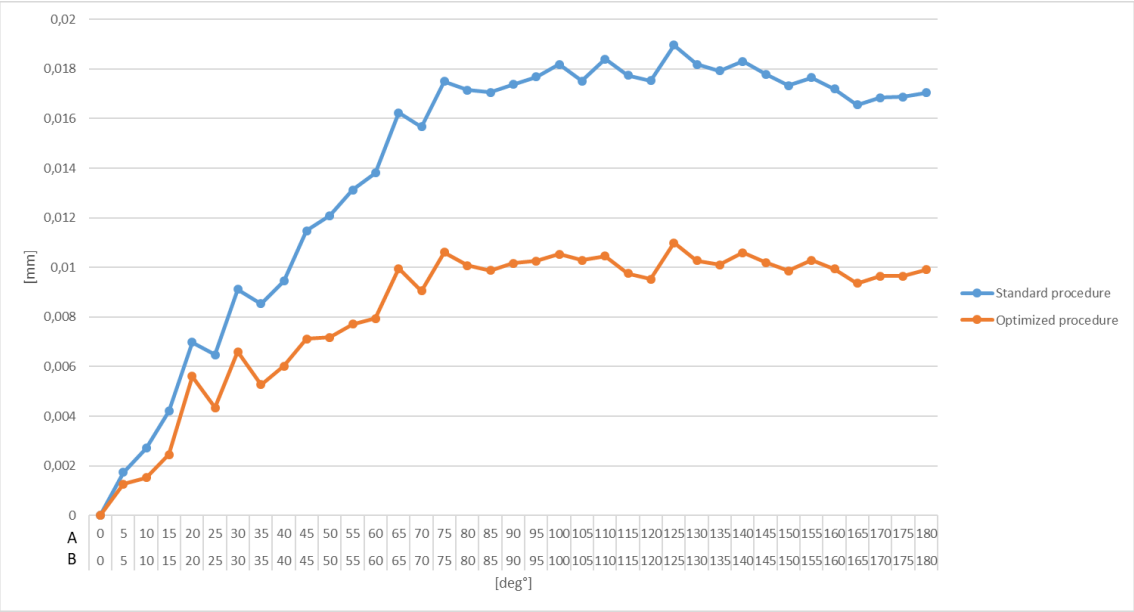

Figure 66: error (point distance) estimation for different values of A-B axes with the standard and the optimized localization method of the rotation centre (i.e. Point C)

In Figure 66 is reported the same example presented in Figure 65 with the superposed data of the same points measured, but rotated around a different rotation centre, which has been corrected with the aforementioned procedure. Note that the measured points used for running the optimization algorithm do not correspond with the ones of the experimental trial reported in Figure 66. As expected, the optimized curve shows lower error values.

	Rotation centre (Point C) spatial coordinates		
	X coordinate [mm]	Y coordinate [mm]	Z coordinate [mm]
Standard procedure	26,6264	54,8357	-193,1341
Optimized procedure	26,6182	54,8481	-193,1247
Difference	**0,0082**	**0,0124**	**0,0094**

Table 7: Rotation centre (Point C) optimization procedure results

In Table 7 are reported the coordinates calculated with the standard rotation centre localization procedure, together with the ones calculated with the optimization procedure showing a difference, in absolute values, in the order of magnitude of 0.01mm.

Since the method has shown satisfactorily results, it has been included in the machine setup and calibration procedure.

3.6. Quality inspection procedure

As stated in the state of the art section, having a laser triangulation sensor integrated on-board the machine tool, gives the opportunity to implement an integrated quality inspection procedure directly on the machine tool. This procedure is substantially standard, and it is usually performed by means of dedicated optical measuring machines based on fringe projection, laser triangulation or autofocus measuring technologies, among others. It consists in the complete reconstruction of the whole work piece already machined which is then best fitted on its CAD nominal geometry through the six points constrained procedure pointed out in 3.5.2. Then deviations, in terms of displacements and inclinations of the cooling channels machined on the surface, can be extrapolated and tolerances can be verified.

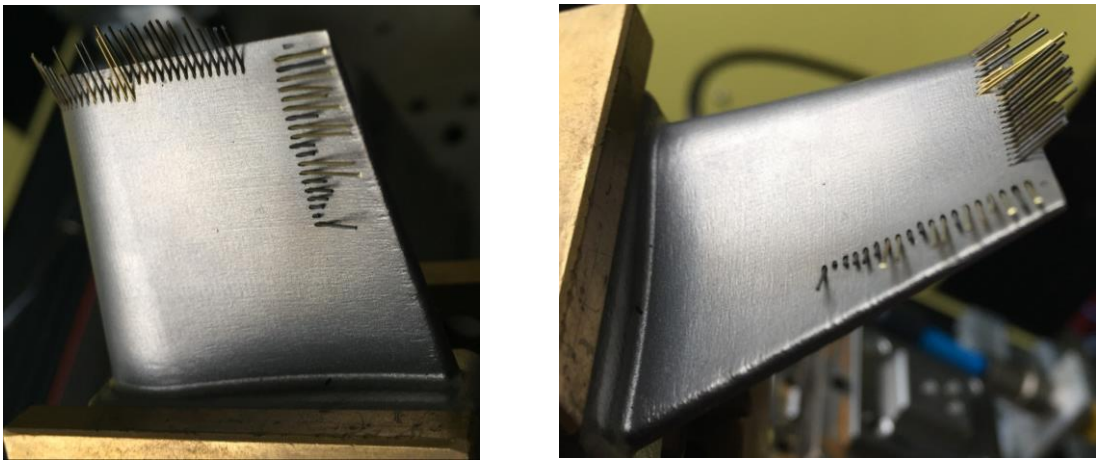

Figure 67: machined turbine blade specimen with calibrated jigs inserted into the cooling channels

Since machined cooling channels, as pointed out in the state of the art section, can have relatively small diameters (e.g. 0.1mm), with lengths up to 30 times the diameter, their complete measurement results to be difficult; the number of points measured in fact, results often to be insufficient to accurately extract the best fitted cylinder representing the machine cooling channel. As a consequence, a wide accepted procedure consists in the insertion of calibrated jigs into the machined cooling channels, in order to enable the measurement of more points and thus increasing the robustness of the measuring procedure. In Figure 67 is reported the turbine blade specimen with calibrated jigs inserted in the machined cooling channels.

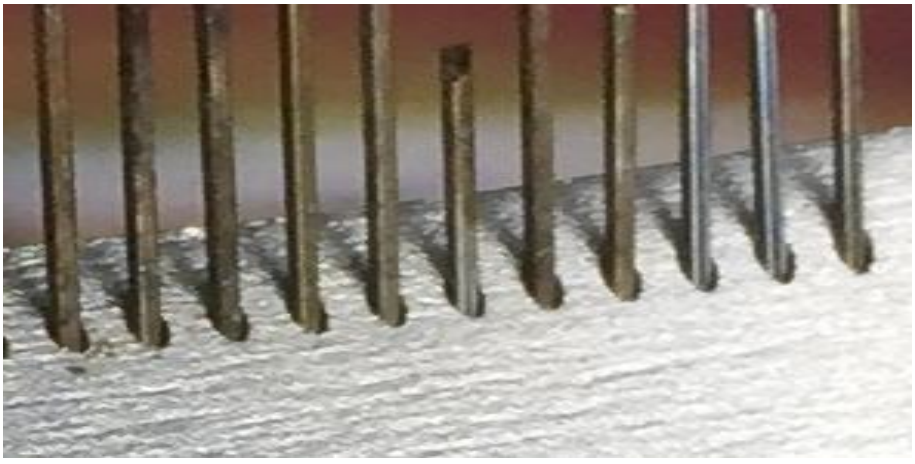

Figure 68: machined turbine blade specimen with calibrated jigs inserted into the cooling channels

In Figure 68 is reported a magnified picture of the aforementioned procedure.

4. Experimental results

4.1. Calibration system experimental tests

This chapter is dedicated to the experimental results of the calibration procedure pointed out in 3.4, showing the outcome of the entire process on the SARIX SX200 Aero machine tool described in 3.1.

The full calibration procedure has been processed 17 consecutive times resulting the calculation of equations (12) where the term R_{sm} corresponds to equation (14).

In Figure 69 are reported the 17 consecutive measurements of X-Y coordinates of reference points C1, C2 and C3 (see Figure 42 for reference), measured via touch probing procedure and expressed in the machine tool reference system.

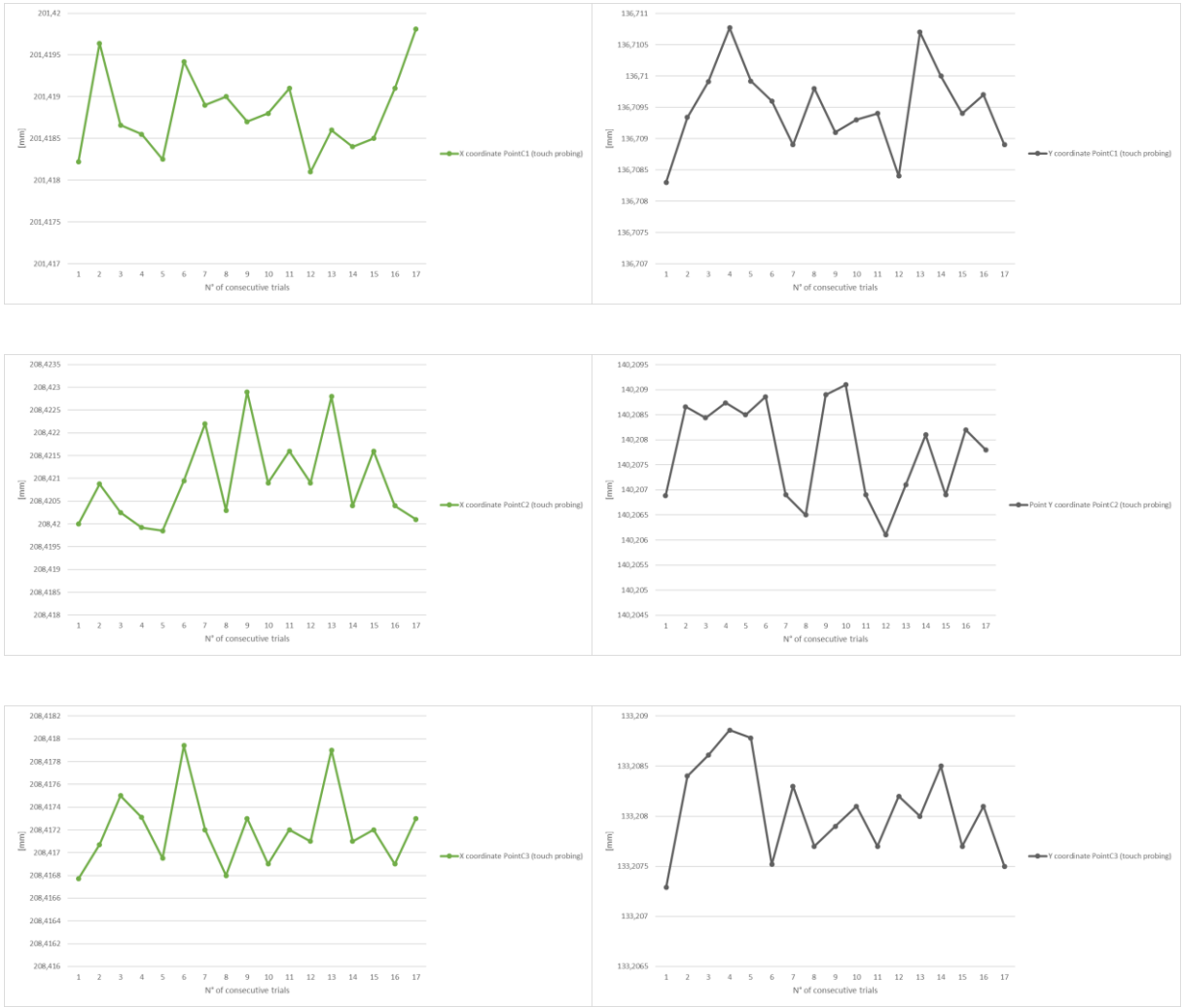

Figure 69: X-Y coordinates of Points C1, C2 and C3 (see Figure 42), measured 17 consecutive times with touch probing procedure expressed in machine tool reference system

The measurements are repeatable, in line with the touch probing declared accuracy (see paragraph 3.1.2); the test demonstrate also that the reference artefact itself does effectively respect the requested tolerances (see Figure 43).

		Min [mm]	Max [mm]	Average [mm]
Point C1	**X coordinate [mm]**	201,4181	201,4207	201,4189
	Y coordinate [mm]	136,7083	136,7199	136,7101
Point C2	**X coordinate [mm]**	208,4199	208,4229	208,4209
	Y coordinate [mm]	140,2061	140,2091	140,2078
Point C3	**X coordinate [mm]**	208,4168	208,4179	208,4172
	Y coordinate [mm]	133,2073	133,2089	133,2081

Table 8: summary table of data reported in Figure 69; maximum, minimum and average values are reported relative to the X-Y coordinates measured 17 consecutive times

In Table 8 is reported a summary table referred to the aforementioned measurements.

Then, according to the procedure explained in 3.4, the same points have been measured 17 times consecutively with 1 step of iterations for the misalignment error compensation (see 3.4.6), leading to the calculation of the displacement and inclinations between the laser triangulation sensor and the machine tool end-effector.

The procedure accuracy can be estimated with the point-to-point distance resulting from the estimation made with the two systems; these results have been reported in Figure 70.

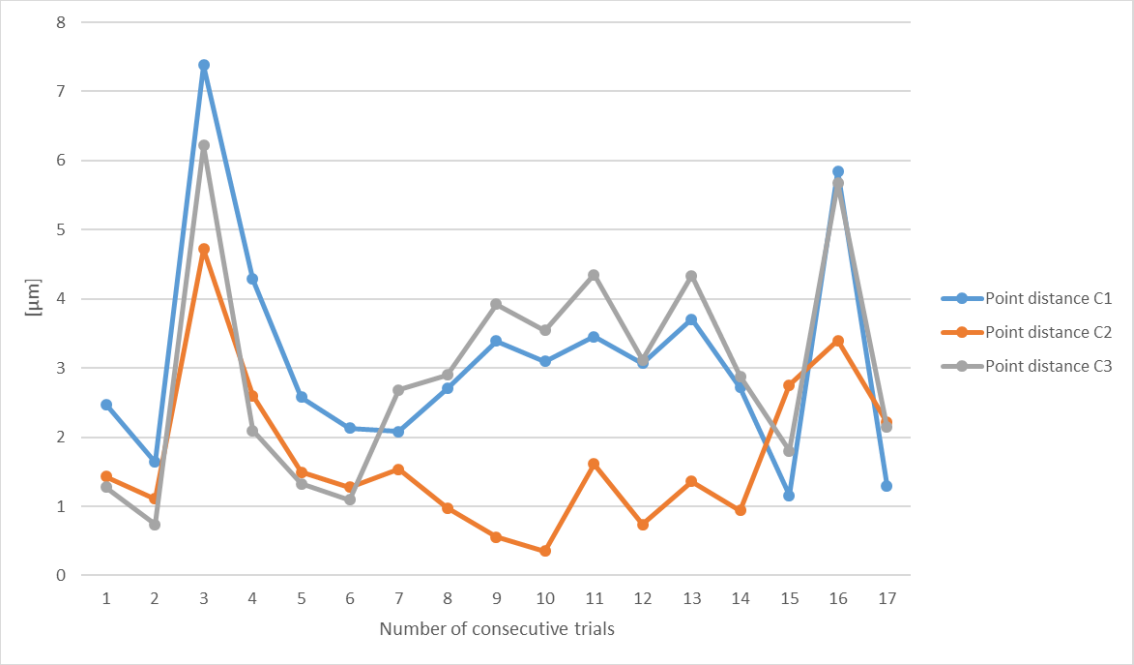

Figure 70: error (point-to-point distance) between centre of cones of calibration artefact (C1, C2 and C3) measured with touch probing and laser triangulation sensor calculated in calibration procedure processed 17 consecutive times

The fact that the trends of the three point coordinates measured (i.e. C1, C2 and C3) are similar along the 17 trials, indicates residual rotations/displacements caused by the uncertainty in the best-fit algorithm (no perfect correspondence between nominal CAD model and real world calibrated artefact), and by the residual deformation caused by the single compensation iteration applied. However, these results can be considered satisfactorily, for the required application.

		Min [µm]	Max [µm]	Average [µm]
Point C1	**Point-to point distance [µm]**	1,161791	7,379179	3,119435
Point C2	**Point-to point distance [µm]**	0,353379	4,721674	1,71021
Point C3	**Point-to point distance [µm]**	0,741787	6,221223	2,947579

Table 9: summary table of data reported in Figure 70; maximum, minimum and average values are reported relative to the X-Y coordinates measured 17 consecutive times

In Table 9 is reported a summary table referred to the aforementioned measurements.

4.2. Positioning procedure experimental tests

This chapter is dedicated to the experimental results of the positioning procedure pointed out in 0, showing the outcome of the entire process on the SARIX SX200 Aero machine tool described in 3.1.

The full positioning procedure has been followed and the turbine blade specimen has been machined consequently. In Figure 71 are reported some pictures of the turbine blade specimen machining.

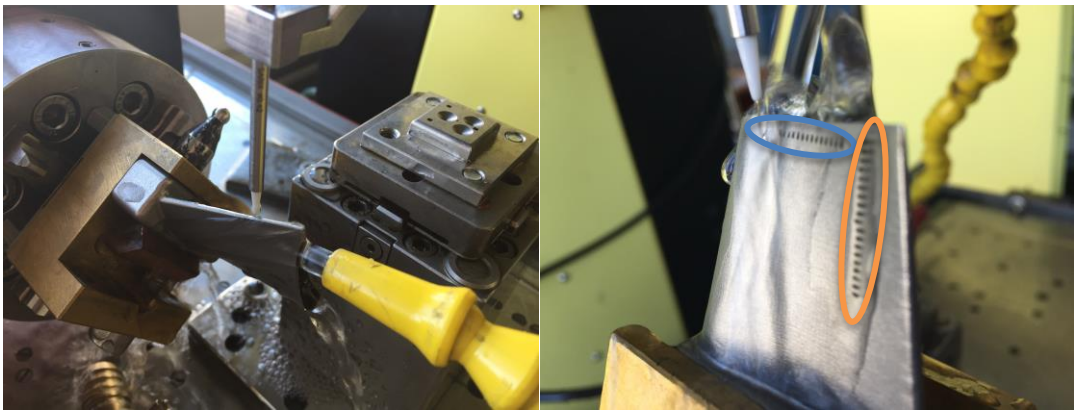

Figure 71: turbine blade specimen micro-EDM machining operations after positioning procedure has been implemented

With reference to the figure, the series of cooling holes circled in blue, have been machined with the six points constraint positioning method (see 3.5.2); the orange circled ones, with the local adaptive procedure (see 3.5.1). Furthermore, some holes have been machined with nominal machining positions, thus with no correction procedures applied. After the blade has been machined, it has been measured again (for example in Figure 72 it is reported a machined blade acquisition best fitted on its CAD model) in order to perform repeatability tests.

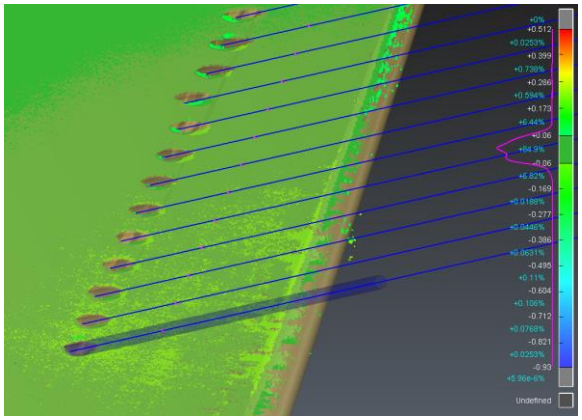

Figure 72: machined turbine blade laser triangulation sensor acquisition

In particular, calibrated foils with different thickness (i.e. 0.6mm, 0.5mm, 0.4mm, 0.3mm, 0.2mm, 0.1mm and 0.05mm) have been randomly inserted in the turbine blade fixturing system in order to introduce voluntarily positioning errors. An example of this procedure is reported in Figure 73.

Figure 73: example of voluntarily positioning error, obtained by manually inserting a calibrated foil of 0.6mm into the turbine blade specimen fixturing system

Then the whole positioning procedure has been processed again with both the methods (i.e. local adaptive correction and six points based alternative method) and the machine tool electrode has been changed with one with a smaller diameter (i.e. 0.2mm vs 0.44mm that has been used for machining). The new electrode has been finally moved again into the new machining positions re-accessing the machined holes and the hole centre has been measured via touch probing procedure.

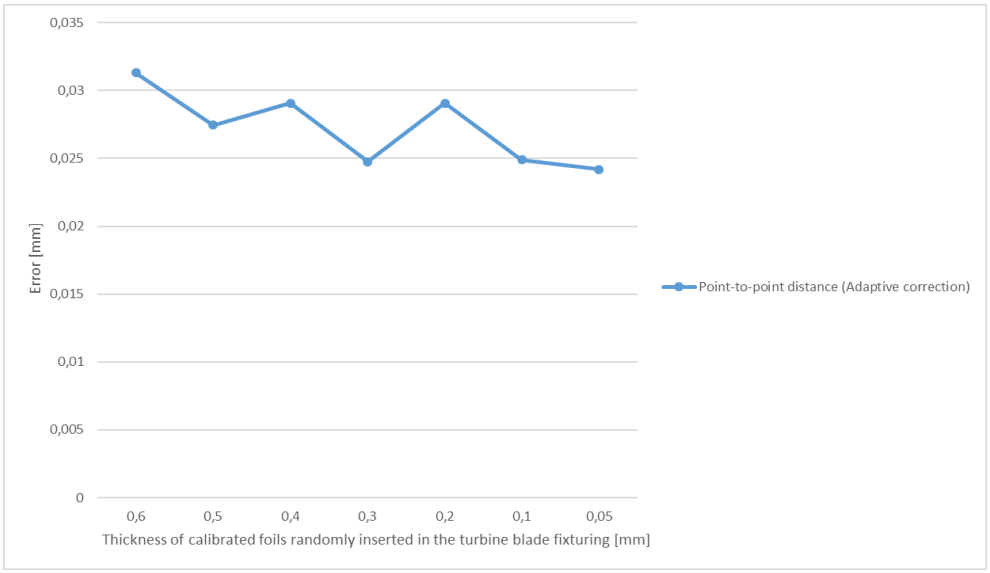

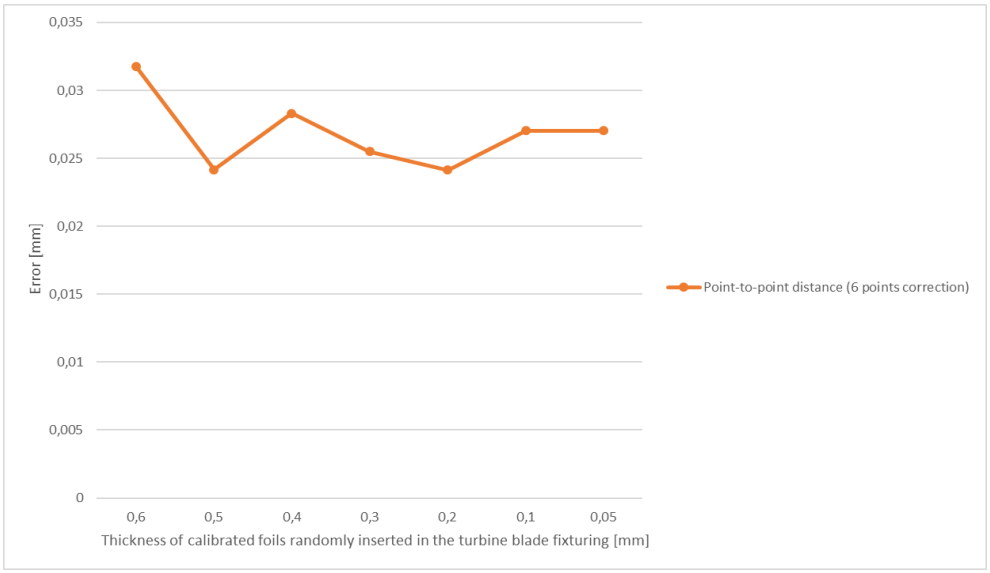

Figure 74: positioning procedures repeatability test; in blue the procedure repeated with the local adaptive positioning procedure, in orange the same test repeated with the six points constrained one

The point-to-point distance (i.e. the distance between the new calculated hole centre and the machined hole centre) has been measured for each of the machined holes, with both the positioning methods. The measured distances in the same holes series (see Figure 71) and within the same trial (i.e. within the same measurement) have been averaged. The results relative the tests with all the calibrated foils are reported in Figure 74.

Both the positioning procedures are similarly repeatable and the error is only slightly affected by the thickness of the calibrated foils inserted in the work piece fixturing.

Note that the results reported are affected by all the error chain described in the previous paragraphs (e.g. A-B axes accuracy).

The nominal positioning error, regarding the holes machined with no corrections applied, was not possible to be estimated with the aforementioned method since the error was too high and the machine tool electrode was not able to re-access the previously machined hole with any of the calibration foils inserted.

In absolute terms, the two positioning procedures differ of a quantity that has been reported as an example for one machined hole in Table 10, also with respect to nominal, CAM generated, coordinates.

Calibrated foil thickness: 0.6mm – Reference hole: Foil1.Group1.Hole1			
Calculated machining coordinates	**Nominal (CAM generated)**	**Adaptive local procedure**	**6 points constrained procedure**
Coordinate X [mm]	202.7765	202.4298	202.4405
Coordinate Y [mm]	67.9014	68.0511	68.0826
Coordinate A [deg°]	0	0.9585	0.9513
Coordinate B [deg°]	55	55.7641	55.7212

Table 10: absolute machining coordinates calculated with three different methods referred to a specific cooling hole where a calibrated foil of 0.6 mm of thickness has been inserted in the turbine blade fixturing system.

In Figure 75 are reported, in two different snapshots, the nominal machining coordinates (i.e. in red) together with the six points constrained positioning method (i.e. in orange) and the local adaptive positioning method (i.e. in blue) which has been used to drive the machining process for the considered hole.

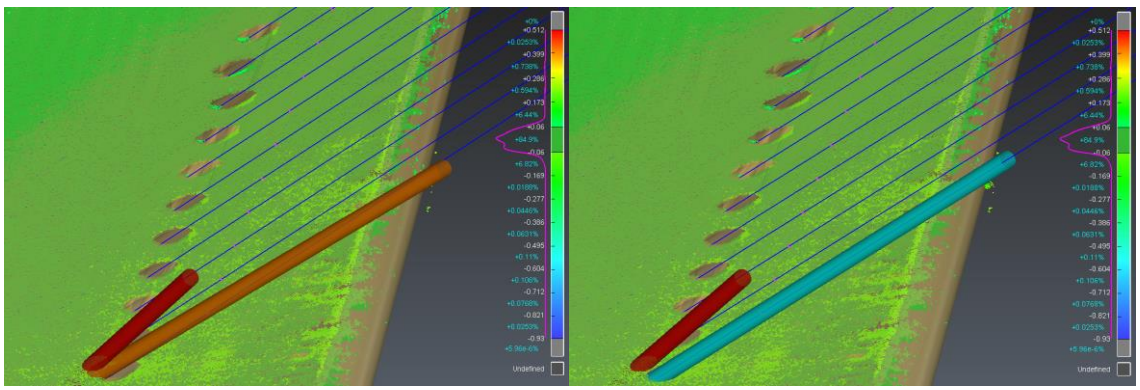

Figure 75: graphical representation of Table 10 content: in red the nominal (i.e. CAM calculated) machining coordinates, in orange the six points constrained procedure, in blue the local adaptive correction

In Figure 76 the three different solutions are represented all together on the same machined cooling channel.

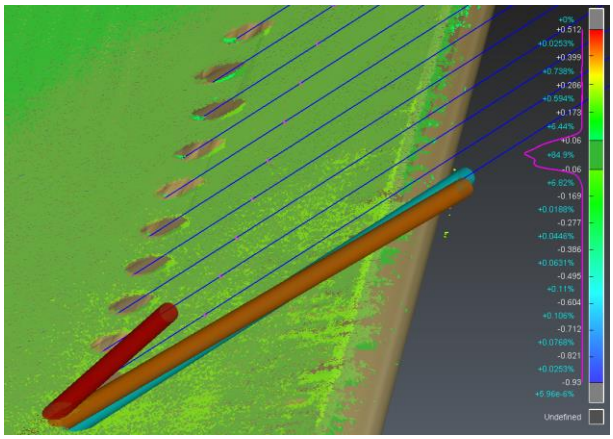

Figure 76: graphical representation of Table 10 content: in red the nominal (i.e. CAM calculated) machining coordinates, in orange the six points constrained procedure, in blue the local adaptive correction

The quality inspection procedure pointed out in paragraph 3.6 has been performed only for real case scenarios production turbine blades (i.e. the calibrated jigs were available only for real case scenarios), for which the results cannot be published due to confidentiality issues.
In the represented case, as stated, the two positioning compensation procedures showed a similar behaviour; this is due to the homogeneity of the distribution of the turbine blade specimen used (i.e. see 3.3.4), since it has been produced via metal additive manufacturing. However, the system has been tested also in real case scenarios, with real, cast produced, aeronautic turbine blades; complete test results cannot be published due to confidentiality issues. In this case the deviations from nominal CAD model are much more non-homogeneous, leading to the presence of areas where the error exceeds 0.3mm. Moreover, cooling holes, as stated in the state of the art section, are not always cylindrical but, on the contrary, can have shaped geometries, leading to the need of complex machine tool trajectories to be machined. An example is reported in Figure 77, where on the left is reported the blade analysis performed with the method explained in 3.5.2, showing deviations greater than 0.3mm. On the right is reported a part of its CAD model, showing that, exactly in the high deviation area, fan shaped holes must be machined. For the realization of these particular features, which are very common in real case scenarios, the positioning must take into account for the blade surface shape deviations, otherwise the machining results would be very poor, resulting finally in scrap work pieces. In this case the local adaptive positioning procedure becomes very helpful: the blade measured portion will be limited to the area where the fan shaped holes must be machined, in this way the best-fit algorithm will compensate for the shape deviations (see Figure 78, where the area to be machined has a shape deviation reduced to ca. 0.08mm) reducing their effect.

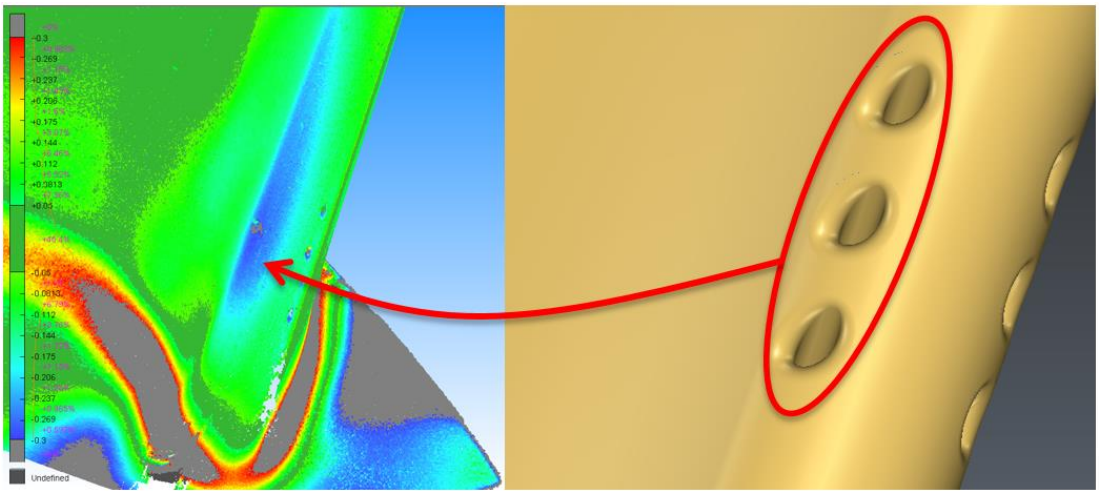

Figure 77: real case scenario of fan shaped holes that must be realized in turbine blade zone with high surface deviation and high curvature

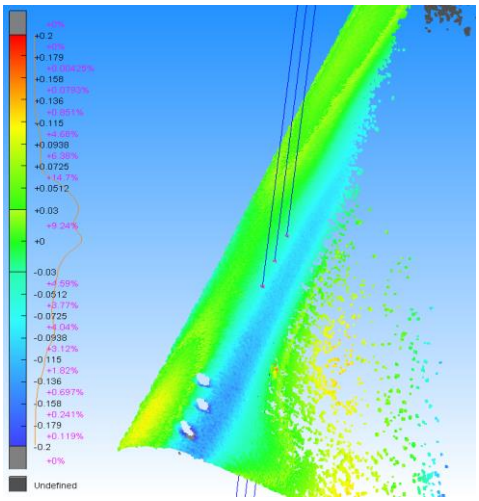

Figure 78: example of partial measurement of turbine blade profile (i.e. the same indicated above in Figure 77), limited to the fan shaped holes machining area.

As a drawback in using this method, there is the fact that the global positioning (i.e. the one calculated with respect to the predefined six points on the blade airfoil) will be significantly deviated from the requirements; however, this is often the only way to machine successfully complex geometries such as fan shaped holes in highly deviated turbine blade surfaces.

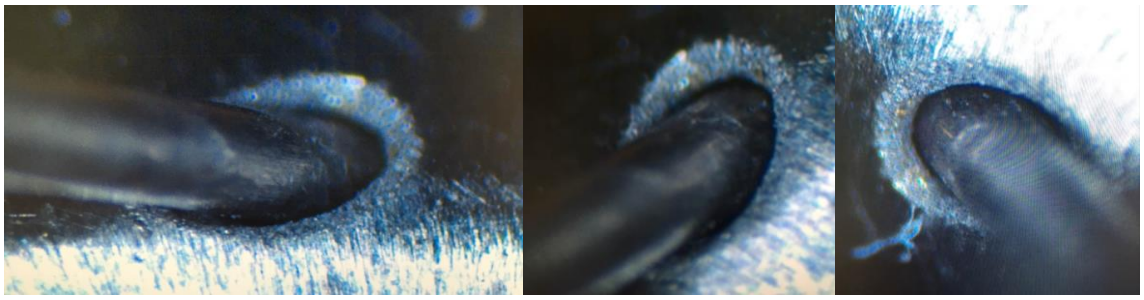

Figure 79: microscope images of the machined fan-shaped hole in a real case turbine blade with high surface deviation and high curvature thanks to the local adaptive positioning procedure

In Figure 79 are reported some microscope images of one of the machined fan shaped holes described above; in this case the shaped geometry was fully compliant with the final customer requirements and the global positioning (i.e. the one calculated with respect to the predefined six points on the blade airfoil, which is the current industrial practice) laid into the requested tolerances leading to final component acceptance (i.e. in this case the quality inspection procedure pointed out in 3.6 has been performed, but results cannot be published due to confidentiality issues).

The whole comparison has been carried out also with the contact based positioning method, which is the actual state of the art method employed by most EDM machine tool manufacturers (i.e. comprehending SARIX SA), as stated in chapter 2. This has shown intermediate results between nominal procedure (i.e. relying on CAM generated coordinates) and the presented methods (i.e. laser triangulation based), however the results cannot be published due to confidentiality issues.

5. Conclusions and next steps

As stated in the introduction section, the present work thesis is part of a wider conceptual framework fostering an in-line inspection and correction system, comprehensive of laser and tomographic measurement systems coupled with fluid dynamic and positioning engines, towards the optimization of micro-scale features machining in freeform shaped parts. The research is focused on gas turbines components with particular focus on turbine blades and vanes cooling system; on these components and their problematics and uncertainties in measurement and machining are centred the state of the art, the research motivation and the market analysis sections.

A part of this framework, consisting in the laser based measurement and inspection system, together with the positioning engine, has been deeply investigated in the present work thesis; the work has been carried out with the support of SARIX SA and the results are being commercialized and patented by the company.

As a consequence, the specific experimental setup comprehensive of machine tool characteristics and technology used for the demonstration, are presented and characterized. Then the sensing equipment choice, together with the design of the specific on-board integration system, are reported.

Then the overall procedures designed for the machine tool calibration and positioning are extensively described, together with their governing equations; the described procedures are generic and valid for any machine tool with small arrangements regarding their kinematic structure.

Since the machining of turbine blades cooling channels is subjected to strict industrial standards, two different procedures have been investigated in order to ensure the full compliancy with these standards: a local adaptive positioning method and a six points constrained one. These two methods have been compared and motivations for the usage of one or another, are reported. In particular, the six points constrained method guarantees the complete compliancy with the actual standards with fast cycle times and respecting the required accuracy and repeatability for the application; on the other hand, the local adaptive procedure becomes very helpful in the machining of components with relatively high local surface shape deviations derived from previous manufacturing operations such as casting, compensating for these deviations, and thus enabling the correct machining of such components where any other state of the art method would have created non-conform pieces. This effect is exacerbated in the case where complex machine tool trajectories must be followed in order to machine the required cooling channel shape, for example in the case of fan shaped holes machining. The comparison with the actual standard procedure, based on the tactile measurement of some predefined points, was not possible to be reported due to confidentiality issues.

Along the work description in the present document, the possible error sources, coming for example from the sensing equipment or from its integration system, have been reported, and quantified through experimental trials, relatively to the specific equipment used for the experiments. In fact, final results are affected by all the error chain contributions, that must be evaluated in strict relationship with the specific equipment adopted.

Finally, overall system tests, comprehensive of both calibration and positioning procedures, have been performed with the described equipment on a custom produced dummy turbine blade, and reported in the present document, together with a few nods regarding real case scenarios (i.e. with real production turbine blades) implementation of the system.

In conclusion, the designed system demonstrated to be a valid method for the positioning and the on-board inspection of freeform shaped parts in high precision machine tools. The extensive knowledge enabled by the adoption of this method, in terms of external surface shape, acquired on each single

machined component, paves the way for the development of the rest of the wide concept presented in the very beginning of the present work thesis. These future developments, enabled by the results presented above, have already started in the form of new research projects involving also other European universities and large gas turbine industries.

6. Bibliography

[1] Freedonia Group: FreedoniaFocusWorldCollection

[2] Credence research: Gas turbine electrical power generation market

[3] Manufacturing Engineering Magazine: Cool is Key to Jet Efficiency

[4] J. P. Holdren, “A National strategic plan for advanced manufacturing,” Report of the Interagency working group on Advanced Manufacturing IAM to the National Science and Technology Council NSTC Committee on Technology CoT, Executive Office of the President National Science and Technology Council, Washington, D.C. (2012).

[5] Westkämper, E., and H-J. Warnecke. "Zero-defect manufacturing by means of a learning supervision of process chains." CIRP Annals-Manufacturing Technology 43.1 (1994): 405-408.

[6] Prnewswire market research

[7] Defining technologies for the next millennium: GE aircraft engines 2000

[8] Manufacturing Engineering Magazine: Cool is Key to Jet Efficiency

[9] EUTurbines Annual reception 2012

[10] Eurostat: statistics on the production of manufactured goods Value ANNUAL 2015

[11] GF Machining Solutions Annual Report 2015

[12] E. Savio, L. De Chiffre, “An artefact for traceable freeform measurements on coordinate measuring machines”, Precision Engineering, 26 (2002), 58-68

[13] ISO/TS 17450-1:2005, Geometrical product specifications (GPS) - General concepts - Part 1: Model for geometrical specification and verification.

[14] M. Konter, M. Thumann, “Materials and manufacturing of advanced industrial gas turbine components”, Journal of Materials Processing Technology, Volume 117, Issue 3, 23 November 2001, Pages 386–390

[15] S.A.M. Rezavand, A.H. Behravesh, “An experimental investigation on dimensional stability of injected wax patterns of gas turbine blades”, Journal of Materials Processing Technology, vol. 182, issues 1–3, 2 February 2007, pp. 580–587

[16] US 6844515 B2, “Method and apparatus for turbine blade machining”

[17] US 7334331 B2, “Methods and apparatus for machining components”

[18] Y. Wang, X. Chen, Q. Liu, N. Gindy “Optimisation of machining fixture layout under multi-constraints”, International Journal of Machine Tools and Manufacture”, Volume 46, Issues 12–13, October 2006, Pages 1291–1300

[19] Patent US6611731: machining aerofoil components

[20] H.Schwenke, U. Neuschafer-Rube, T.Pfeifer, H.Kunzmann “Optical methods for dimensional metrology in production engineering”, Keynote paper, Annals of the CIRP, 51/2:685-699

[21] Sirat, G.Y., 1992, Conoscopic holography. I. Basic principles and physical basics, Journal of the Optical Society of America A, 9, 70-83.

[22] Chen, F. et al., 2000, Overview of three-dimensional shape measurement using optical methods, Optical Engineering, 39/1, 10-22. 68.

[23] Reich, C., et al., 2000, 3-D shape measurements of complex objects by combining photogrammetry and fringe projection, Optical Engineering, Vol. 39, No. 1,224-231

[24] S. V. Ekkad and J.-C. Han, “A Review of Hole Geometry and Coolant Density Effect on Film Cooling,” in Frontiers in Heat and Mass Transfer, 2013.

[25] J.-C. Han and L. M. Wright, “Enhanced Internal Cooling for Turbine Blades and Vanes, Ch. 4.2.2.2,” in The Gas Turbine Handbook, U.S. DOE-National Energy Technology Laboratory (NETL), 2006, pp. 321-354.

[26] D. G. Bogard, “Airfoil Film Cooling, Ch. 4.2.2.1,” in The Gas Turbine Handbook, U.S. DOE-National Energy Technology Laboratory (NETL), 2006, pp. 309-321.

[27] R. S. Bunker, “The Effect of Manufacturing Tolerances on Gas Turbine Cooling,” Journal of Turbomachinery, vol. 131, pp. 1-11, October 2009.

[28] S.Lee, D.-H. Rhee and K. Yee, “Optimal Arrangement Of The Film Cooling Holes Considering The Manufacturing Tolerance For High Pressure Turbine Nozzle,” in ASME Turbo Expo 2016: Turbomachinery Technical Conference and Exposition, Seoul, South Corea, 2016.

[29] F. Montomoli, A. D'Ammaro and S. Uchida, “Numerical and Experimental Investigation of a New Film Cooling Geometry with High P/D Ration,” International Journal of Heat and Mass Transfer, vol. 66, pp. 366-375, 2013.

[30] D. Bohn and R. Krewinkel, “Conjugate Simulation of the Effects of Oxide Formation in Effusion Cooling Holes on Cooling Effectiveness,” in Proceedings of ASME Turbo Expo 2009: Power for Land, Sea and Air, Orlando, Florida, 2009.

[31] J. Han, S. Dutta and S. Ekkad, Gas Turbine Heat Transfer And Cooling Technology, Boca Raton: CRC Press, 2012.

[32] A. McNally, I. R. Pashby and J. Flokes, “Laser drilling of cooling holes in aero-engines: State of the art and future challenges,” Materials Science and Technology, no. 20(7), 2004.

[33] Y. L. H.-Y. F. F. Xi, “Error compensation for three-dimensional line laser scanning data,” The International Journal of Advanced Manufacturing Technology, vol. 18, p. 211–216, 2001.

[34] J. N. C. Che, “A ball-target-based extrinsic calibration technique for high-accuracy 3-D metrology using off-the-shelf laser-stripe sensors,” Precision engineering, vol. 24, p. 210–219, 2000.

[35] B. Z. X. L. Z. H. P. R. G. Wang, “Modelling and calibration of the laser beam-scanning triangulation measurement system,” Robotics and autonomous systems, vol. 40, p. 267–277, 2002.

[36] S. C. P. B. J.-P. K. Nick Van Gestel, “A performance evaluation test for laser line scanners on CMMs,” Optics and Lasers in Engineering, p. 336– 342, 2009.

[37] J. I. U. N.-R. Markus Bartscher, “ISO test survey on material influence in dimensional computed tomography,” in Case Studies in Nondestructive Testing and Evaluation, Elsevier, 2016.

[38] S. Webzell, “That first step into EDM, in: Machinery”, 159, (4040) Findlay Publications Ltd, Kent, UK, November 2001, p. 41

[39] Anonymous, History and development, in: “The Techniques and Practice of Spark Erosion Machining”, Sparcatron Limited, Gloucester, UK, 1965, p. 6.

[40] A.L. Livshits, Introduction, in: “Electro-erosion Machining of Metals”, Department of Scientific & Industrial Research, Butterworth & Co., London, 1960, p. x

[41] L. Houman, Total EDM, in: E.C. Jameson (Ed.), “Electrical Discharge Machining: Tooling, Methods and Applications”, Society of Manufacturing Engineers, Dearbern, Michigan, 1983, pp. 5– 19.

[42] H.C. Tsai, B.H. Yan, F.Y. Huang, “EDM performance of Cr/Cu based composite electrodes”, Int. J. Mach. Tools Manuf. 43 (3) (2003) 245–252.

[43] E.I. Shobert, “What happens in EDM”, in: E.C. Jameson (Ed.), Electrical Discharge Machining: Tooling, Methods and Applications, Society of Manufacturing Engineers, Dearbern, Michigan, 1983, pp. 3–4

[44] G. Boothroyd, A.K. Winston, “Non-conventional machining processes”, in: Fundamentals of Machining and Machine Tools, Marcel Dekker, Inc, New York, 1989, p. 491.

[45] S.F. Krar, A.F. Check, “Electrical discharge machining”, in: Technology of Machine Tools, Glencoe/McGraw-Hill, New York, 1997, p. 800.

[46] S. Kalpajian, S.R. Schmid, “Material removal processes: abrasive, chemical, electrical and high-energy beam”, in: Manufacturing Processes for Engineering Materials, Prentice Hall, New Jersey, 2003, p. 541.

[47] K.P. Rajurkar, Z.Y. Yu, “3D micro-EDM using CAD/CAM”, Ann. CIRP 49 (1) (2000) 127–130.

[48] T. Masuzawa, “State of the art of micromachining”, Ann. CIRP 49 (2) (2000) 473–488.

[49] S.H. Yeo, G.G. Yap, “A feasibility study on the micro electro discharge machining process for photomask fabrication”, Int. J. Adv. Manuf. Technol. 18 (1) (2001) 7–11.

[50] I. Ishida, Y. Takeuchi, “L-shaped curved hole creation by means of electrical discharge machining and an electrode curved motion generator”, Int. J. Adv. Manuf. Technol. 19 (4) (2002) 260–265.

[51] F. Zhao, X. Xu, S.Q. Xie, "Computer-Aided Inspection Planning - The state of the art", Computer in Industry, No. 60, pp. 453-466, 2009